DIFFERENT COORDINATION MODES OF BIS(IMINE-PYRIDINE) AND BIS(QUINALDINECARBOXAMIDE) LIGANDS

by

DIPESH PREMA

B.Sc., Nottingham Trent University, 2001

AN ABSTRACT OF A DISSERTATION

submitted in partial fulfillment of the requirements for the degree

DOCTOR OF PHILOSOPHY

Department Of Chemistry
College of Arts and Sciences

KANSAS STATE UNIVERSITY
Manhattan, Kansas

2007

Abstract

2-Formylbenzoquinoline and a selection of novel chiral bis(pyridine-imine) and bis-amide ligands derived from (1*R*,2*R*)-cyclohexanediamine and (*R*)-[1,1'-binaphthalene]-2,2'-diamine have been synthesized and thoroughly characterized. Subsequently, their coordination chemistry has been investigated. Metallation with Zn(II), Ni(II) and Fe(II) has resulted in the formation of a series of helical complexes, some of which exhibit unusual coordination modes.

Bis(imine-pyridine) ligands were found to form dinuclear complexes upon reaction with $ZnCl_2$. In one case, the use of $Zn(CF_3SO_3)_2$ resulted in the formation a single stranded monohelix, after the ligand had undergone a reduction at one imine bond. The use of NiI_2 as the metal salt resulted in the formation of penta-coordinate complexes with N_3-coordination and helical dinuclear complexes with bridging iodo ligands. $Ni(CF_3SO_3)_2$ was also used, this resulted in the formation of a double stranded mononuclear complex. The ligand, in this case was hydrolyzed to yield a tridentate ligand, subsequently two of these new ligands coordinate to one metal center to form the complex.

Bis-amide ligands were reacted with $FeCl_2$ and $Fe(CF_3SO_3)_2$ to form complexes with various different colors. In all but one case, several attempts to structurally characterize the Fe(II) complexes were unsuccessful. Suitable crystals of this complex revealed a double stranded helicate complex that coordinates through carbonyl oxygens rather than amide nitrogens. The work described herein, is an account of the synthesis, characterization and study of a new family of tetradentate nitrogen donor ligands and their respective transition metal complexes.

DIFFERENT COORDINATION MODES OF BIS(IMINE-PYRIDINE) AND BIS(QUINALDINECARBOXAMIDE) LIGANDS

by

DIPESH PREMA

B.Sc., Nottingham Trent University, 2001

A DISSERTATION

submitted in partial fulfillment of the requirements for the degree

DOCTOR OF PHILOSOPHY

Department Of Chemistry
College of Arts and Sciences

KANSAS STATE UNIVERSITY
Manhattan, Kansas

2007

Approved by:

Major Professor
Dr Christopher J. Levy

Abstract

2-Formylbenzoquinoline and a selection of novel chiral bis(pyridine-imine) and bis-amide ligands derived from (1*R*,2*R*)-cyclohexanediamine and (*R*)-[1,1'-binaphthalene]-2,2'-diamine have been synthesized and thoroughly characterized. Subsequently, their coordination chemistry has been investigated. Metallation with Zn(II), Ni(II) and Fe(II) has resulted in the formation of a series of helical complexes, some of which exhibit unusual coordination modes.

Bis(imine-pyridine) ligands were found to form dinuclear complexes upon reaction with $ZnCl_2$. In one case, the use of $Zn(CF_3SO_3)_2$ resulted in the formation a single stranded monohelix, after the ligand had undergone a reduction at one imine bond. The use of NiI_2 as the metal salt resulted in the formation of penta-coordinate complexes with N_3-coordination and helical dinuclear complexes with bridging iodo ligands. $Ni(CF_3SO_3)_2$ was also used, this resulted in the formation of a double stranded mononuclear complex. The ligand, in this case was hydrolyzed to yield a tridentate ligand, subsequently two of these new ligands coordinate to one metal center to form the complex.

Bis-amide ligands were reacted with $FeCl_2$ and $Fe(CF_3SO_3)_2$ to form complexes with various different colors. In all but one case, several attempts to structurally characterize the Fe(II) complexes were unsuccessful. Suitable crystals of this complex revealed a double stranded helicate complex that coordinates through carbonyl oxygens rather than amide nitrogens. The work described herein, is an account of the synthesis, characterization and study of a new family of tetradentate nitrogen donor ligands and their respective transition metal complexes.

Table of Contents

List of Figures

List of Tables

Acknowledgements

Firstly, I would like to thank my advisor Dr. Christopher J. Levy for his help, advice, support and encouragement, whilst a member of his research group. I've taken great strides as a chemist under his supervision and learnt so much. I would also like to express my gratitude to Dr. Eric Maatta and Dr. Christer Aakeroy, who were both very helpful when I first came to Kansas State, as well as John Desper (crystallography) and everybody else in the chemistry department; coworkers, friends, faculty and support staff. My time here has been an enjoyable and positive one. In addition, my regards to Dr. Wallace at Nottingham Trent University for giving me the opportunity to come to Kansas State University in the first place.

Most importantly, I'd like to thank my parents; none of this would be possible without them. Their undying love, support and motivation over the past few years has allowed me to achieve my goals and further my career as a chemist. Also, regards to my brother Paresh and sister Rina, for their help and understanding, especially through the hard times.

DEDICATION

To my parents, for their love and support.

Chapter 1

Introduction

1.1 Helical Complexes

Design and synthesis of suitable chiral ligands for catalysis is a key goal in the field of asymmetric catalysis. One approach has been to incorporate a helical motif. A helix is defined as a twisted shape like a spring, screw or spiral staircase, it can be either left or right handed (*M* or *P*) respectively. If the helix spirals in the same direction the four fingers of the right hand are pointing, then it is a right handed helix (Figure 1.1). Contrary, if the helix spirals in the direction that the four fingers of the left hand are pointing then it's a left handed helix.

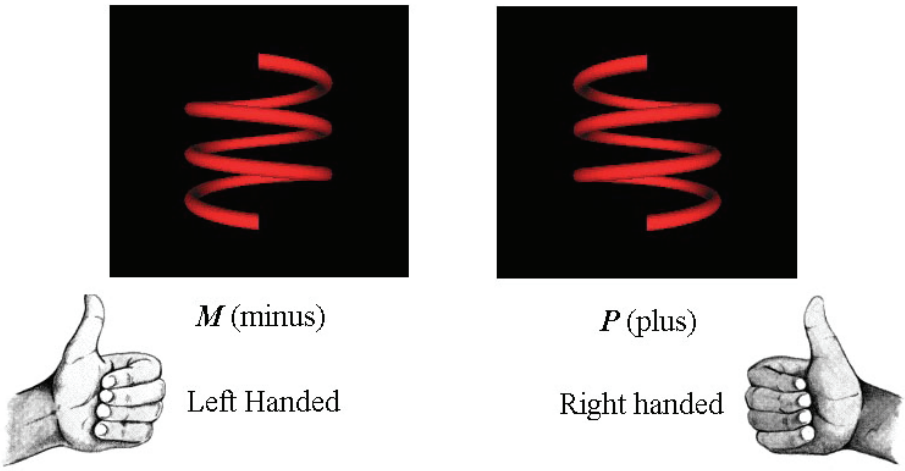

Figure 1.1 *M* and *P* configurations

The most well known example of molecular helices in nature is deoxyribonucleic acid (DNA), a double helix in which the two strands are connected by hydrogen bonding between

complimentary bases. In recent years there has been increasing interest in helical transition metal complexes and related supramolecular structures as potential scaffolds for chiral catalysts.[1]

1.2 Monohelices and Helicates

Molecular complexes of transition metals can be grouped into two general classifications, monohelices and helicates. Monohelices contain a single metal ion and can be single, double, or triple stranded depending on the nature of the ligand. Examples of each of these are illustrated in Figure 1.2. A single stranded monohelix can be produced when a single multidentate ligand wraps around a single metal center, as for the europium complex shown.[2] A double stranded helix is formed when two chelating ligands coordinate to the same metal, as for the platinum complex.[3] Triple-stranded monohelices such as $[Co(en)]_3^{3+}$ can be formed when three chelating

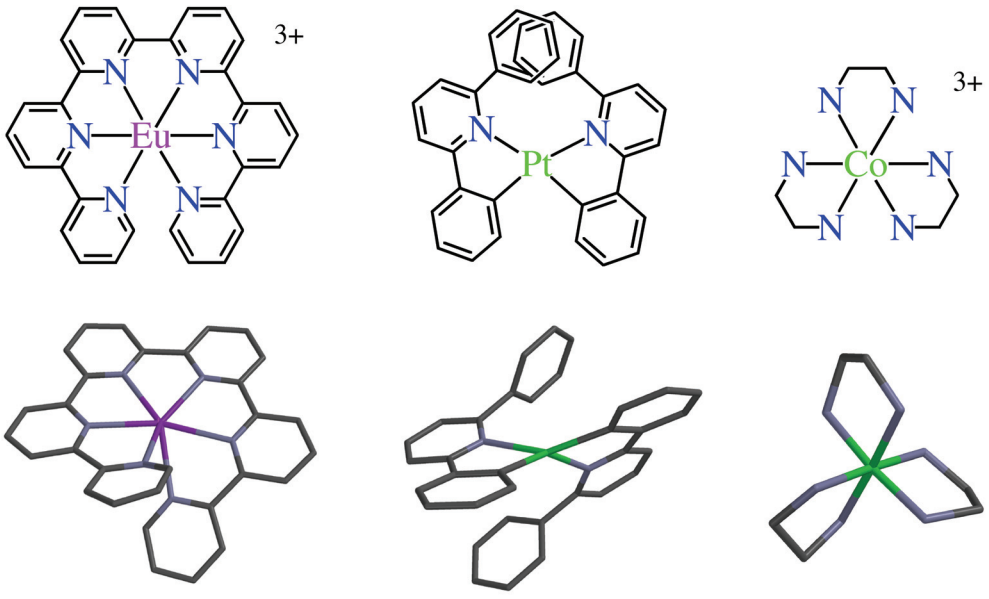

Figure 1.2 Examples of single, double, and triple-stranded monohelices

ligands coordinate to a single metal center.[4] Double and triple stranded monohelices resemble two and three-bladed propellers, respectively.

The majority of investigations to date have been concerned with helicates.[5] A helicate as defined by Lehn and co-workers in 1987, is a polymetallic helical double stranded complex.[6] This original definition has been expanded to include all helical complexes with two or more metal centers. There is a wide array of different helicates, but some of the most common forms are double and triple stranded dihelicates produced when ligands with two chelating sections coordinate to two metal centers (Figure 1.3).

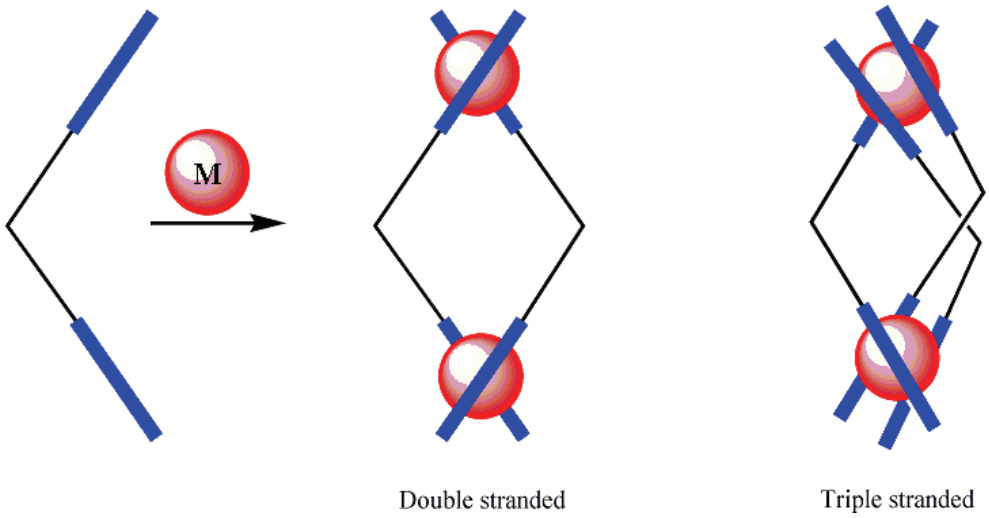

Figure 1.3 Double and triple stranded helicates

1.3 Types of Single-Stranded Monohelices

A primary goal of the research presented in this thesis is the production of single-stranded monohelical complexes. In order for these complexes to be useful as catalysts, they should have

labile coordination sites. One way of achieving this, is to coordinate a tetradentate ligand to an octahedral metal center, therefore there remain two reactive positions. For this approach three different morphologies that can be created; *trans*, *α-cis*, *β-cis* (Figure 1.4). The different arrangements are likely to lead to complexes that exhibit very different selectivities and catalytic activity. For four coordinate metal centers there is no distinction between these, since the tetradentate ligand coordinates to all available coordination sites.

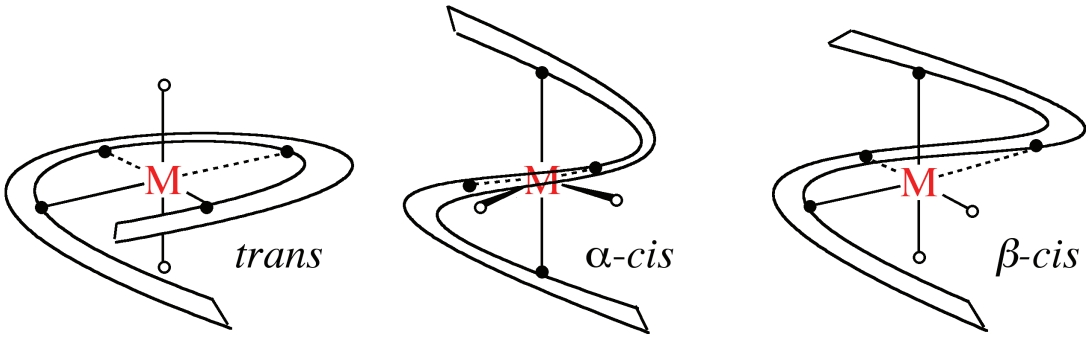

Figure 1.4 Morphologies for single-stranded monohelices of octahedral metal ions

Single-stranded monohelices are highly attractive as asymmetric catalysts due to their well defined reaction centers and their highly twisted conformations (high asymmetry). In order to be useful as catalysts a complex should exist in a single helical type (*M* or *P*). Predetermination of helical chirality around a metal center can be achieved if ligands themselves are chiral. The chiral centers may be present in the central section of the ligand (the backbone) or at the ends of the ligand (the sidearms). Both approaches can be successful, and some examples of these will be presented in subsequent sections. First some of the important factors that determine helix formation for tetradentate ligands will be considered.

1.4 Design Considerations: Ligand Donor Arrangement and Flexibility

The nature of the type of helicate produced is not only dependent on the design of the ligand (nature of binding sites, spacer groups, flexibility) but also the metal (coordination preference, geometry, charge, size). The most important factor in the design of the ligand is the way it is partitioned into its distinct metal binding sites or domains. Multidentate ligands often contain several bidentate or terdentate domains that are separated by rigid or bulky groups. For the production of helicates, these domains and spacer groups are then arranged so that each site will bind to different metal ions rather than chelating to a single metal center. A rigid or bulky spacer is not required for helicate formation. For example, Van Koten[7], has shown that the use of ligands with flexible spacer groups can result in the formation of dinuclear helicate complexes (Figure 1.5).

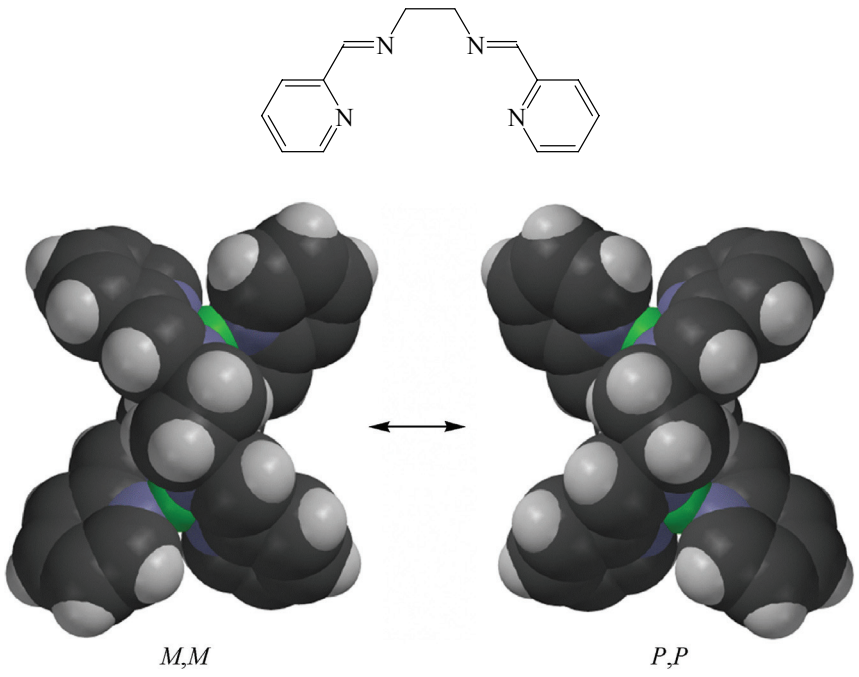

Figure 1.5 Van Koten's ligand (top) and space filing models of dinuclear silver complexes

In order for multidentate ligands to form monohelices the donor pockets should be directed so that they prefer to be adjacent to one another, instead of separated so that there is no opportunity for them to complex to a single metal. The use of ligand backbones that enforce this type of arrangement has been a successful strategy for producing monohelices. This implies a certain degree of rigidity for the backbone, however, it is also important that there is sufficient flexibility for the ligand to be able to wrap around one metal ion and to accommodate different sidearms and various sizes of metal ions. So the best ligands for single-stranded monohelix formation are those that direct the donor groups toward a single metal ion, allow sufficient flexibility for binding and avoid unfavorable steric interactions.

1.5 Design Considerations: Metal Ions

The nature of the helical complex produced with a given ligand depends on the metal as well as the ligand itself. The size, charge and geometry preferences of the metal will all factor into determining how a given ligand will bind to it. There are many examples where a change in metal ions has produced a change in the type of helix produced. For example, a poly-bidentate ligand will likely form a dihelicate with metal cations preferring tetrahedral geometry (e.g. Cu^{+}), but a triple helicate with metals that prefer octahedral geometry (e.g. Fe^{2+}). If a poly-tridentate ligand is coordinated to an octahedral metal, then it is likely a double-stranded helicate will be formed. On the other hand, Pallavicini[8] reported that his bidentate ligands formed double helices with Ag^{+} and Cu^{+}, but did not form triple helices with Fe^{2+}due to steric crowding.

In general, metals that prefer a square planar (e.g. Cu(II)) or octahedral geometry (e.g. Fe(II)) are more likely to form monohelices. Some ligands, such as the tetradentate H_2Fs ligands of Bermejo[9] (Figure 1.6), will form monohelices regardless of preferred metal coordination geometry.

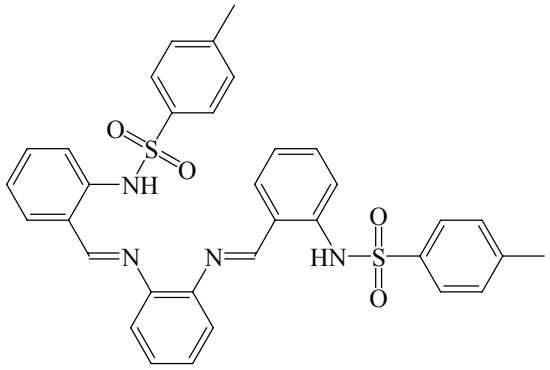

Figure 1.6 Bermejo's H_2FTs ligand

The results outlined above suggest that a match between the geometry of the ligand donor groups and the metal coordination preference is an important consideration in designing helical complexes. The possible steric interactions of the ligand(s) will also vary considerably with different coordination geometries, and strong interactions must be avoided if the desired helical form is to be produced. Ward[10] and Fabrizzi[11] have reported that the charge of the metal can also have a profound effect on the nuclearity. Their respective tetradentate bis(pyridyl-pyrazolyl) and bis(imine-pyridine) ligands (Figure 1.7), form monohelical complexes with Cu^{2+}, but dihelicates complex with Cu^{+}. In general, it appears that metals with higher charges are better able to form monohelices, probably because the stronger metal ligand bonding is enough to overcome the steric and torsional restrictions associated with ligand wrapping and monohelix formation.

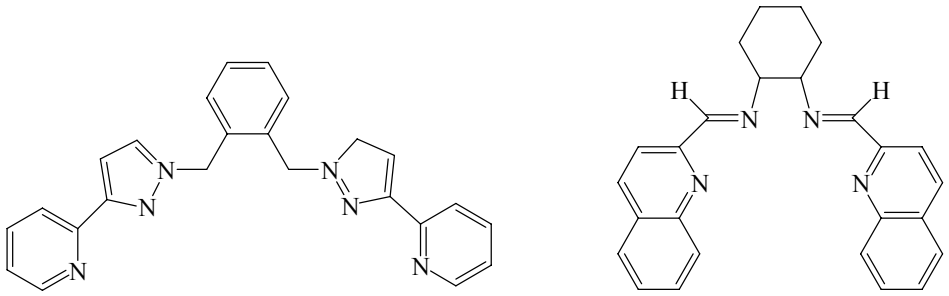

Ward Fabrizzi

Figure 1.7 Bis(pyridyl-pyrazolyl) (left) and bis(imine-pyridine) ligands (right)

1.6 Single-Stranded Monohelices from Non-Racemic Chiral Ligands

Monohelical complexes can be produced from achiral ligands. Matsumoto,[12] Chung-Ying,[13] Mak,[14] Stoeckli-Evans[15] and Kovacs[16] have also reported the formation of monohelical complexes from achiral ligands. In these cases there is generally no control of the helical form produced, and a racemic mixture of *M* and *P* helices results. Of much greater catalytic interest are systems where a chiral ligand leads to the formation of only one helical type. There are a number of examples of this approach in the literature, and those that are most relevant will now be described.

Pfaltz[17] recently reported the synthesis of a new type of chiral tetradentate bis(oxalamide) ligand. The ligand is capable of forming monohelical complexes with Cu(II) and Ni(II) (Figure 1.8). The three dimensional structures of these complexes were similar; each has a distorted square planar coordination geometry. The metal ion is coordinated to two oxazoline nitrogen donors and two anionic nitrogen donors from the oxalamide bridge. Zhou[18] has studied bis(oxazolinyl) type tetradenate ligands, with chiral elements incorporated in terminal oxazoline

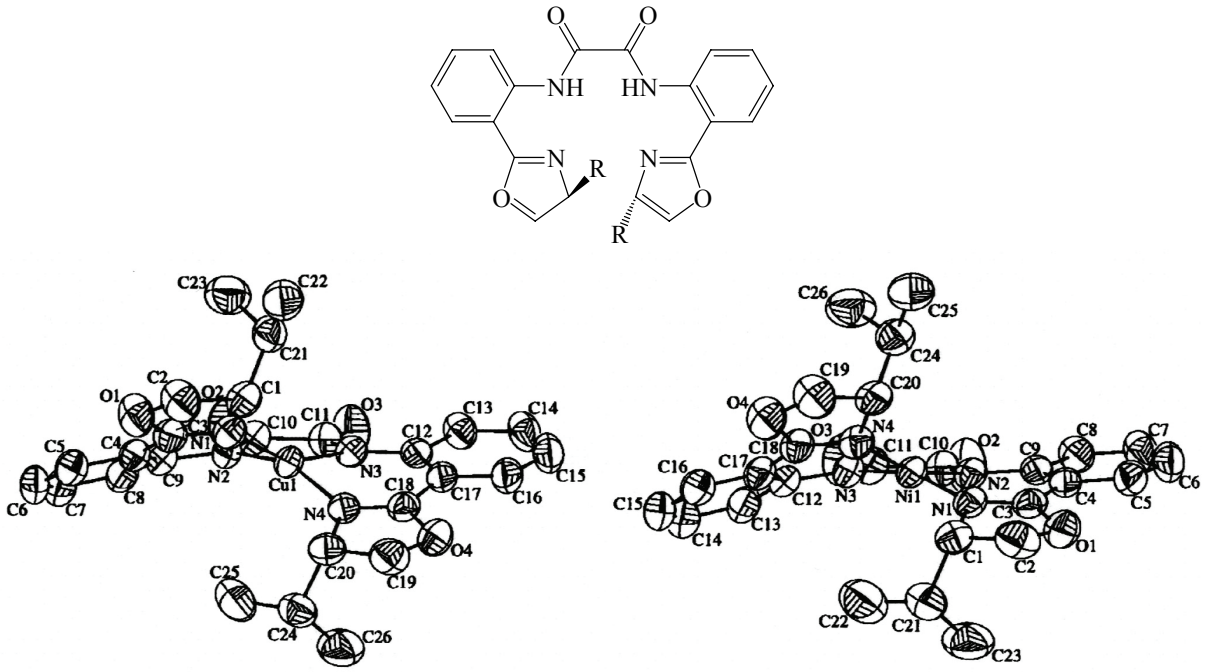

Figure 1.8 Pfaltz's bis-amide ligand (top) and crystal structures of Cu(II) and Ni(II) complexes (bottom)

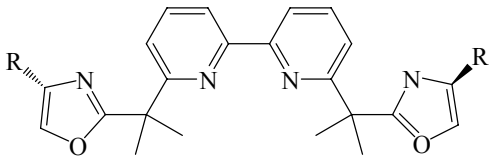

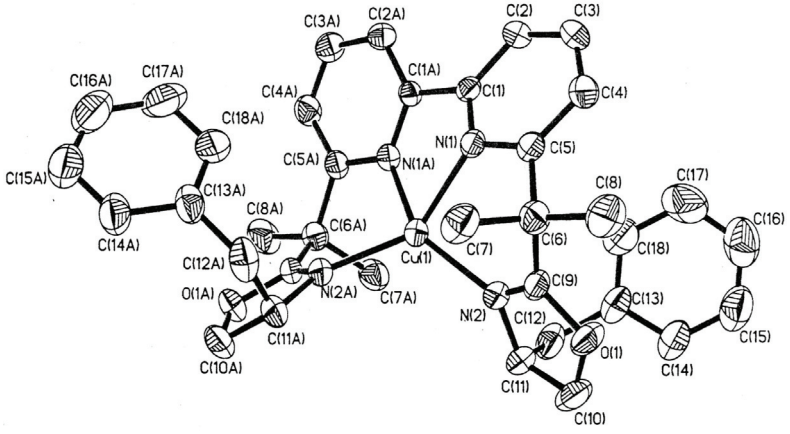

Figure 1.9 Zhou's bis(oxazolinyl) ligand (top) and structure of Cu(I) complex

fragments. The *S*,*S*-enantiomer of the ligand (Figure 1.9, R = Bn) is metallated with Cu(I) to form a complex of *P* handedness. The metal complex is coordinated to four nitrogen atoms and is C_2 symmetric.

Kinoshita[19] and coworkers were able to synthesize and study the monohelical copper complex shown in Figure 1.10. On addition of base, it was found that there was a rapid conversion to a dinuclear helicate. Furthermore the process was reversible via HBr addition/removal. They were able to monitor the conversion via circular dichroism.

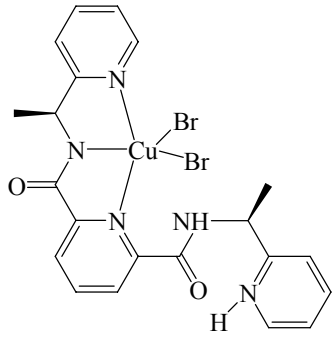

Figure 1.10 Kinoshita's mononuclear copper complex

More recently Reiser[20] has utilized a pentadentate bis(oxazoline) ligand to form monohelices with iron and cadmium. In each case the *R*,*R*-enantiomer is employed to yield helices of only *P* handedness. Even though the oxazoline units are slightly tilted to induce helicity, the driving force for the formation of the helical hepta-coordinate complexes was attributed to the π-π stacking of the two phenyl moieties. The bis(oxazoline) ligand forms monohelical complexes with Fe(II) and Cd(II) (Figure 1.11).

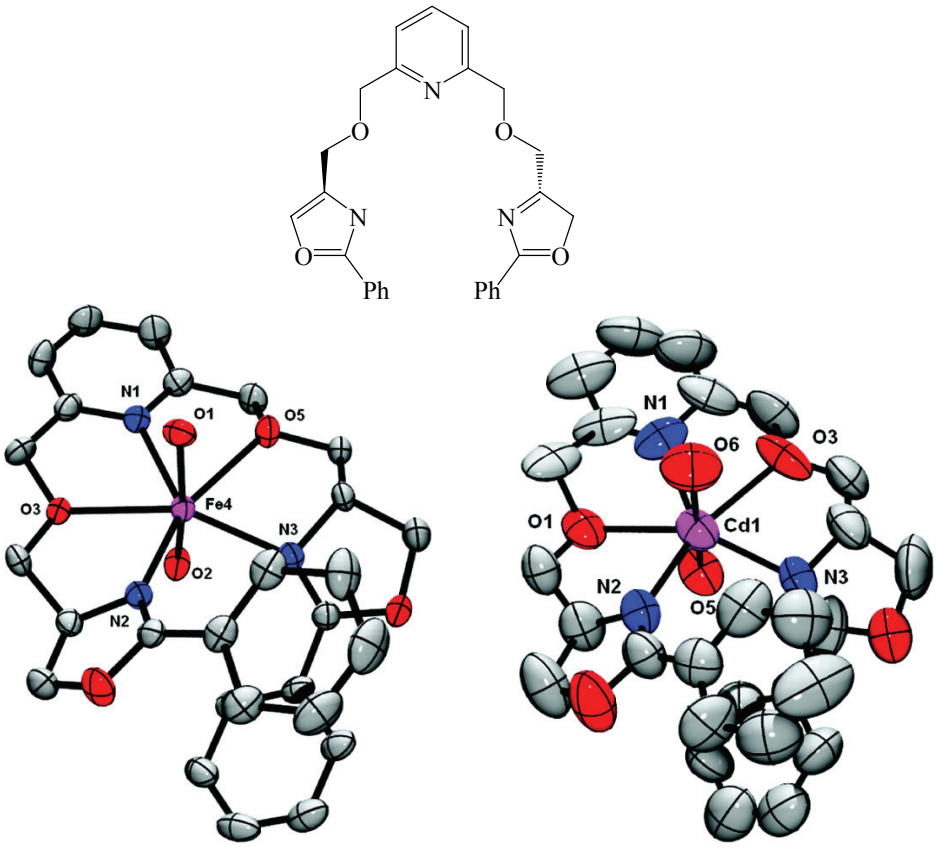

Figure 1.11 Reiser's bis(oxazoline) ligand (top) and structures of iron and cadmium complexes

The ligands described thus far, are examples where chirality has been incorporated in the terminal groups of the ligand (sidearm). In the complexes to be studied in this work, chiral elements are incorporated in the central section of the ligand (backbone). Below is an example where chiral backbones are utilized in salen type ligands. A series of monohelical salen Fe(II) and Zn(II) complexes have been synthesized previously in the Levy group.[21] Ligands bearing phenanthryl and benz[a]anthryl siderams attached to a binaphthyl or cyclohexyl backbone bridging groups were utilized (Figure 1.12). Upon deprotonation and subsequent metallation,

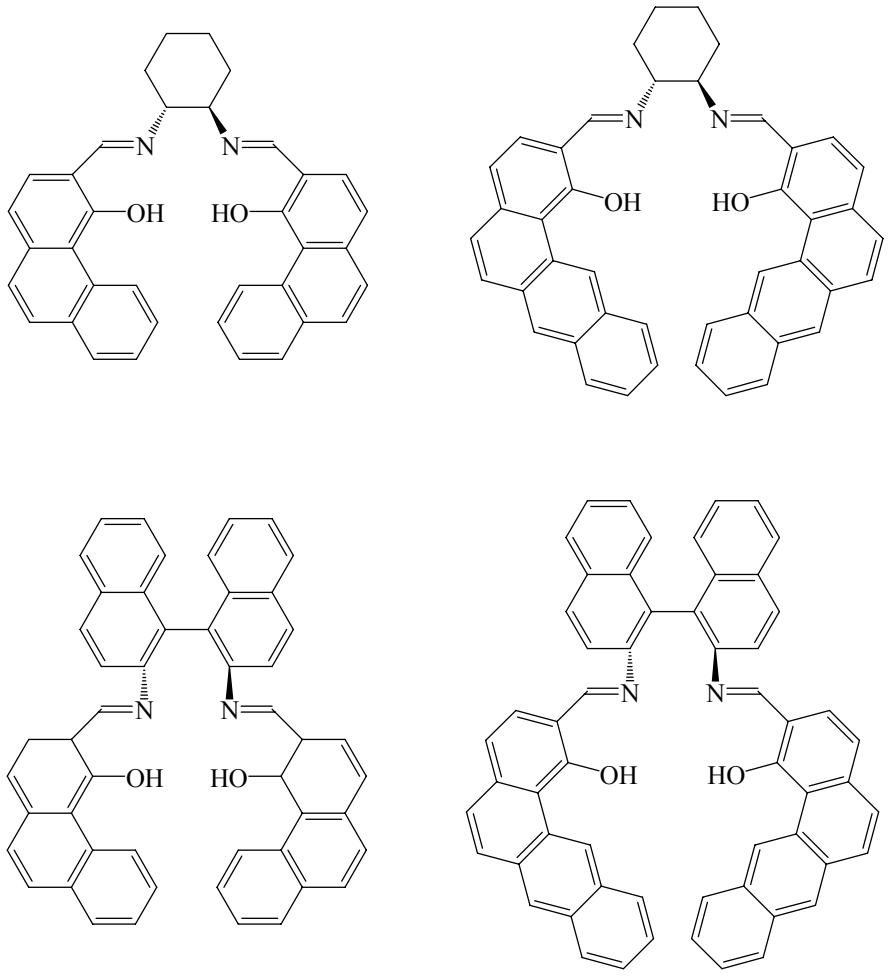

Figure 1.12 Salen ligands bearing phenanthryl and benz[a]anthryl siderams

mononuclear single stranded helical complexes were formed through coordination of two phenoxide and two imine donors. The binaphthyl complexes afforded exclusively *M*-helimers, while those incorporating the cyclohexyl bridge gave a 1:1 mixture of *P* + *M* helimers. A significantly greater degree of sidearm overlap was apparent when the benz[a]anthryl sidearm was employed compared with its phenanthryl counterpart. The example is shown in Figure 1.13 is of a zinc complex synthesized from a ligand derived from the benz[a]anthryl sidearm and binaphthyl backbone.

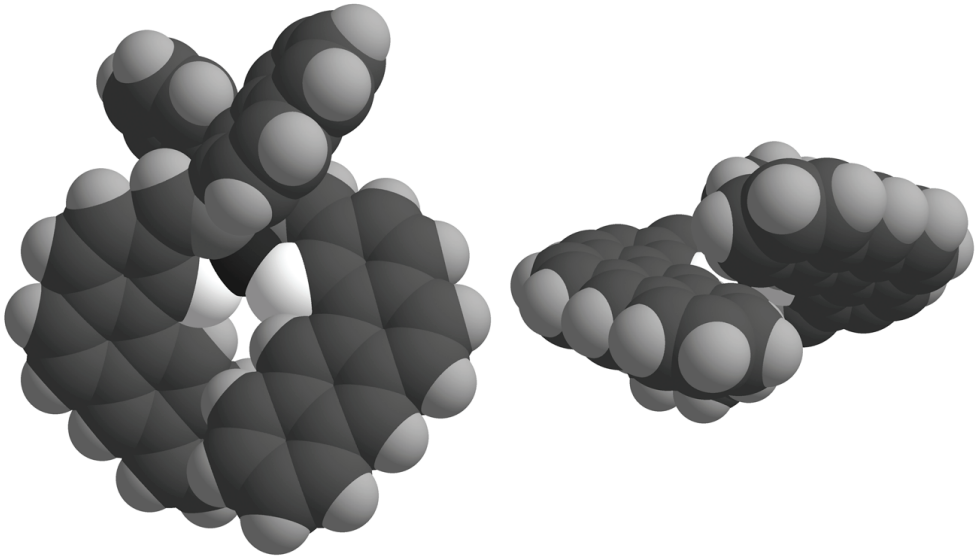

Figure 1.13 Space filling model of a Zinc complex with overlapping benz[a]anthryl sidearms

1.7 Design of New Chiral Ligands for Monohelices: Donor groups

In the previous sections the factors that are important for monohelix formation have been discussed and a survey of some important examples was presented. Now, this information must be used in order to design new ligands for producing single-stranded monohelical complexes. One of the most important components of a ligand system is the nature of the donor groups, since they influence the structure, electronic properties and reactivity of the resultant complexes. Schiff base and bis-amide ligands (Figure 1.14) are of particular interest because their respective metal complexes resemble metalloporphyrins, which are excellent catalysts for many transformations. The ligands typically have a wide application and are open to diverse structural modifications.

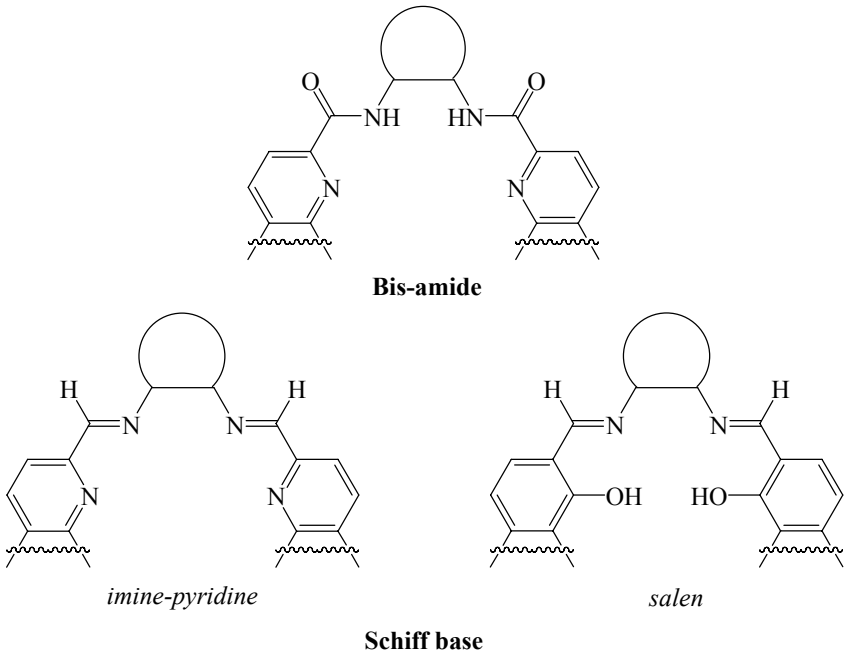

Figure 1.14 General structures of Schiff base and bis-amide ligands

Metal complexes derived from Schiff base ligands (imine-pyridine and salen) have been known since 1840 when Ettling[22] isolated bis(salicylideneamido) copper(II). Since then, they have been vital in the development of coordination chemistry and their transition metal complexes are able to stabilize various oxidation states. They are ubiquitous in the areas of catalysis, biological modeling, materials chemistry and design of molecular ferromagnets.[23] The most famous recent examples are perhaps the manganese salens of Jacobsen[24] (Figure 1.15). They have been shown to be efficient for alkene epoxidations. Salen ligands are dianionic, containing two imine donors and two phenoxide donors. Salen complexes are much more common in the literature then their neutral Schiff base counterparts in which the phenoxide donors are replaced with neutral fragments. However, the use of neutral pyridine-type donors can be advantageous. The donor is now incorporated into aromatic sidearm and this effectively pulls the ligand framework closer to the metal. This allows for smaller sidearms to be used,

while still maintaining terminal overlap for helix formation (*M* or *P*). Moreover, with ligand arms held closer to the metal, there is a greater twist to the complex and therefore the potential of a higher effective chirality at the coordination site. One disadvantage of using a neutral ligand is that the metal ion is less-tightly bounds, and this can favor the formation of helicates,[25] just as reducing the charge on the metal has the same effect (*vide supra*).

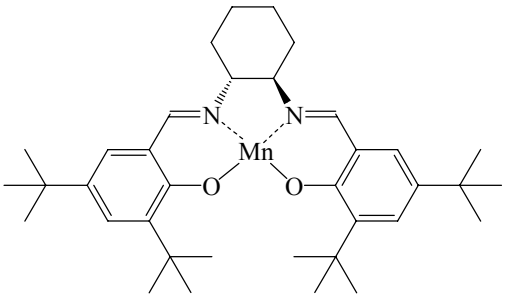

Figure 1.15 Jacobsen's salen catalyst

From a catalytic standpoint, neutral ligands with nitrogen donors have been shown to be effective for a number of important transformations (Figure 1.16). Jacobsen[26] and Stack[27] have reported epoxidations of unactivated olefins with hydrogen peroxide and peracetic acid respectively. Que[28] has reported the hydroxylation of C–H bonds to give alcohols; this reaction is of extreme importance for functionalizing normal unreactive hydrocarbons. In most cases only achiral catalysts systems have been examined. The production of catalysts that could carry out asymmetric transformations of these types is a long term goal of the ongoing research project described herein. For example, if asymmetric C–H hydroxylation could be achieved, then simple (and inexpensive) hydrocarbons such as butane could be oxidized to give a non-racemic alcohol which would be an important chiral precursor for applications such as pharmeceuticals, agrochemicals, and materials production.

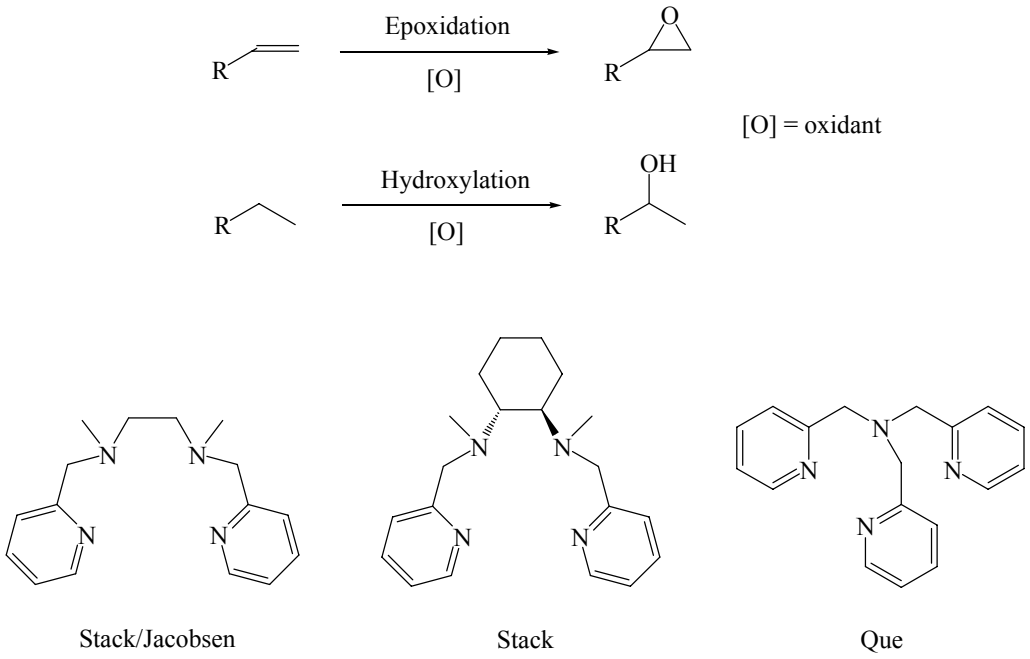

Figure 1.16 Ligands of Stack, Jacobsen and Que. A general scheme of epoxidation and hydroxylation is also shown (top)

As noted above, the main problem with neutral ligands is the relatively weak coordination of the metal ions due to significantly decreased ionic bonding. From this standpoint, it would be beneficial to have an anionic ligand. This can be accomplished, without disturbing the beneficial aspects of the terminal pyridine donors if the anionic donors are located in the ligand backbone. A deprotonated bis-amide ligand can have these characteristics. Amide donors are an excellent choice for oxidation catalysts, since they are known to stabilize high oxidation states of coordinated metal ions,[29] and amide ligands generally have high resistance to oxidation. The majority of investigations concerning metal complexes of bis-amide ligands has been with the use of achiral ligands[30] A selection of those reported by Che and the crystal structure of the Ru(bpb) complex is depicted in Figure 1.17. There is coordination from the four

nitrogen donors of the ligand and two pyridine molecules to form an octahedral complex. The ligand donors are co-planar and the two pyridine molecules occupy the axial positions.

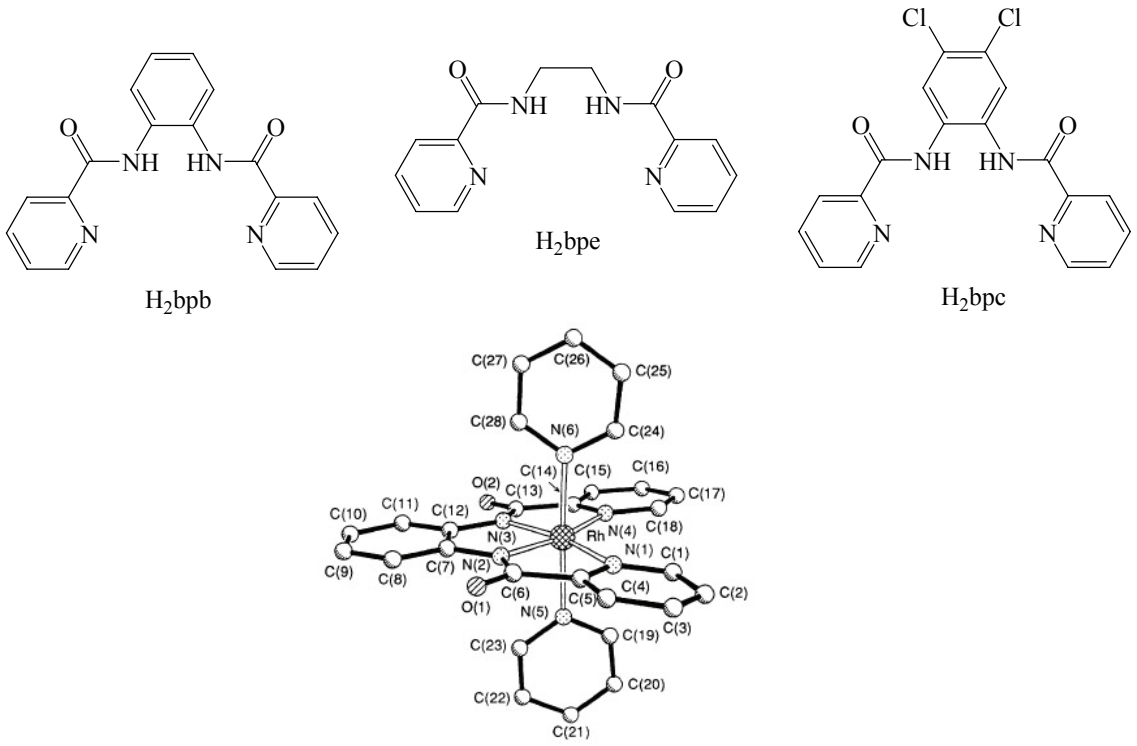

Figure 1.17 Bis-amide ligands of Che (top) and crystal structure of ruthenium complex (bottom) $[Rh(bpb)(py)_2]^+$ (two pyridine molecules are also coordinated in axial positions)

Chiral bis-amide ligands synthesized by Pfaltz (discussed earlier in section 1.3) were found to form monohelices upon complexation. Perhaps those that are more relevant and similar to the chiral ligands studied in this text have been reported by Trost[31] and coworkers. They have designed and synthesized a series of chiral bis-amide ligands for use in molybdenum catalyzed asymmetric alkylations, some of which are shown in Figure 1.18. However, the exact nature of the catalytic species in not known. It is postulated that complexes of these ligands often involve coordination through only one pyridine and one amide nitrogen. Moberg[32] has reported similar

results. It seems coordination through the four nitrogen donors is not always favored with bis-amide ligands, and there is also a tendency to form complexes through amide-oxygen coordination. The ambivalent coordinating ability of bis-amide ligands has been discussed by both Yamakasi[33] and Vagg[34]. In any case as described above, there is clear presidence for the use of bis-amide ligands in catalysis.

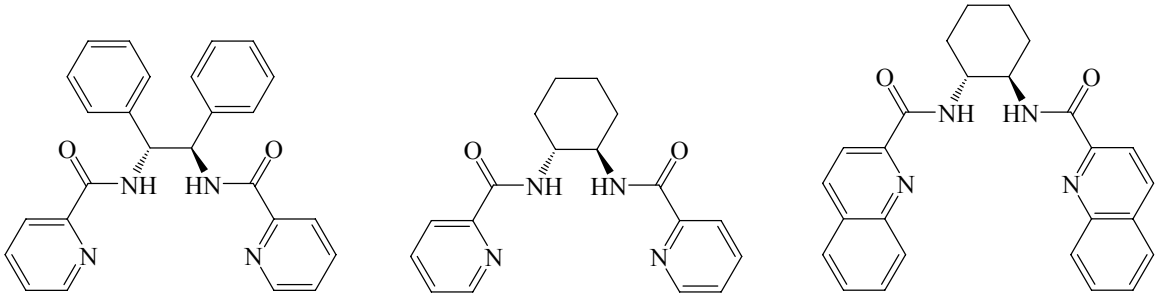

Figure 1.18 Chiral bis-amide ligands of Trost

1.8 Design of New Chiral Ligands for Monohelices: Chiral Backbones

Chirality must be incorporated into any new ligand systems in order to produce monohelical complexes of only one handedness. It has been shown that the chiral components can either be located at the ends of the ligand (sidearm) or in the central portion (backbone). One goal of the research detailed in this thesis is to create complexes with significantly overlapped arms. This goal is difficult to achieve when bulky groups are located at the ends of the ligands, since there will be significant steric interactions. To avoid this, planar aromatic sidearms can be used. These are able to stack on top of one another without significant steric interactions: in fact attractive π-π stacking becomes possible, providing an additional helix-

stabilizing interaction. In order to use this strategy the chiral elements are best located in the backbone of the ligand, allowing the ligand arms to remain roughly planar.

In order to produce Schiff base and bis-amide backbones, a chiral C_2-symmetric diamine can be employed: the ligands are prepared by condensation reactions with these backbones. A series of commercially and synthetically available backbones are indicated in Figure 1.19. There is a progression from left to right for several factors that will impact the properties of the resulting ligands and complexes. Two of these backbone precursors have been examined in this thesis: the cyclohexyl backbone, (1*R*, 2*R*)-diaminocyclohexane, and the binaphthyl backbone, (*R*)-1,1'-binaphthyl-2,2'-diamine. The cyclohexyl backbone is an excellent choice since the ring forces the donors to be near one another, thus encouraging monohelix formation. In fact, several of the examples of monohelices presented in previous sections utilized this backbone. It has alkyl substituents on the amine groups, making them relatively basic. This will result in stronger imine or amide donors in the ligands produced after condensation. The electron rich nature of the imine groups of Schiff bases with this backbone make them relatively inert to hydrolysis.

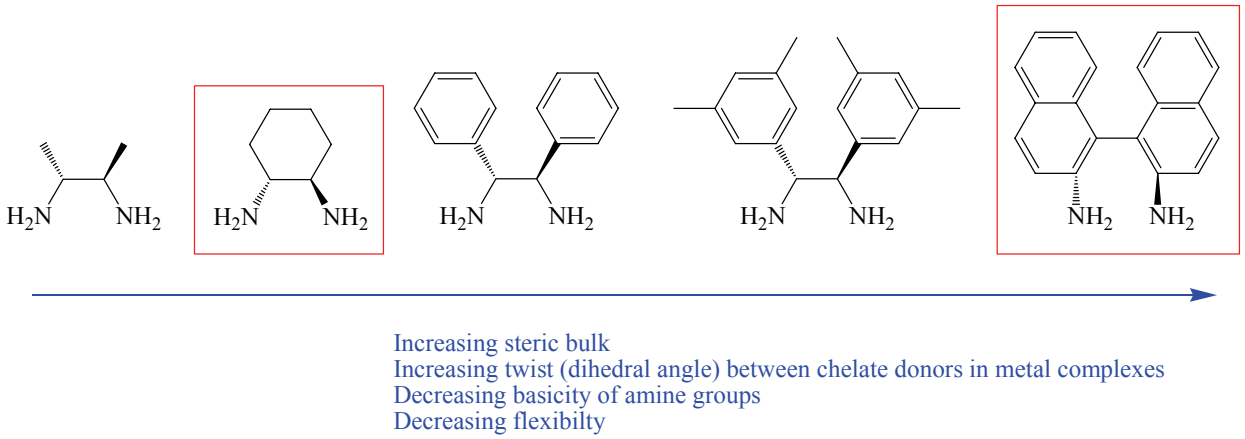

Figure 1.19. Chiral backbone units: those studied in this work are indicated

Binaphthyl backbones have received considerably less study that their cyclohexyl, ethylene, and benzyl counterparts.[35] An advantage of the binaphthyl backbone is that it is highly twisted and typically results in the formation of only one helical conformer. Compared to the backbones discussed thus far, the binaphthyl backbone has much less conformational mobility. Rotational isomerism is not possible at normal temperatures, and the steep energy well to rotation restricts the binaphthyl dihedral angle to ~60-130°.[36] Salen derived binaphthyl ligands have to date received more attention[37] than the analogous tetradentate nitrogen type (bis-imine and bis-amide). Hannon[38] and coworkers have shown that the binaphthyl derived ligands L^R and L^S react with Ag(I) to form dinuclear dihelicate complexes (Figure 1.20). The crystal structures clearly demonstrate how the chiral twisting of the binaphthalene can be used to control the helicity of the complex. The coordination of two L^R ligands around two silver ions results in the formation of a complex that exhibits *P* handedness. The coordination of two L^S ligands results in an *M* handed double helix. Each silver is four coordinate, pseudo tetrahedral and bound to two pyridyl-imine units. Similar results were obtained with Cu(I) complexes.

Leznoff[39] more recently has investigated reactions of the same ligand (L^R) with metal ions that prefer non-tetrahedral coordination geometries. Reaction of ligand L^R with Ni(II) resulted in a complex that is missing one of its pyridyl groups, this is due to hydrolysis of one imine bond. Two molecules of the resulting tridentate ligand coordinate to nickel to form a double stranded monohelix that has a distorted octahedral coordination geometry (Figure 1.21). In further studies, ligand L^R was metallated with $CuCl_2$ to form a dinuclear complex with bridging chlorides (Figure 1.22). The ligand cradles a planar, rhomboidal [$Cu_2(\mu^2\text{-}Cl_2)$ unit. Each copper also has a non-bridging chloride group attached and is coordinated to one pyridine and one amine nitrogen atom. The binaphthyl framework adopts an open framework to

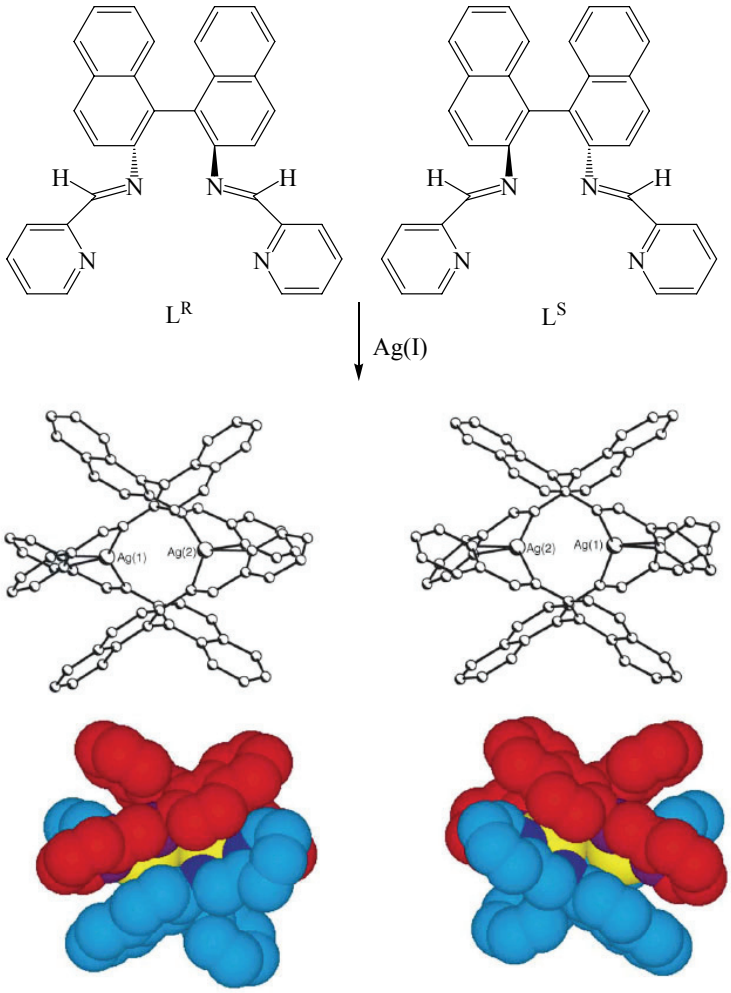

Figure 1.20 *P* (left) and *M* (right) double helixes formed by Hannon's L^R and L^S ligand

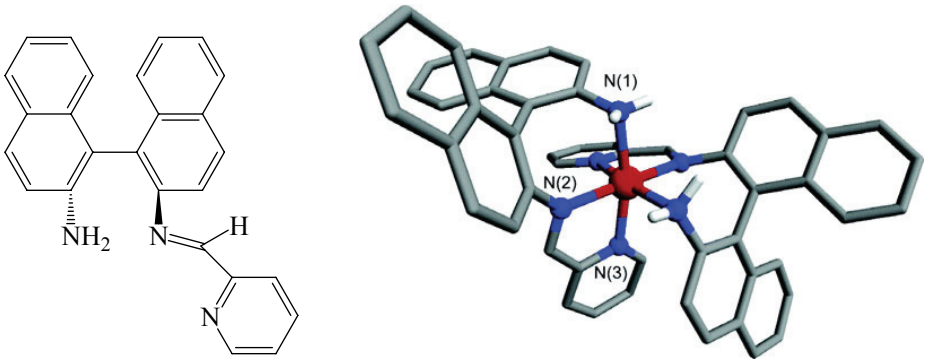

Figure 1.21 Leznoff's hydrolyzed ligand (left) and crystal structure of double stranded nickel complex (right)

accommodate the $CuCl_2$ fragment. The geometry of each of the copper centers was reported to be intermediate between square pyramidal and trigonal bypyramidal.

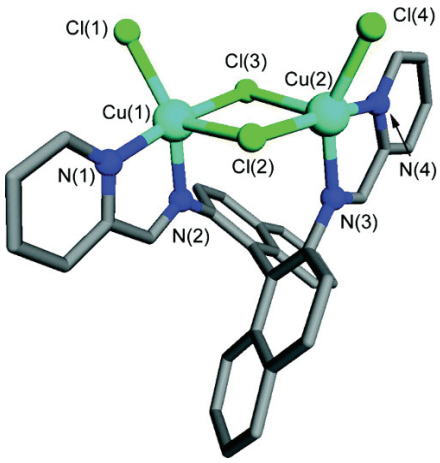

Figure 1.22 Dinuclear copper complex with bridging chloride anions

In studies with the analogous binaphthyl bis-amide ligand (Figure 1.23), Che,[40] has reported a mononuclear osmium oxo complex. The ligand in its free form features four nitrogen donors arranged in a tetrahedral fashion. However, upon complexation each nitrogen becomes more coplanar. The resulting complex exhibits a distorted octahedral coordination geometry, with two oxo ligands completing the coordination sphere.

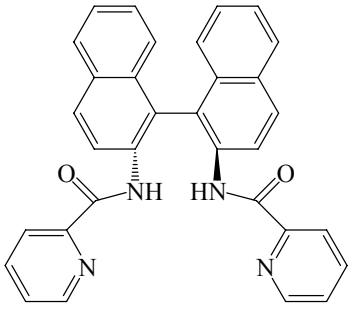

Figure 1.23 Binaphthyl bis-amide ligand of Che

1.9 The New Ligand Systems

This section will introduce the specific ligand systems that have been studied in this thesis, with reference to the factors that have been discussed so far in this introductory chapter. Following is a list of important design considerations:

1. A chiral non-racemic C_2-symmetric backbone should be used. This provides the twist to the ligand and therefore creates a preference for one helical form over another (*M* or *P*). Locating the chirality in the backbone section of the ligands allows the ligands arms to be roughly planar and avoid unfavorable steric interactions that would prevent the ligand wrapping around the metal.

2. The backbone should be neither too rigid nor too flexible. This avoids unwanted coordination modes, such as helicates, while still providing the ligand pliability that is necessary for wrapping.

3. The backbone must direct the ligand siderams so that they can be next to one another, and thus coordinate to the same metal. The cyclohexyl and binaphthyl backbones discussed in the previous section clearly fulfill this criterion, as well as the two previous ones in this list.

4. The ligand sidearms should be rigid and have relatively low steric bulk so that they do not interact strongly upon wrapping and overlap. The implementation of extended planar

polyaromatic ring systems is an obvious solution, and this approach has been used in this work. This criterion will be most important for *trans* coordination to an octahedral metal center. For *cis* coordination modes and coordination to tetrahedral metal centers some steric bulk at the ligand termini may not be detrimental, and may in fact help to enforce the desired coordination geometry by making other geometries sterically unfavorable. This avenue has been explored in this work by including isopropyl groups at the ligand termini in some cases.

5. The choice of metal is also critical as different considerations must be kept in mind. The use of a metal that will allow for facile complex characterization is desirable. In this regard Zn(II) is ideal, it likely will form diamagnetic complexes that can readily be characterized by ^{1}H NMR spectroscopy. Since Zn(II) is a d^{10} metal ion, it does not have a strong preference for one coordination geometry over another, and can readily adapt to the coordination preferences of the ligands. This makes it an excellent choice for structural studies of ligands.

6. In terms of potential for high catalytic activity, more reactive transition metals with incomplete *d*-shells will be of importance. However, such metals often produce compounds that are paramagnetic (hence difficult to characterize) and highly air and/or moisture sensitive (difficult to prepare and handle). A representive metal from this class, Fe(II) has been examined in this work. This is a metal that has potential for catalytic activity in transformations such as epoxidations and hydroxylations. A moderately-reactive d^{8} metal ion, Ni(II), has also been studied in this work. Unlike the other metals

examined, nickel generally prefers square-planar geometries. Other beneficial aspects of Ni(II) are its potential to form diamagnetic complexes, and its relatively low air and moisture sensitivity.

With these design considerations in mind, the chiral backbones (1*R*,2*R*)-cyclohexanediamine (DAC) and (*R*)-[1,1'-binapthalene]-2,2'-diamine (DAB) were chosen. Three different sidearms were used; 2-formylbenzoquinoline (BZQ), 8-Isopropyl-2-quinolinecarboxaldehyde (IPQ) and quinaldic acid (QNL) (Figure 1.24). The different combinations of backbones and sidearms give rise to six different ligands (Figure 1.25): (*R*,*R*)-**5**, (*R*)-**6**, (*R*,*R*)-**26** and (*R*)-**27** were synthesized in this work. (*R*,*R*)-**10**, (*R*)-**22** were synthesized in previous studies. The ligands were subsequently metallated with Zn(II), Ni(II) and Fe(II). The ligands and complexes were characterized with various NMR experiments, X-ray analysis and elemental analysis, UV and ECD spectroscopy.

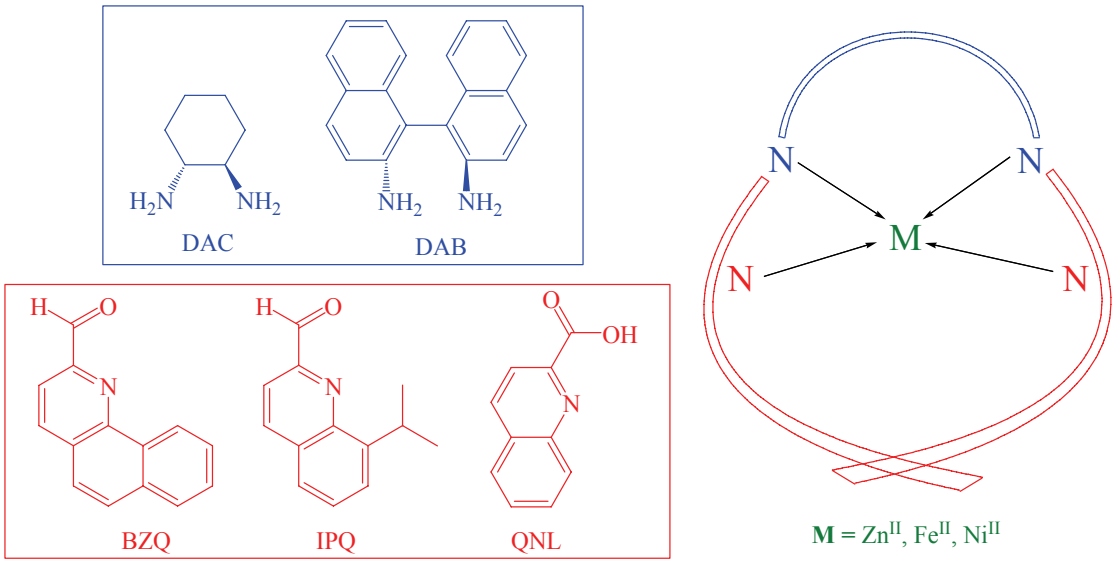

Figure 1.24 Chiral backbones and rigid sidearms

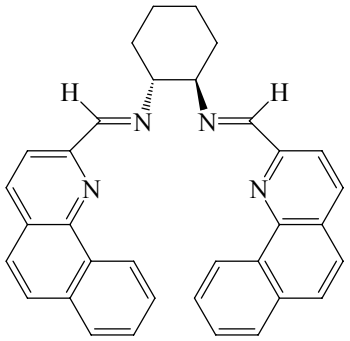

(*R*,*R*)-**5**

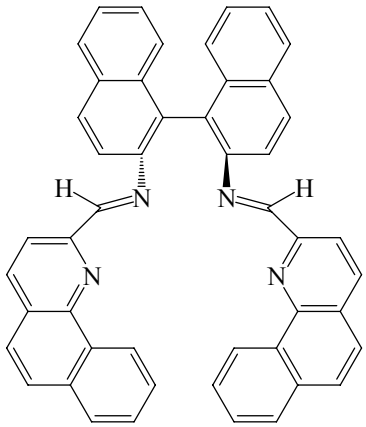

(*R*)-**6**

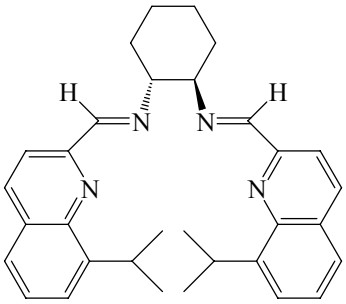

(*R*,*R*)-**10**

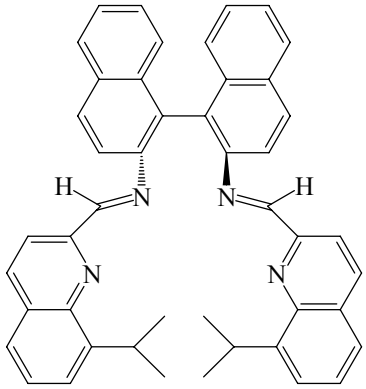

(*R*)-**22**

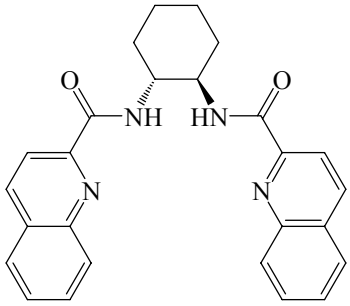

(*R*,*R*)-**26**

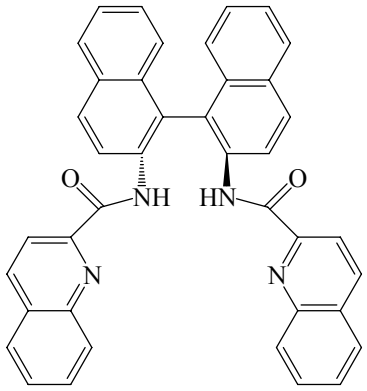

(*R*)-**27**

Figure 1.25 Structural formulae of new ligands

1.10 Research Objectives

1. To synthesisze single-stranded mononuclear helical transition metal complexes with chiral bis(imine-pyridine) and bis-amide ligands (Figure 1.26).

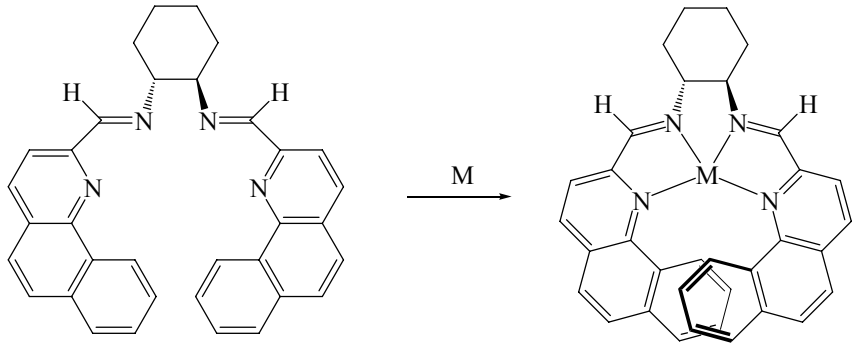

Figure 1.26 Formation of a monohelix upon metallation of chiral ligand

2. To produce helical complexes of one 'hand'. Upon complexation the overlapping sidearms will produce a conformation that is 'locked' in either the *M* or the *P* form, hence there will be no inter-conversion between the two forms.

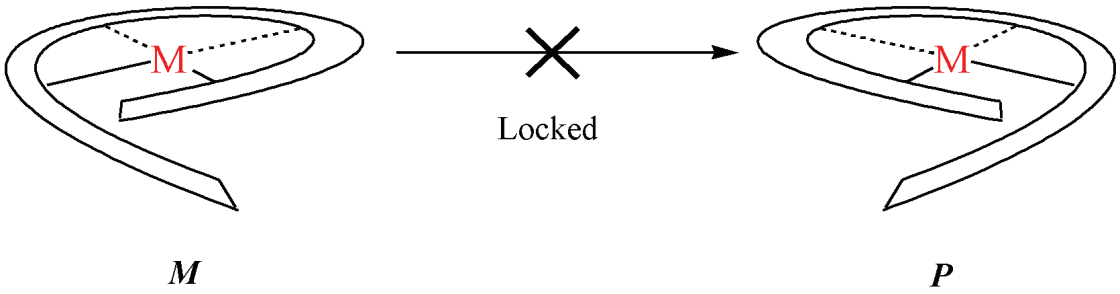

Figure 1.27 Locked *M* and *P* helices

3. Use the new systems to understand the nature of helix formation. Looking at the effect of the chiral backbone, donor groups, and metal centers. Can we control helix/helicate formation?

4. Examine the scope of coordination chemistry of new ligand designs. As will be seen, the ligands developed in this work can form monohelices, but also have a number of other interesting coordination modes.

5. Examine some of the reaction chemistry of the new ligands and helical complexes.

Chapter 2

Synthesis and characterization of new ligands

2.1 Introduction

In general, the synthesis of bis(imine-pyridine) ligands involves a Schiff base condensation reaction between a diamine and two equivalents of the appropriate aldehyde (Figure 2.1). This can often be achieved by simply refluxing the two in ethanol. Of course, the

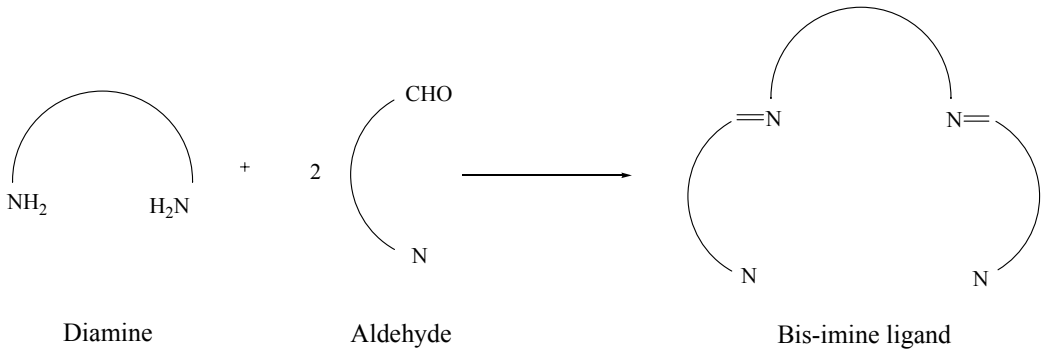

Figure 2.1 General scheme of Schiff base condensation

aldehydes and diamines must first be prepared (Figure 2.2). The chiral diamines (1*R*,2*R*)-cyclohexanediamine (*R*,*R*)-**1** and (*R*)-[1,1'-binapthalene]-2,2'-diamine (*R*)-**2** are available commercially, however due to ease of preparation and relatively inexpensive starting materials they were synthesized following well documented literature procedures.[41]

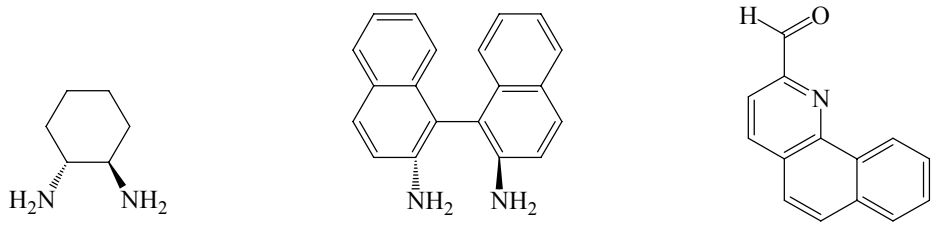

(*R*,*R*)-**1** (*R*)-**2** **3**

Figure 2.2 Diamines and aldehyde precursors

2.2 Synthesis

The aldehyde required for the condensation reaction is 2-formylbenzoquinoline (**3**), this is not available commercially, nor is there a documented literature procedure for the synthesis. It was synthesized in two steps, the first being a modification of Skraup's procedure.[42] Reaction of 1-aminonapthylene and crotanaldehyde in sulfo mix yielded the 2-methylbenzoquinoline (**4**) precursor in 25% yield (Figure 2.3). The second step involves oxidation of the methyl group

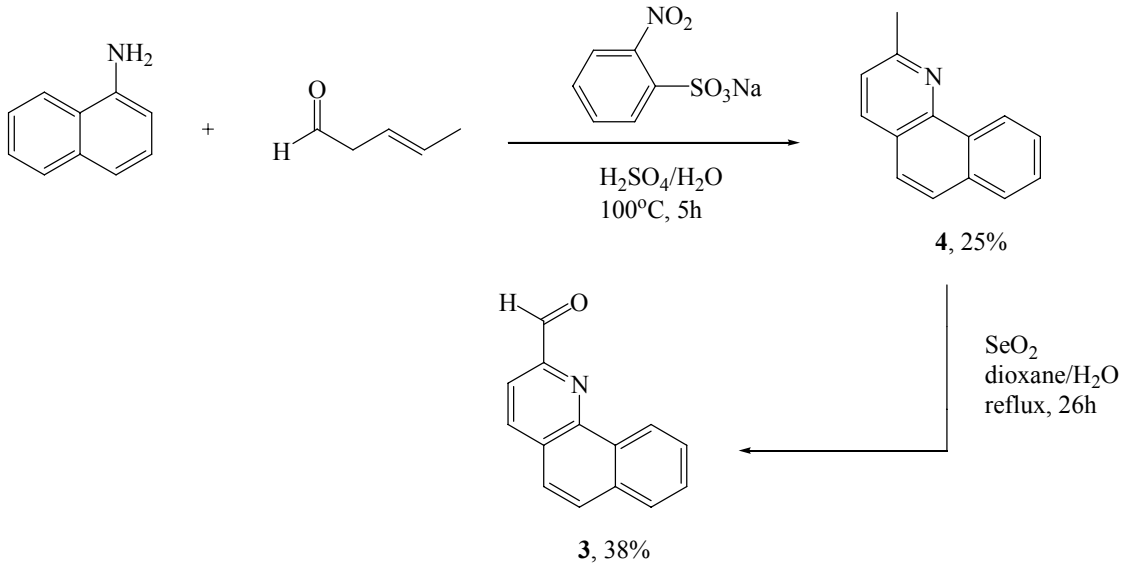

Figure 2.3 Synthesis of 2-formylbenzoquinoline

to an aldehyde using selenium dioxide[43]. Purification of the aldehyde is achieved through a series of silica gel filtrations, both selenium byproducts and excess starting materials were removed this way. The final yield of the aldehyde after purification was fairly low (38%) but, ^{1}H NMR and elemental analysis data indicated a compound of high purity.

Synthesis of ligands (*R*,*R*)-**5** and (*R*)-**6** involves a simple Schiff base condensation reaction of **3** with the appropriate diamine backbone, (*R*,*R*)-**1** or (*R*)-**2** respectively (Figure 2.4). The yields and purity are generally high and because both reactants are completely soluble in ethanol while the products are not, ligands are of high purity without further purification. The

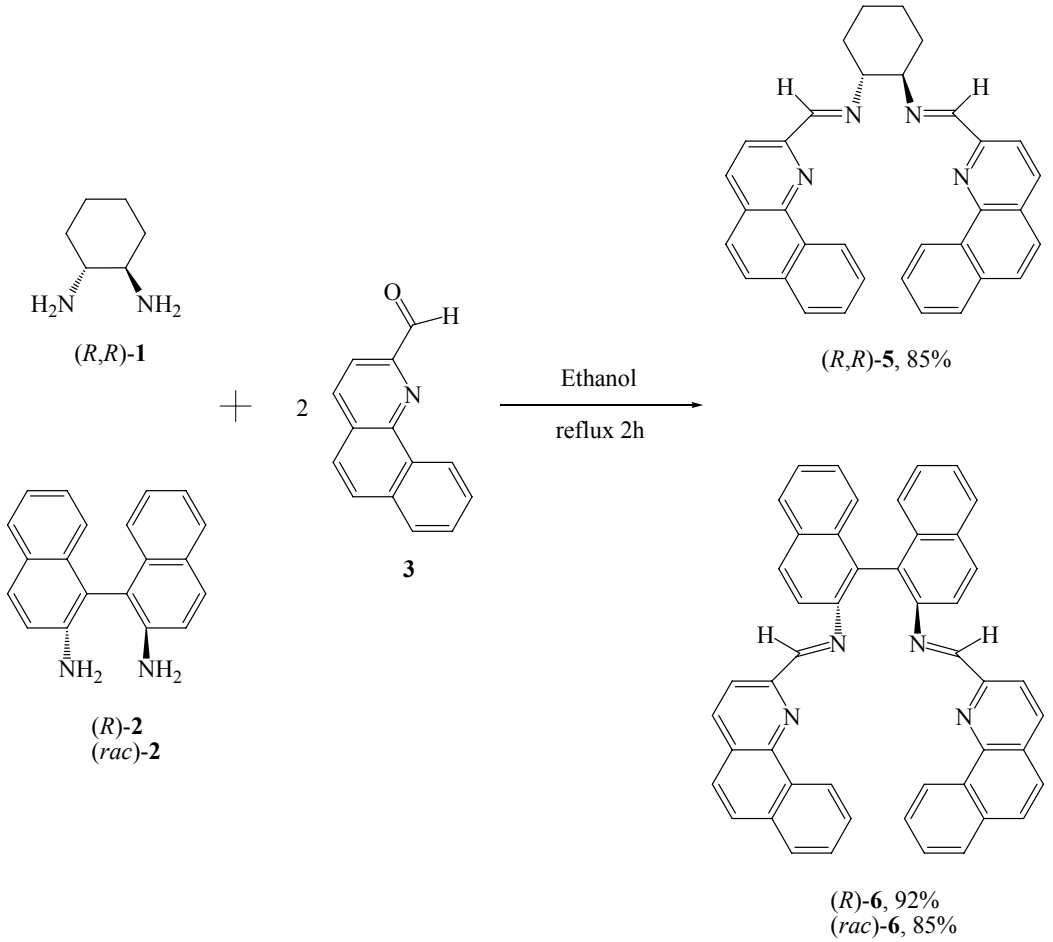

Figure 2.4 Synthesis of new ligands

same methodology was used to prepare the racemic ligand (*rac*)-**6**, utilizing (*rac*)-[1,1'-binapthalene]-2,2'-diamine as starting material. Synthesis of ligands was carried out without using inert conditions, however subsequent analysis ($^{1}H/^{13}C$ NMR) required the use of dry solvent as there is facile decomposition via hydrolysis of the imine bonds. As solids, the ligands are stable to decomposition from atmospheric moisture.

2.3 NMR spectroscopy of 2-formylbenzoquinoline and ligands

2-Formylbenzoquinoline and the ligands were analyzed by NMR spectroscopy. The ^{1}H NMR spectrum for 2-formylbenzoquinoline, with assignments is shown in Figure 2.5. The spectra provided sufficient resolution that each peak was visible clearly along with its respective splitting, albeit two doublet resonances (7.95 and 7.96 ppm) remain overlapped and deceptively appear as a triplet. The aldehyde peak is unique in that its resonance appears characteristically at 10.36 ppm, and therefore this can be assigned easily. The absolute assignment of each proton in **3** was achieved through the use of Correlation Spectroscopy (COSY) and Nuclear Overhauser Effect Spectroscopy (NOESY) experiments (Figure 2.6).

The peak at 9.43 ppm is due to the bay region hydrogen at the 5 position. It appears at a low field respective of the remaining aromatic protons due edge position aromatic deshielding and repulsive Van der Waals interactions.[44] It is well known that the substituent at the 4 position also greatly affects the chemical shift of this bay region hydrogen.[45] It is likely the lone pair of electrons on the pyridyl nitrogen is exerting an anisotropic deshielding effect, causing the proton

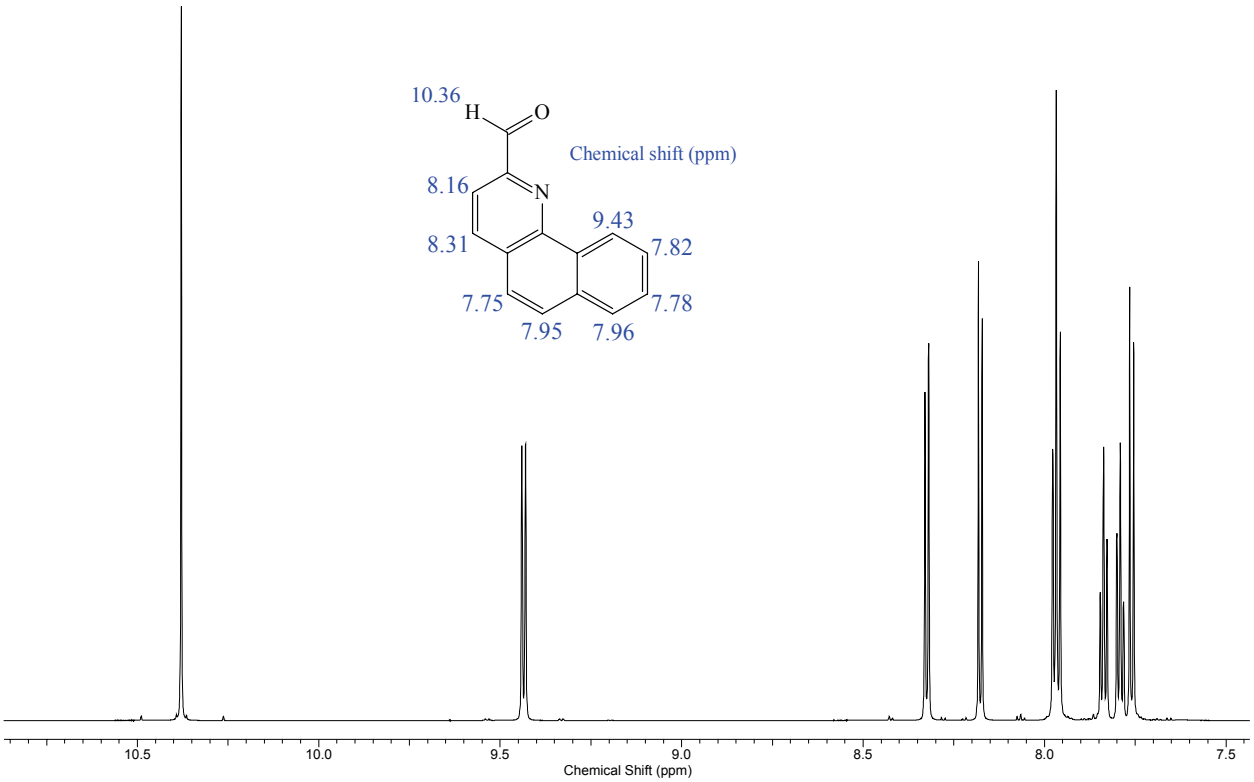

Figure 2.5 800 MHz ^{1}H NMR spectra of **3** ($CDCl_3$) with assignment of peaks

to shift upfield. There are only two triplets in the molecule, and these are adjacent to each other (7.82 and 7.78 ppm). These factors provided a convenient starting point for assigning the remaining proton resonances in the molecule using a combination of COSY and NOESY (Figure 2.6). For example, there is COSY correlation between the triplet peak at 7.78 ppm and the doublet at 7.96 ppm. A NOESY correlation is seen between the doublet peak at 7.96 ppm, and the one at 7.95 ppm. In this way, we are able to make our way around the molecule, assigning the chemical shift of each hydrogen in turn. A correlation between the aldehyde proton (10.36 ppm) and the proton residing at 8.16 ppm was not observed in the NOESY spectrum of **3**. This is likely due to free rotation of the aldehyde in solution.

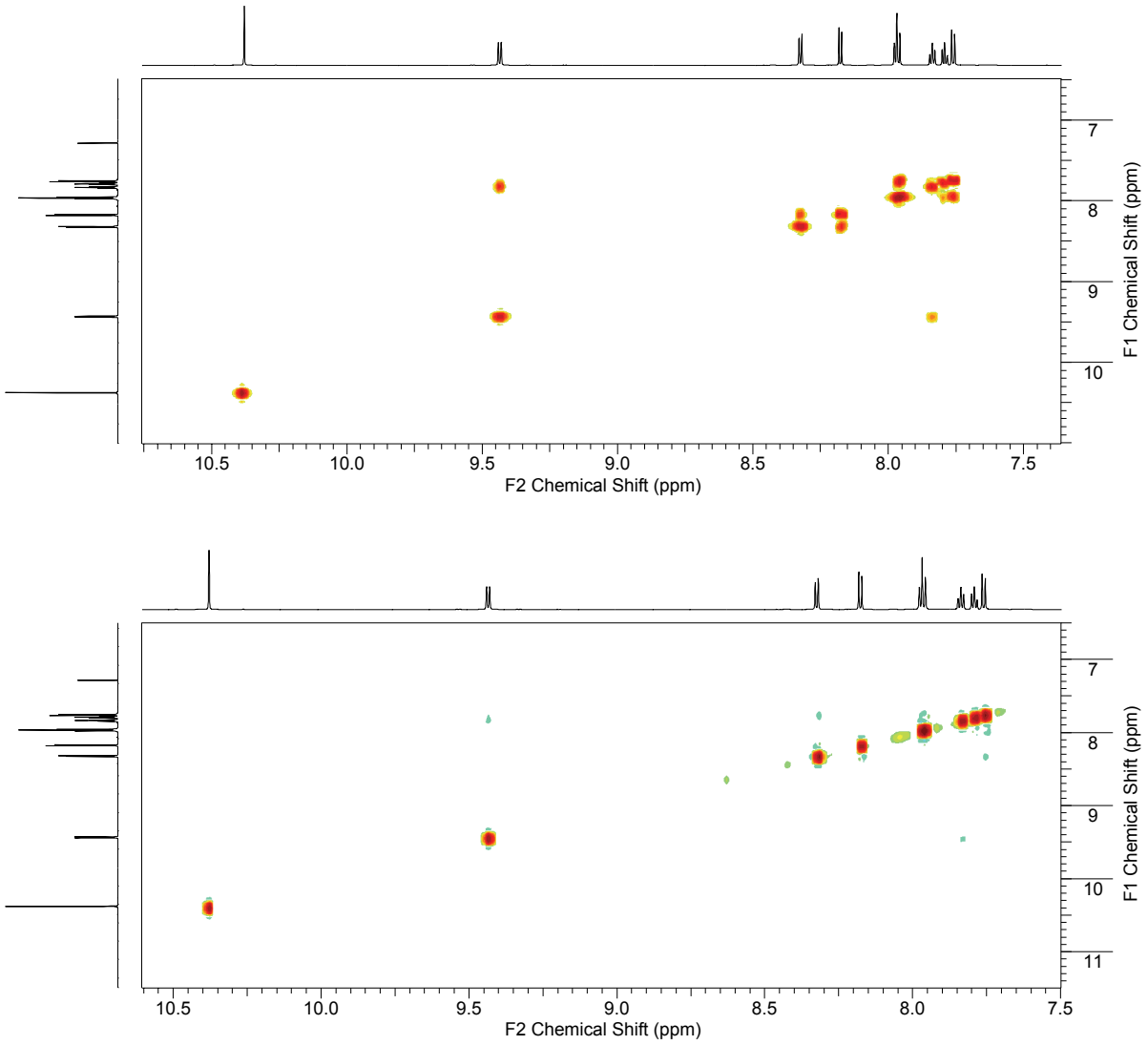

Figure 2.6 800 MHz COSY (top) and NOESY (bottom) NMR spectra for **3** ($CDCl_3$)

A similar 1D and 2D NMR analysis was undertaken of the ligand, (*R*,*R*)-**5.** The ^{1}H NMR spectrum of (*R*,*R*)-**5** with specific assignments is shown in Figure 2.7. Complete assignment of the cyclohexyl backbone was not attempted due to the appearance of broad multiplet peaks in the aliphatic region. This is likely due to fluctuation of the ring and second order effects, not to the presence of multiple conformers. The total number of resonances is half of that possible since the molecule is C_2 symmetric. The imine proton is unique in that it appears as a singlet peak at

8.69 ppm. The doublet peak at 9.26 is also easily assigned as there is a characteristic upfield shift due to a ring current effect in the bay region of the molecule.

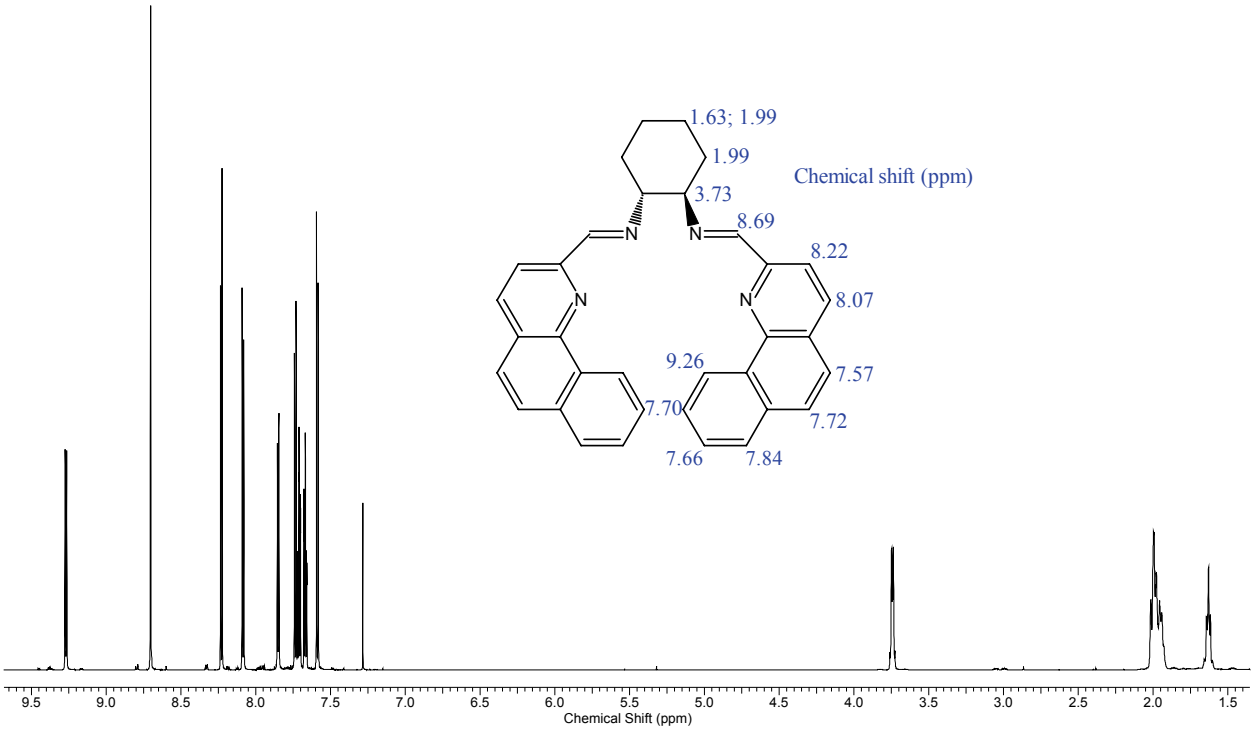

Figure 2.7 800 MHz ^{1}H NMR spectra of (*R*,*R*)-**5** ($CDCl_3$) with assignments

The assignments described above and the distinct triplet resonances allows for a convenient starting point to assign the remaining aromatic protons of the molecule using the COSY and NOESY spectra (Figure 2.8). For example, there is a COSY correlation between the triplet resonance at 7.66 ppm and the doublet at 7.84 ppm. Subsequent analysis by NOESY, revealed there was a correlation between the doublet resonances at 7.84 and 7.72 ppm. A correlation between the imine proton and the one at 8.22 ppm was not observed in the NOESY, however there was a correlation to one of the cyclohexyl protons (3.73 ppm). This allowed the general assignment of signals corresponding to the protons of the cyclohexyl backbone.

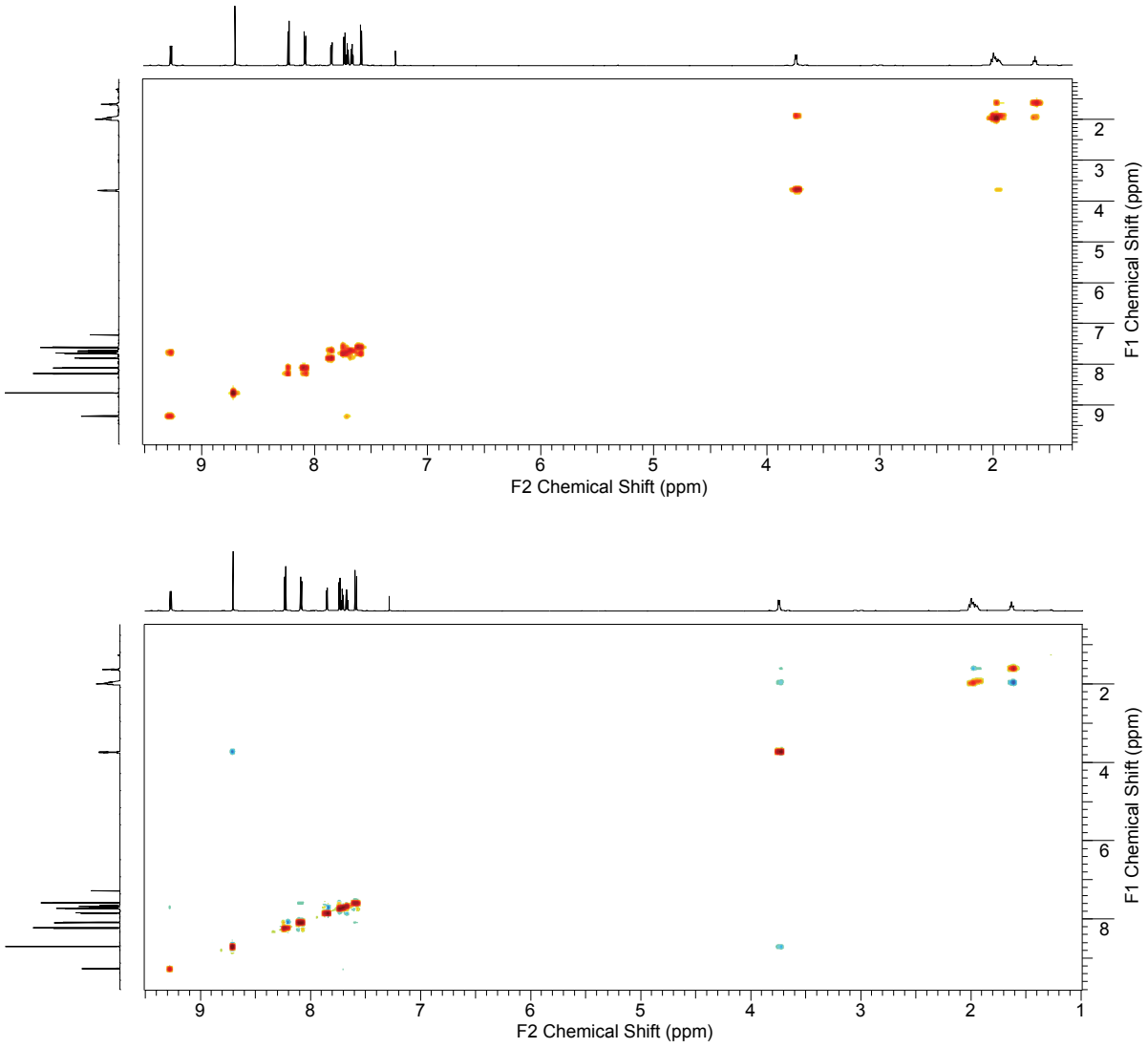

Figure 2.8 800 MHz COSY (top) and NOESY (bottom) NMR spectra for (*R*,*R*)-**5** ($CDCl_3$)

The complete analysis of the ligand (*R*)-**6** was also undertaken. The ^{1}H NMR spectrum along with assignments is shown in Figure 2.9. Again the molecule is C_2 symmetric and so the only half the total number of possible resonances are visible, however the spectrum remains rather complicated owing to the large number of resonances over a relatively small chemical shift range. Nevertheless the complete proton assignment of the molecule was deciphered (Figure 2.9).

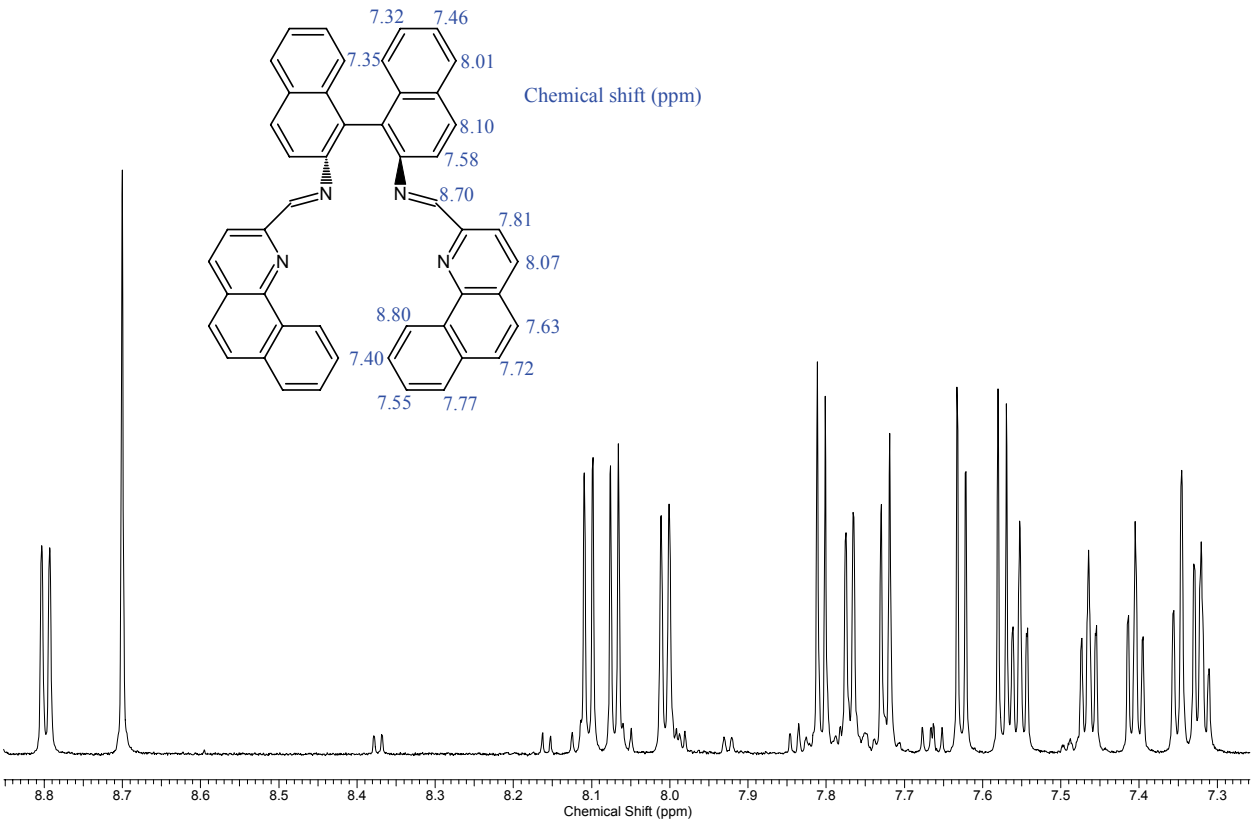

Figure 2.9 800 MHz ^{1}H NMR spectra of (*R*)-**6** (CD_2Cl_2) with assignments

The imine hydrogen appears as a singlet resonance and is found characteristically at 8.70 ppm. The peak at 8.80 ppm is shifted farther upfield respective to any other resonance due to the ring current effect that is experienced by the bay region hydrogen. There are two sets of adjacent triplet peaks in the spectrum; one set resonates from the binaphthyl backbone (7.32, 7.46 ppm) and the other from the sidearm (7.40, 7.55 ppm). These peaks were assigned after analysis of COSY and NOESY spectra (Figure 2.10). This information and the assignment of the bay region hydrogen allowed for straight forward assignment of the remaining resonances.

Notably, there is a NOESY correlation between the imine hydrogen at 8.70 ppm and the hydrogen at 7.58 ppm, i.e. the two protons are close enough to each other that they experience

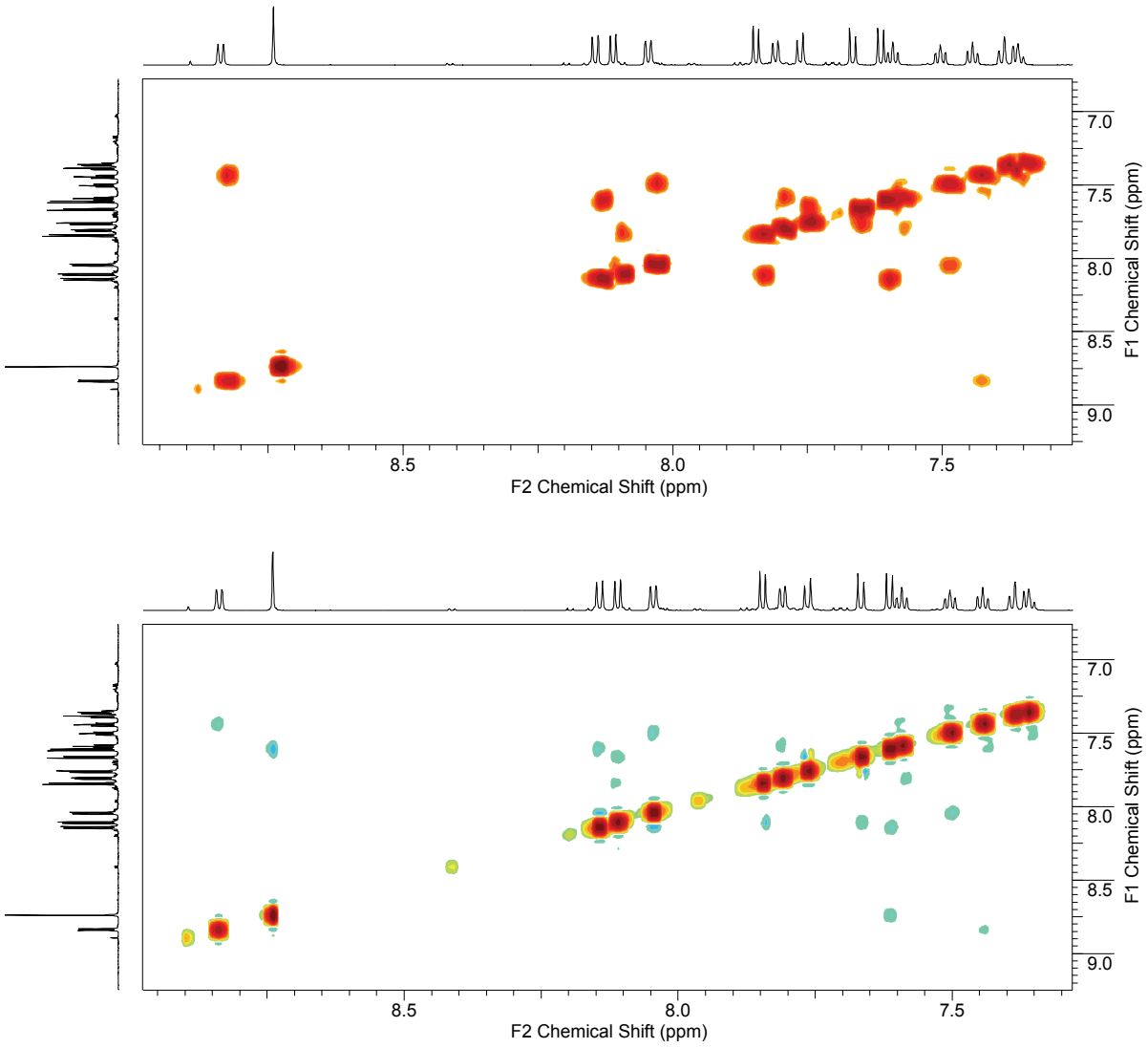

Figure 2.10 800 MHz COSY (top) and NOESY (bottom) NMR spectra for (*R*)-**6** (CD_2Cl_2)

NOE (Figure 2.11). However, there is no correlation of the imine hydrogen to the one at 7.81 ppm on the sidearm, the two protons in this case are too far apart to interact with each other through NOE. ^{13}C NMR spectra for **3**, (*R*,*R*)-**5** and (*R*)-**6**, were also collected. However, due to little additional structural information yielded they have not been included here. See Appendix I the and experimental section for more details.

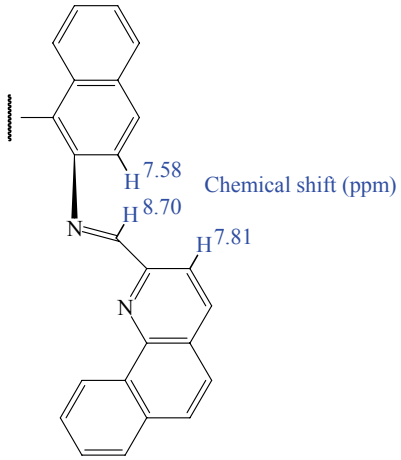

Figure 2.11 Some ^{1}H NMR shifts for (*R*)-**6**

2.4 Structural studies of 2-formylbenzoquinoline and ligands

Single crystals that were suitable for X-ray analysis were grown of the aldehyde **3** and the ligand (*R*,*R*)-**5** via solvent diffusion. Suitable crystals of the aldehyde were grown from chloroform over which was layered petroleum ether. The crystal structure, which has not been previously reported, is shown in Figure 2.12. There is only one distinct molecule in the unit cell, and the structure is as expected; a planar aromatic system and a formyl group at the 2 position. Crystals of (*R*,*R*)-**5** were grown from methylene chloride over which was layered diethyl ether. The crystal structure (Figure 2.13) clearly shows the planar arrangement of the each arm. Furthermore, the arms orient themselves so as to point away from each other. Unfortunately, it was not possible to grow suitable crystals of (*R*)-**6**: several attempts resulted in only very fine, hair like needles. Further attempts with the use of the racemic ligand (*rac*)-**6** also resulted in only hair like needles that did not diffract well.

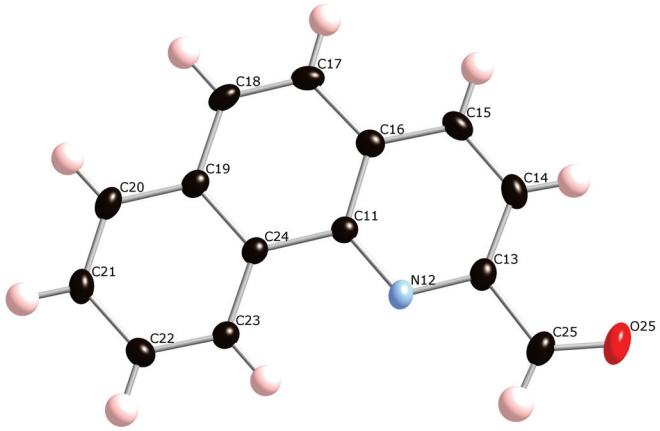

Figure 2.12 Thermal ellipsoid plot (50% probability) of **3**. Selected bond length: C_{25}-O_{25} 1.206(3) Å.

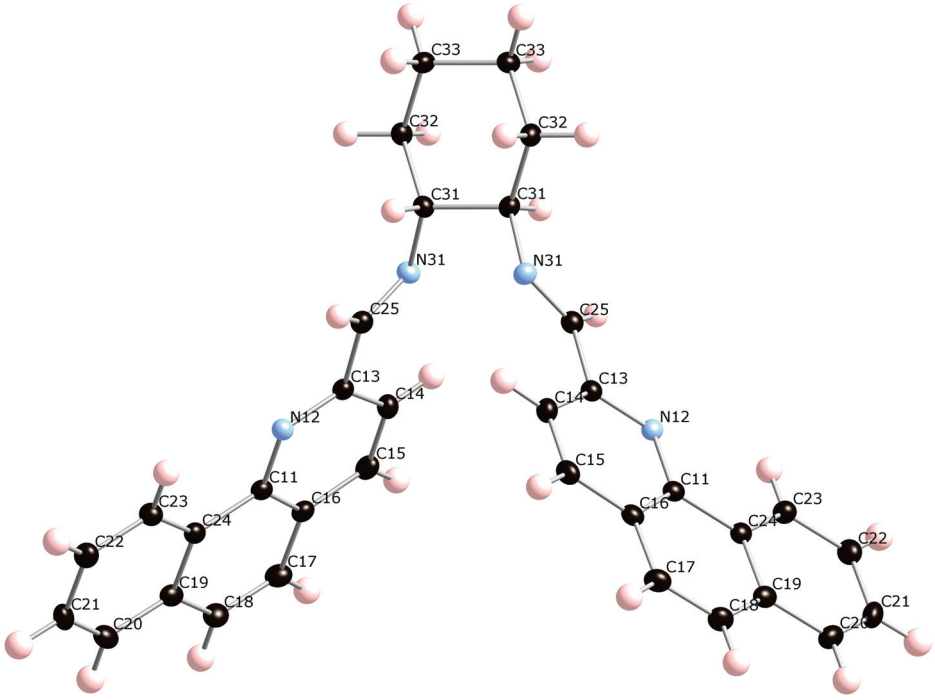

Figure 2.13 Thermal ellipsoid plot (50% probability) of (*R*,*R*)-**5**. Selected bond lengths: C_{31}-N_{31} 1.455(3) Å; C_{25}-N_{31} 1.258(3) Å.

Chapter 3

Syntheisis and characterization of

complexes with the cyclohexyldiamine backbone

3.1 Synthesis

The ligand (*R*-*R*)-**5** was metallated with zinc chloride to afford the dinuclear complex (*R*-*R*)-**8**, rather than the anticipated monohelical one, (*R*,*R*)-**7**. The yield for (*R*,*R*)-**8** is low due to the stoichiometric addition of $ZnCl_2$ rather than the use of two equivalents, i.e. there is an excess

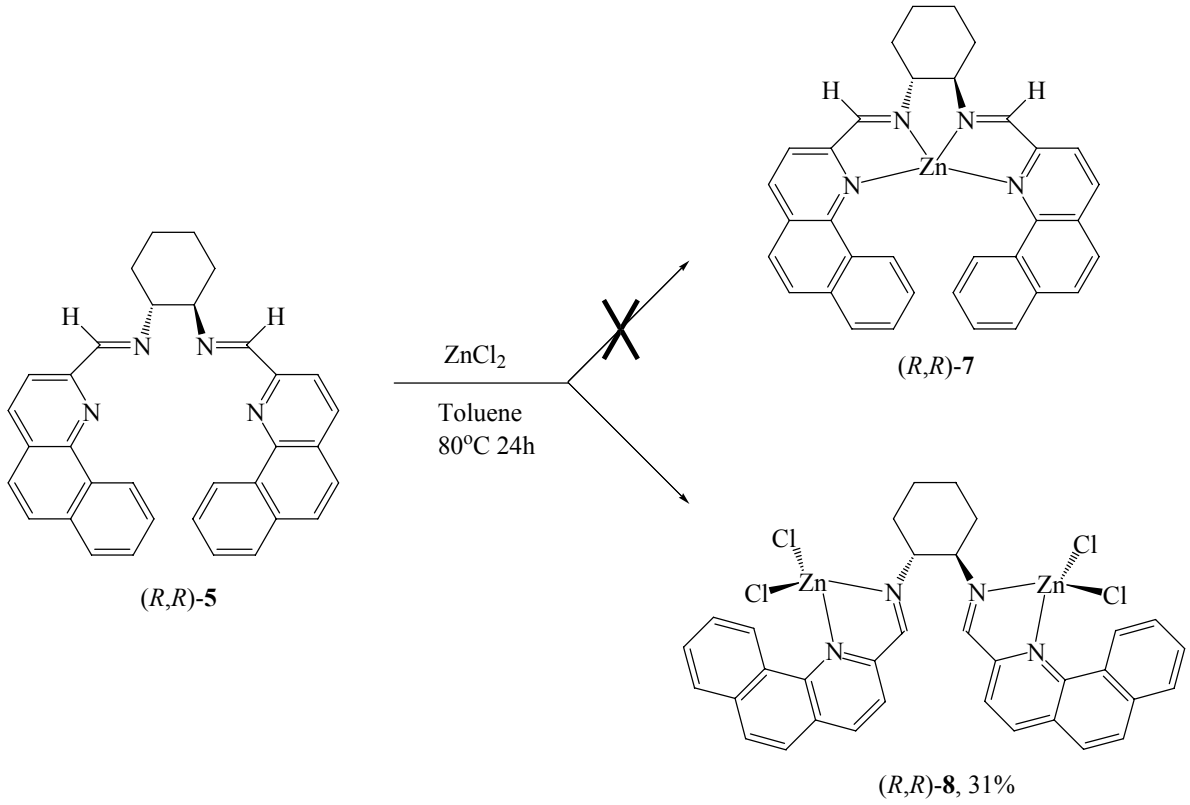

Figure 3.1 Synthesis of dinuclear zinc complex (*R*,*R*)-**8**

of ligand. The complex, (*R*,*R*)-**8** is afforded as a pale yellow colored precipitate and is of high purity, as was indicated by $^{1}H/^{13}C$ NMR. The high solubility of the ligand versus the high insolubility of the complex in toluene allows for facile purification. Comparably, the dinuclear zinc complex (*R*,*R*)-**9** is also formed under similar reaction conditions with the analogous isopropylquinoline ligand (Figure 3.2).

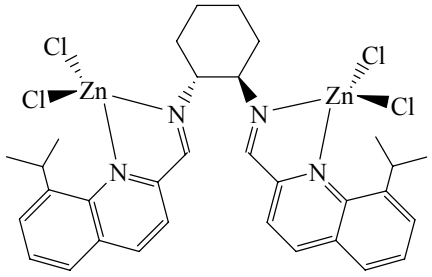

(*R*,*R*)-**9**

Figure 3.2 Dinuclear zinc complex (*R*,*R*)-**9**

In further studies, ligands (*R*,*R*)-**5** and (*R*,*R*)-**10** were metallated with nickel iodide, to afford the complexes (*R*,*R*)-**11** and (*R*,*R*)-**12** respectively (Figure 3.3). Subsequent crystal structure analysis revealed that they were mononuclear 5-coordinate nickel complexes. In each case there is coordination from both imine donors but from only one of the pyridyl donors. Two coordinated iodide anions complete the coordination sphere. A mixture of solvents was used for the reaction; ethanol was used to facilitate the solvation of the metal salt and toluene for the ligand. Nickel complexes (*R*,*R*)-**11** and (*R*,*R*)-**12** are afforded in moderate yields, and ^{1}H NMR spectra indicate that they are of high purity. Due to their paramagnetic nature and low solubility, it was not possible to obtain ^{13}C NMR data for (*R*,*R*)-**11** and (*R*,*R*)-**12**. Both complexes are sensitive to atmospheric oxygen and moisture, therefore inert conditions must be employed.

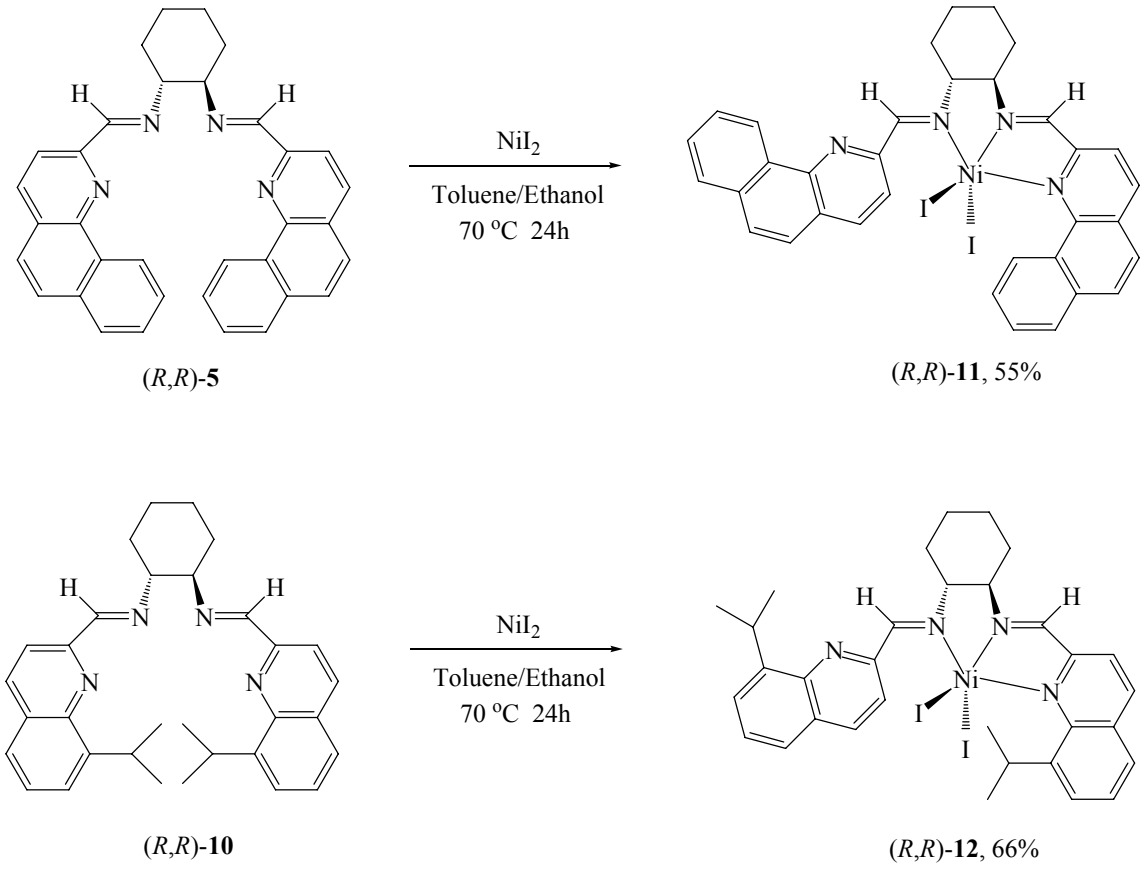

(*R*,*R*)-**5**

(*R*,*R*)-**11**, 55%

(*R*,*R*)-**10**

(*R*,*R*)-**12**, 66%

Figure 3.3 Synthesis of nickel complexes (*R*,*R*)-**11** and (*R*,*R*)-**12**

Unfortunately the formation of a monohelical complex was not realized (Figure 3.3). This is attributed to the insufficient lability of the anion and the inability of neutral ligand donors to displace anionic halides. It was believed that removal of one the iodide moieties using a halogen abstraction agent would allow for coordination of the second pyridyl nitrogen, and therefore the formation of a monohelix. With this in mind the complex (*R*-*R*)-**11** was reacted with silver triflate in methylene chloride. It was hoped that silver triflate would act as a halogen abstraction agent, removing one of the iodide anions to form the helical complex (*R*,*R*)-**13** and insoluble AgI. Surprisingly, a dinuclear complex (*R*,*R*)-**14** was the result (Figure 3.4). The

mechanism here is unclear, since the product is not the result of halide abstraction, but rather loss of ligand.

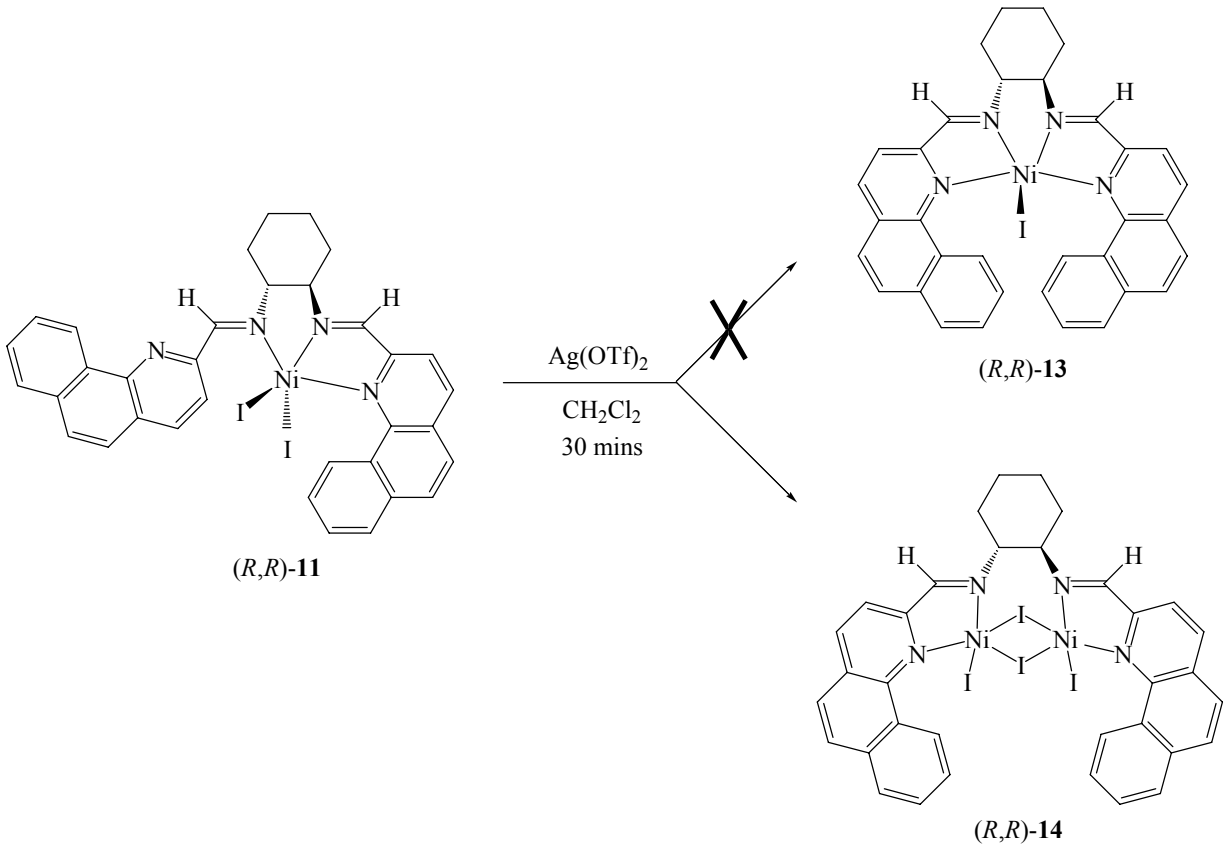

Figure 3.4 Attempted halogen abstraction from (*R*,*R*)-**11**

Analysis of reaction mixtures by ^{1}H NMR resulted in complicated paramagnetic spectra that indicated the presence of multiple species in solution. Crystals were grown of complex (*R*,*R*)-**14** by dissolving it in chloroform and then layering toluene over the solution. Upon diffusion a crystalline material as well as a white solid had formed. After crystal structure analysis had indicated the formation of a dinuclear complex, it was obvious the white precipitate was actually excess ligand. A similar reaction was attempted with the analogous

ispropylquinoline complex (*R*,*R*)-**12** to yield the monohelical complex (*R*,*R*)-**15**. Crystal structure analysis revealed a complex that remains coordinated to three nitrogen donors; (*R*,*R*)-**16**. Additionally there is partial occupancy of a coordinated oxygen atom and one of the coordinated iodide anions (Figure 3.5).

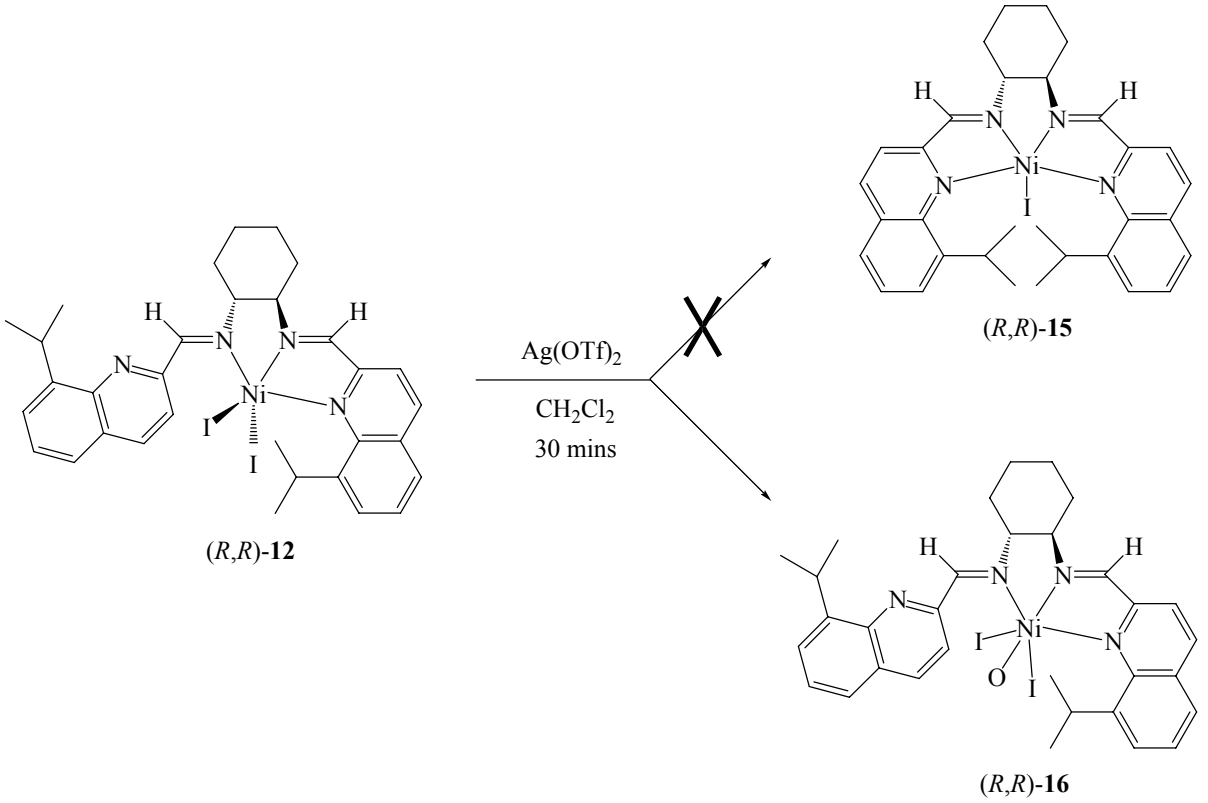

(*R*,*R*)-**12**

(*R*,*R*)-**15**

(*R*,*R*)-**16**

Figure 3.5 Attempted halogen abstraction from (*R*,*R*)-**12**

The ^{1}H NMR spectrum of the reaction mixture after attempted halide abstraction from (*R*,*R*)-**12** indicates a paramagnetic compound and the presence of multiple species in solution. Crystals were grown of complex (*R*,*R*)-**16** by dissolving the mixture in chloroform and then layering diethyl ether over the solution. The source of the oxygen is as of yet unclear, since rigorous anhydrous and oxygen free conditions were employed for the synthesis.

The unsuccessful attempt to remove the iodide anion led us to explore the use the more labile trifate anion. Nickel triflate (**17**) is not available commercially and therefore was synthesized following, in part, documented literature procedures[46] (see experimental section for further details). Subsequently, ligand (*R*,*R*)-**5** was metallated with nickel triflate to afford the mononuclear, double stranded helical complex (*R*,*R*,*R*,*R*)-**18** (Figure 3.6).

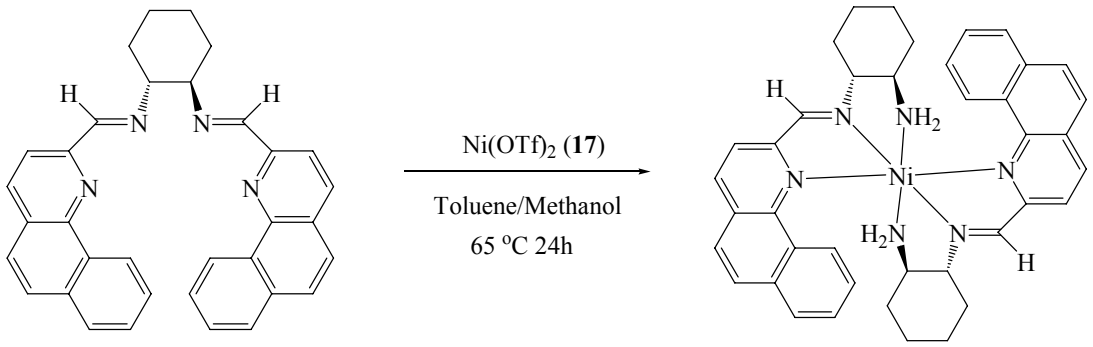

(*R*,*R*)-**5** (*R*,*R*,*R*,*R*)-**18**

Figure 3.6 Synthesis of double stranded nickel complex (*R*,*R*,*R*,*R*)-**18**

Analysis by ^{1}H NMR was inconclusive due to complicated paramagnetic spectra, but initial indications pointed towards the presence of more than one species in solution. Crystals were grown of complex (*R*,*R*,*R*,*R*)-**18** from methylene chloride over which was layered hexanes. Once more, as well as crystalline material being present, there was also a white precipitate. Crystal structure analysis revealed a mononuclear complex that is coordinated to two ligands, where both ligands are now tridenatate. Each ligand has undergone hydrolysis at one imine bond causing the loss of a sidearm. This provides rationale for the appearance of the white precipitate.

3.2 NMR spectroscopy of zinc and nickel complexes

The diamagnetic zinc and the paramagnetic nickel complexes were analyzed by NMR spectroscopy. Due to the presence of unpaired electrons in the nickel complexes a comprehensive NMR analysis was not possible. However, this was not the case with zinc complexes and a detailed NMR analysis was undertaken with the aid of 2D NMR. The ^{1}H NMR (800 MHz) spectrum of (*R*,*R*)-**8** with assignments is shown in figure 3.7. There are clearly both upfield and downfield shifts when the spectrum is compared to that of the ligand (*R*,*R*)-**5** (Figure 2.7). For example, the imine hydrogen has shifted upfield from 8.67 to 9.35 ppm, whereas the resonance at 8.22 ppm has shifted downfield to 8.03 ppm upon metallation. There were also

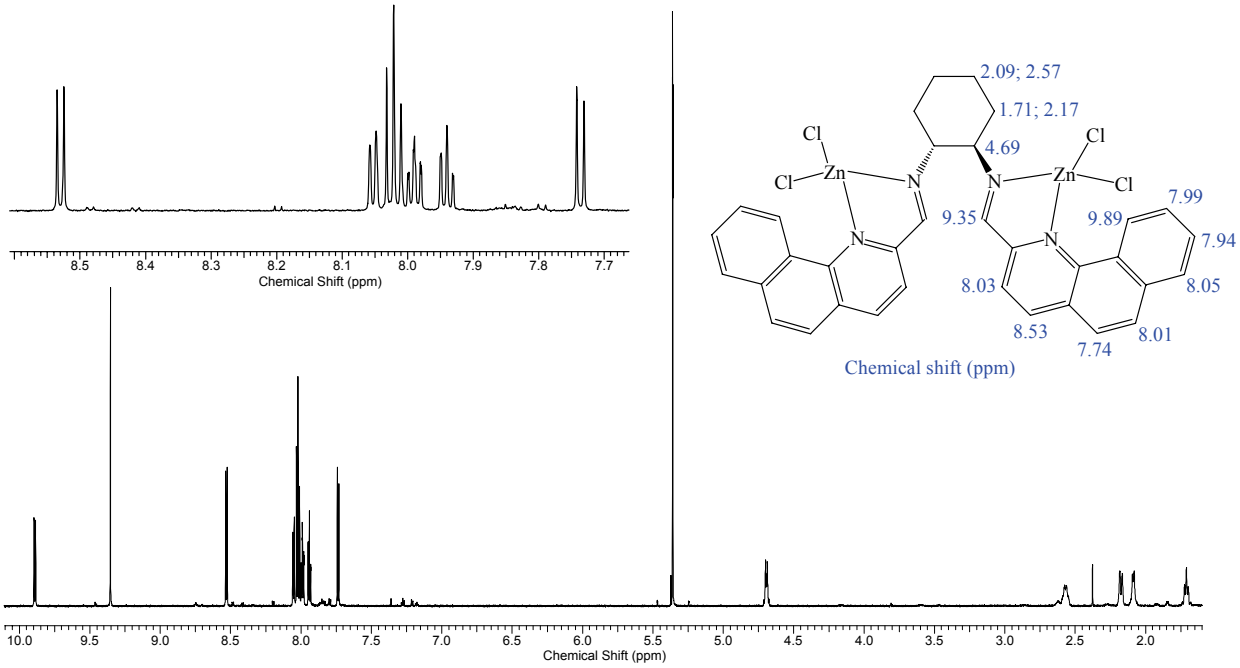

Figure 3.7 800 MHz ^{1}H NMR spectra of (*R*,*R*)-**8** (CD_2Cl_2) with assignments

notable shifts in the aliphatic region, for example the multiplet at 3.73 ppm in the ligand spectrum now appears at 4.69 ppm. As in the ligand spectrum, there are two unique triplet peaks in the spectrum (7.99 and 7.94 ppm), providing a convenient starting point to assign the remaining proton signals in the spectrum. This was achieved using a combination of COSY and NOESY analysis (Figure 3.8).

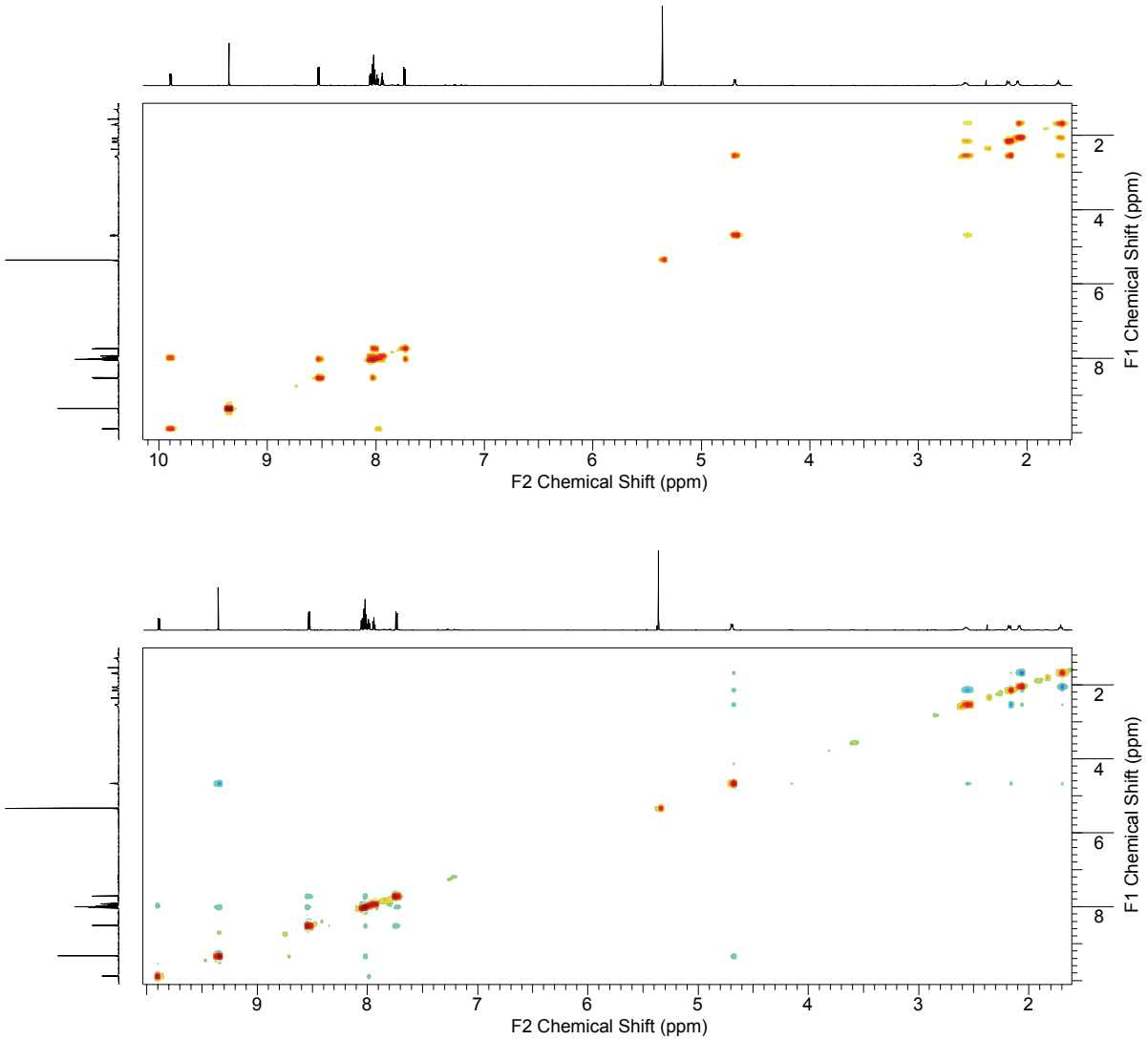

Figure 3.8 800 MHz COSY (top) and NOESY (bottom) NMR spectra for (*R*,*R*)-**8** (CD_2Cl_2)

The NOESY spectra indicated through space correlations between not only the imine hydrogen and the cyclohexyl proton at 4.69 ppm, but in contrast to the ligand, also to the aromatic proton at 8.03 ppm. This is likely due to the adopted conformation as a result of dinucleation (Table 3.1 and Figure 3.9).

Table 3.1 Some ^{1}H NMR data and bond distances for (*R*,*R*)-**5** and (*R*,*R*)-**8**

	Protons (ppm)	Distance Between (Å)	NOESY correlation
(*R*,*R*)-**5**	3.73-8.69	2.127	yes
	8.69-8.22	3.596	no
(*R*,*R*)-**8**	4.69-9.35	2.212	yes
	9.35-8.03	2.484	yes

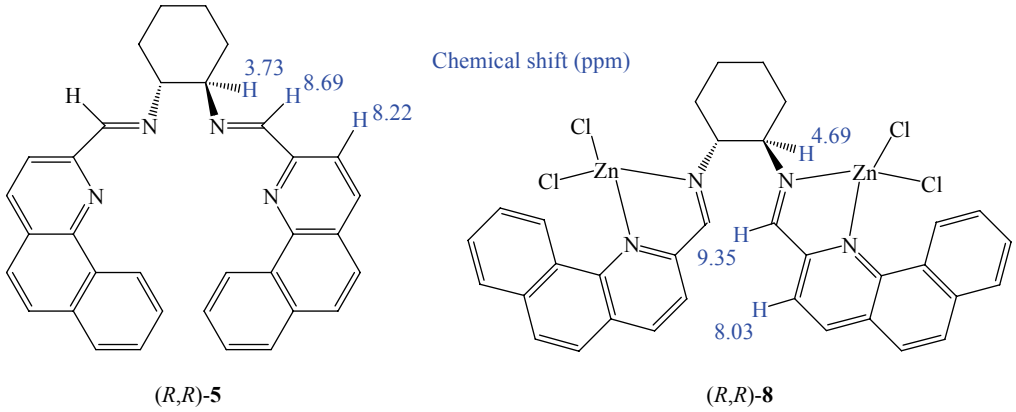

(*R*,*R*)-**5** (*R*,*R*)-**8**

Figure 3.9 Some ^{1}H NMR data for (*R*,*R*)-**5** and (*R*,*R*)-**8**

Nickel(II) complexes have a $3d^8$ electronic configuration. When the complex is octahedral or tetrahedral there are two unpaired electrons, but a square planar arrangement results in a diamagnetic complex with no unpaired electrons.[47] It was hoped that complexes formed with ligands (*R*,*R*)-**5** and (*R*,*R*)-**10** would be square planar, and therefore diamagnetic.

This would allow for facile characterization via ^{1}H NMR. X-ray analysis revealed that nickel complexes (*R*,*R*)-**11** and (*R*,*R*)-**12** were 5-coordinate. Five coordinate nickel complexes can be high or low spin depending on the nature of the ligand, therefore there is a possibility that the complex can be either diamagnetic or paramagnetic. However, the paramagnetic spectra clearly indicate unpaired electrons. The ^{1}H NMR spectra of the nickel complexes (*R*,*R*)-**11** and (*R*,*R*)-**12** were collected. The ^{1}H chemical shift data is listed in table 3.1 and the spectra are shown in Figure 3.10. Peaks are often highly broadened and range from -7.15 to 24.66 ppm. Complete assignment of the spectra was not attempted due to the difficulty in interpreting highly broadened spectra.

Unpaired electrons affect the NMR linewidth and give rise to paramagnetic shifts, yet there remains some valuable information that can be extracted. For example, there are resonances in both the aromatic and aliphatic regions of the spectra. There are also resonances present outside the normal diamagnetic chemical shift range; these are likely due to protons that are closer in proximity to the metal center. Proton resonances occurring from the sidearm are likely to experience a greater paramagnetic shift compared to those of the cyclohexyl backbone; this is due to the conjugation that is present through the sidearm to the metal center. With respect to specific ^{1}H NMR assignments no further conclusions were drawn for (*R*,*R*)-**11** and (*R*,*R*)-**12**.

Table 3.2 400 MHz ^{1}H NMR ($CDCl_3$) chemical shift data for (*R*,*R*)-**11** and (*R*,*R*)-**12**

	Chemical shifts, δ
(*R*,*R*)-**11**	-7.15, -5.70, 7.91, 10.87, 11.34, 11.95, 13.50, 17.57, 24.66
(*R*,*R*)-**12**	-6.05, 0.90, 1.28, 8.83, 10.74, 13.00, 24.15

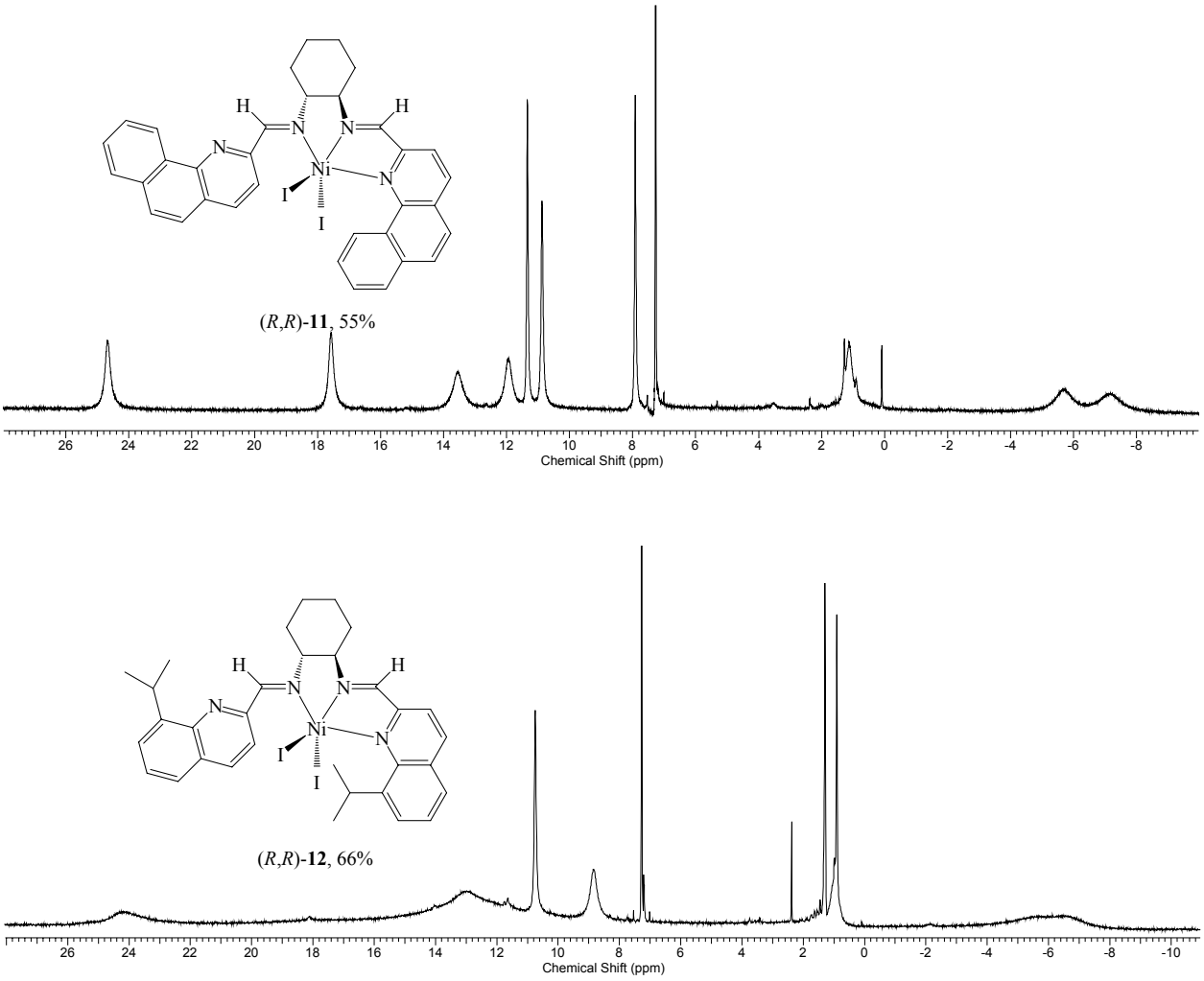

Figure 3.10 400 MHz ^{1}H NMR spectra ($CDCl_3$) of (*R*,*R*)-**11** (top) and (*R*,*R*)-**12** (bottom)

It was hoped that reaction of (*R*,*R*)-**11** with silver(I) triflate would result in the formation of a monohelix, however X-ray analysis indicated the formation of the dinuclear complex, (*R*,*R*)-**14**. ^{1}H NMR analysis again revealed a broadened spectrum due to unpaired electrons. The complicated nature of the spectrum pointed to the presence of more than one species in solution (Figure 3.11). It is clear that one of these species is in fact the starting material (*R*,*R*)-**11**. Comparing the two spectra (Figure 3.11), the following resonances occur in both starting material and product spectra; 25, 17.5, -6, -7 ppm. Given the number and nature of signals

present, it is likely that there are three different metal-containing species in solution. As was mentioned earlier in the synthesis section a white precipitate was formed on crystallization of (*R*,*R*)-**14**. This is consistent with the presence of excess ligand due to non-stoichiometric formation of a dinuclear complex. Of the remaining peaks in the ^{1}H NMR spectrum for (*R*,*R*)-**14**, those resonating from the dinuclear complex and those from excess ligand can be generally

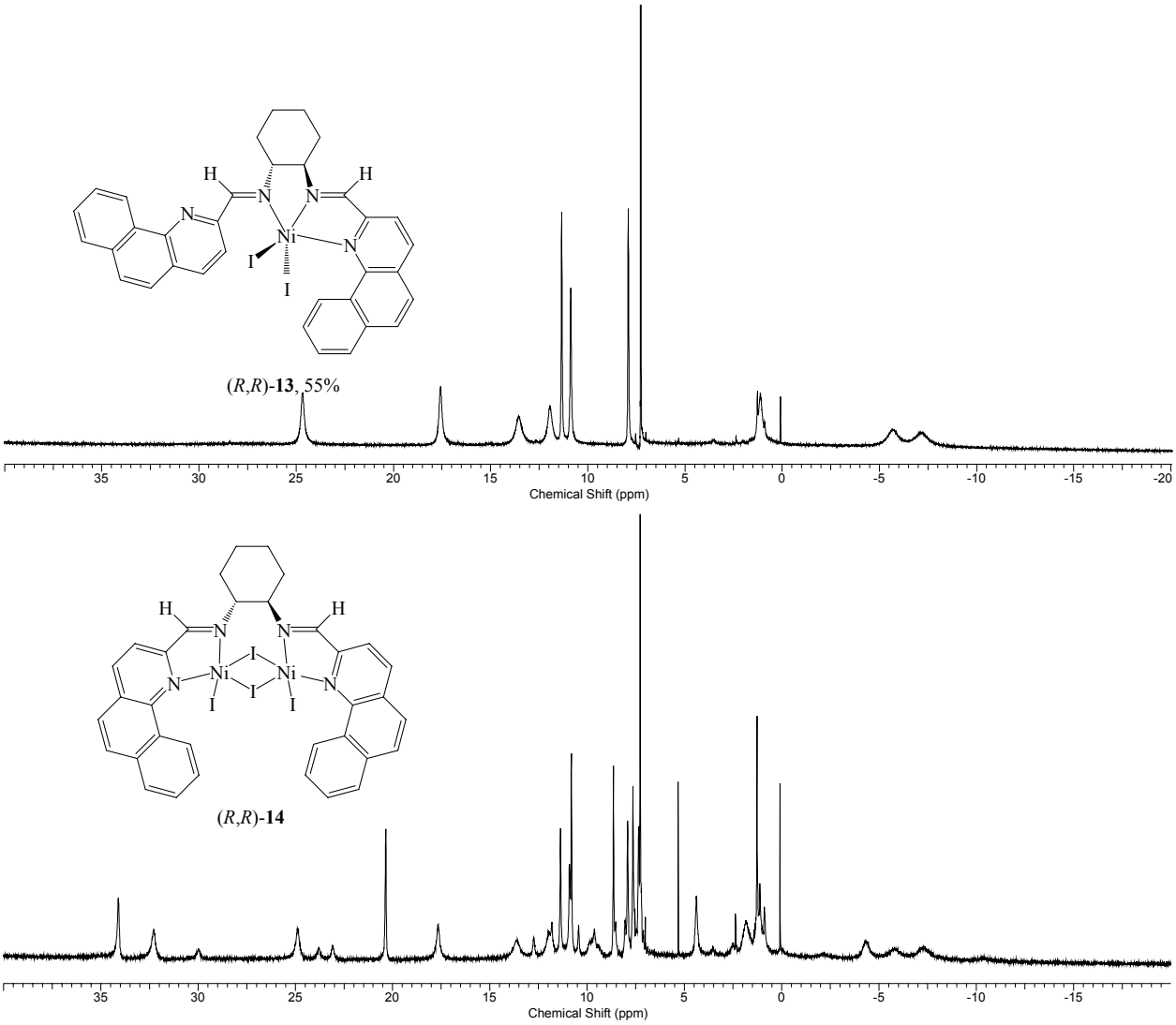

Figure 3.11 400 MHz ^{1}H NMR spectra ($CDCl_3$) of (*R*,*R*)-**11** (top) and (*R*,*R*)-**14** (bottom)

assigned. Peaks corresponding to free ligand will appear in the normal diamagnetic chemical shift range of the spectrum whereas resonances from the dinuclear complex (*R*,*R*)-**14** are likely to be highly shifted and broadened. For example the peaks at approximately 34 and 32 ppm (Figure 3.11) are expected to resonate from (*R*,*R*)-**14**.

The complex (*R*,*R*)-**16** was also analyzed by ^{1}H NMR spectroscopy. Again a highly broadened spectrum was obtained, this time with multiple overlapping peaks (Figure 3.12). The complicated spectrum suggests the presence of more than one species in solution. Full peak assignment is not possible; however there are peaks present that clearly correspond to starting material.

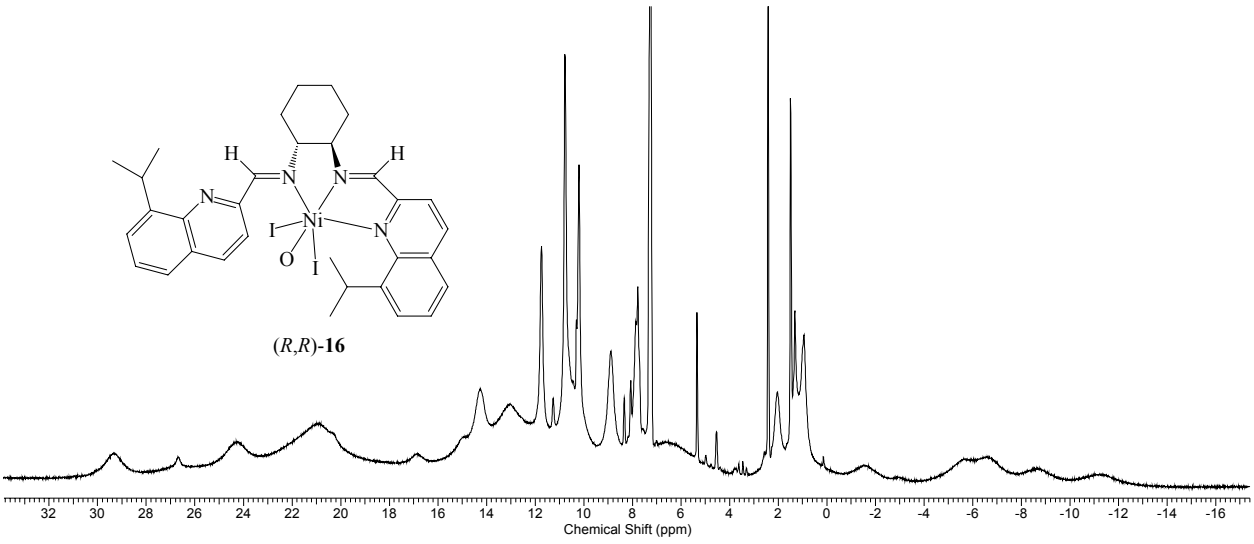

Figure 3.12 400 MHz ^{1}H NMR spectra of (*R*,*R*)-**16** ($CDCl_3$)

Reaction of ligand (*R*,*R*)-**5** with nickel triflate (**17**) resulted in the formation of the double stranded helicate (*R*,*R*,*R*,*R*)-**18**. Not surprisingly ^{1}H NMR analysis revealed a paramagnetic spectrum (Figure 3.13). With respect to the ligand spectrum, peaks now appear broader and some of these resonate outside the normal diamagnetic range. Unlike the ligands and zinc

complexes a comprehensive NMR analysis was not possible for the paramagnetic nickel complexes.

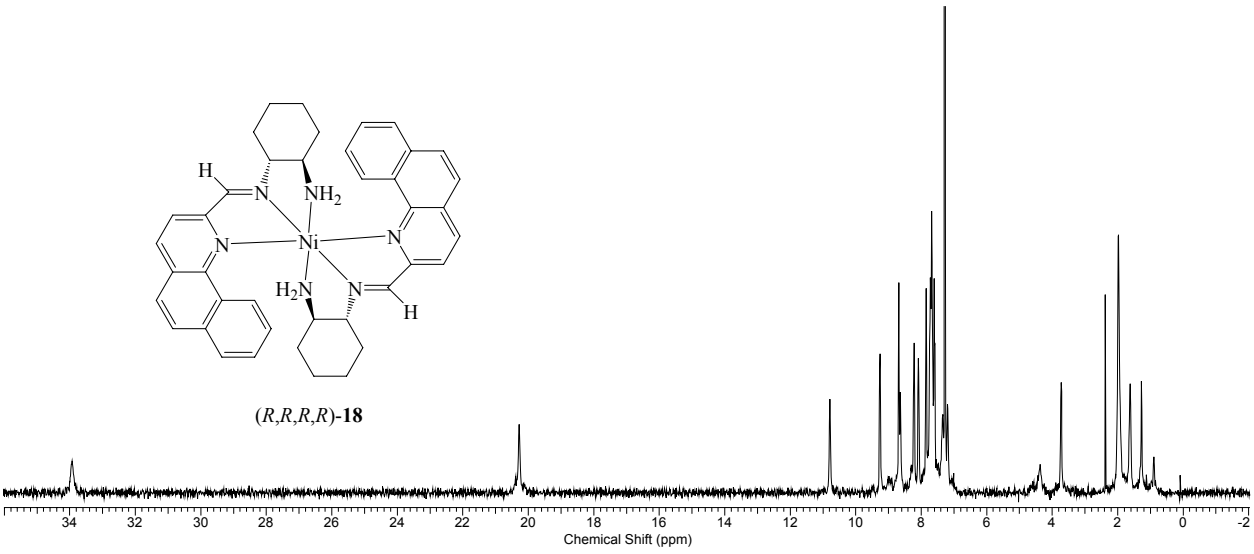

Figure 3.13 400 MHz ^{1}H NMR spectra of (*R*,*R*,*R*,*R*)-**18** ($CDCl_3$)

3.3 Structural studies of zinc and nickel complexes

The zinc and nickel complexes were characterized by X-ray crystallographic analysis. Single crystals were grown employing the solvent diffusion method and rigorously inert conditions. The crystal structure for the dinuclear complex (*R*,*R*)-**8** is shown in Figure 3.14, there are two molecules (1 and 2) in the unit cell with only minimal differences between them. Single crystals were grown of (*R*,*R*)-**8** from methylene chloride over which was layered diethyl ether. A dinuclear complex where the ligand is coordinated to two $ZnCl_2$ groups is the result.

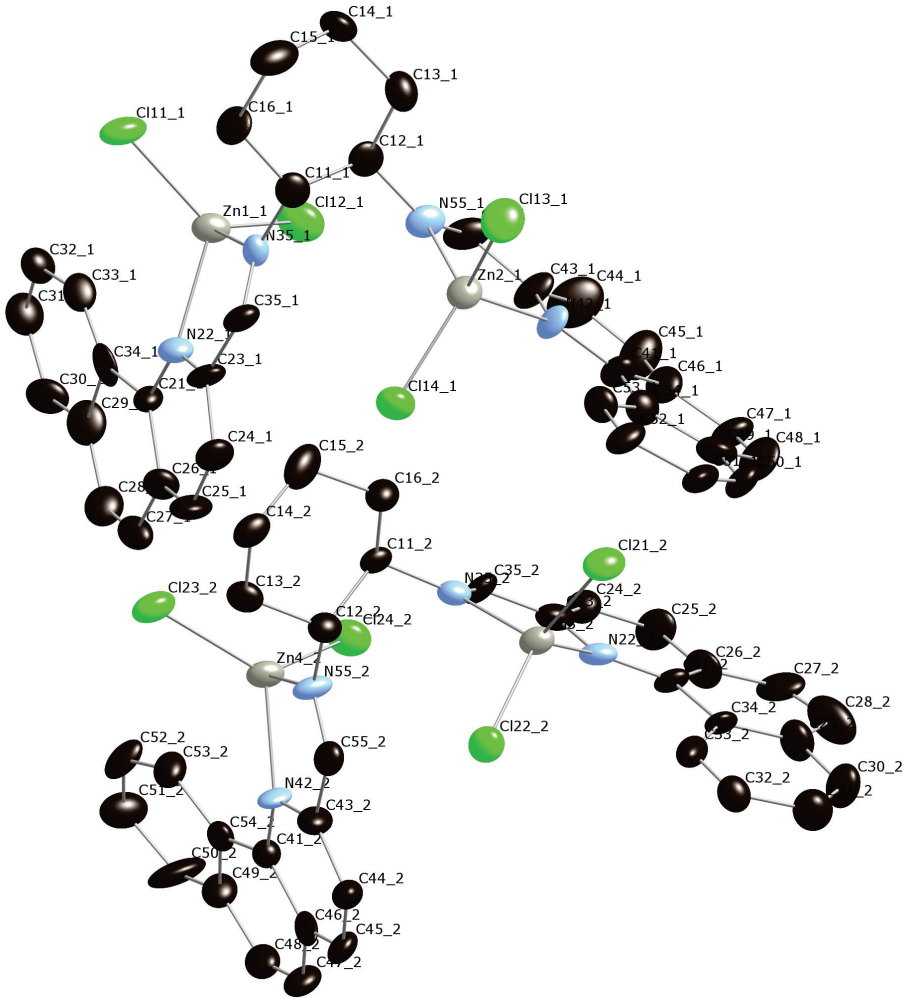

Figure 3.14 Thermal ellipsoid plots (50% probability of (*R*,*R*)-**8**

The crystal structure (Figure 3.14) clearly shows how each sidearm orients in such a way as to twist outwards. The ligand then coordinates to each $ZnCl_2$ moiety through one pyridyl donor and one of the imine donors. Clearly a monohelical structure was not realized, rather a helical dinuclear complex is formed. The molecule can therefore be classed as a single-stranded helicate. Analyzing some selected bond lengths and angles for (*R*,*R*)-**8** (Table 3.3), it is clear that there are only minimal differences in geometry between the two molecules in the unit cell (1 and 2). Zn-N bond lengths are typical to those found in complexes with nitrogen donor ligands.[48]

Table 3.3 Selected bond lengths (Å) and bond angles (°) for (*R*,*R*)-**8**

	Molecule 1		Molecule 2	
Bond lengths	Zn_1-N_{35}	2.054(11)	Zn_3-N_{35}	2.041(11)
	Zn_1-N_{22}	2.170(11)	Zn_3-N_{22}	2.112(11)
	Zn_2-N_{55}	2.029(11)	Zn_4-N_{55}	2.046(12)
	Zn_2-N_{42}	2.090(12)	Zn_4-N_{42}	2.099(9)
	Zn_1-Cl_{12}	2.193(5)	Zn_3-Cl_{21}	2.210(4)
	Zn_1-Cl_{11}	2.219(4)	Zn_3-Cl_{22}	2.214(4)
	Zn_2-Cl_{13}	2.191(4)	Zn_4-Cl_{23}	2.206(4)
	Zn_2-Cl_{14}	2.215(4)	Zn_4-Cl_{24}	2.231(5)
Bond angles	N_{35}-Zn_1-N_{22}	78.5(5)	N_{35}-Zn_3-N_{22}	81.4(5)
	N_{55}-Zn_2-N_{42}	83.7(5)	N_{55}-Zn_4-N_{42}	81.8(4)
	Cl_{12}-Zn_1-Cl_{11}	118.1(18)	Cl_{21}-Zn_3-Cl_{22}	111.4(16)
	Cl_{13}-Zn_2-Cl_{14}	123.4(2)	Cl_{23}-Zn_4-Cl_{24}	115.8(17)

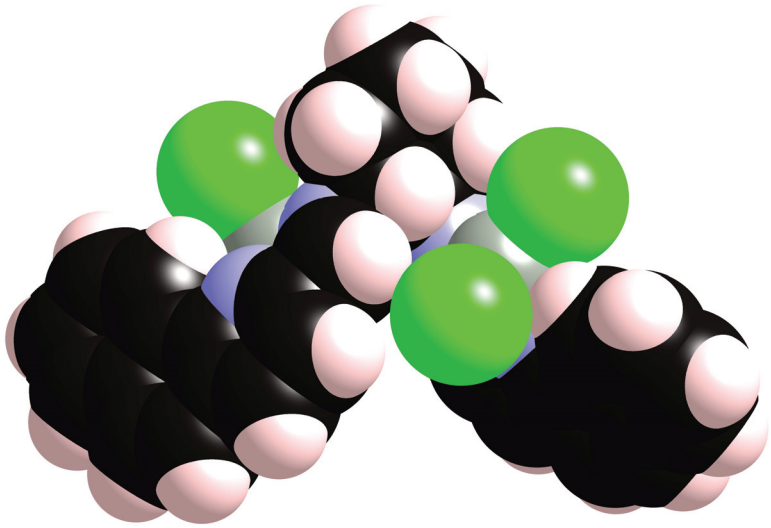

Figure 3.15 Space filling model of (*R*,*R*)-**8**

It appears that the formation of a monohelix is not favorable for this system. One factor is that the chloride anions are insufficiently labile. As a result the coordination of a tetradentate ligand to a single metal would result in an octahedral complex. This is unfavourable, since it

will result in a coordination sphere that is overcrowded. Furthermore, the space filling model of the dinuclear complex observed, (Figure 3.15) indicates that there is in fact very little free space around the zinc atoms. The bis(bidentate)[49] coordination behavior of the ligand (*R*,*R*)-**8** is not the only one of its type. As mentioned earlier in this chapter, the analogous isopropyl ligand also forms a similar dinuclear complex when metallated with zinc chloride (Figure 3.2). There are also some examples in the literature: Puddephatt[50] and Perez[51] have reported formation of platinum and molybdenum dinuclear complexes (Figure 3.16). In the case of the platinum complex, unsurprisingly there is a square planar geometry around each metal. In (*R*,*R*)-**8**, the zinc atoms are arranged more closely to a tetrahedral geometry.

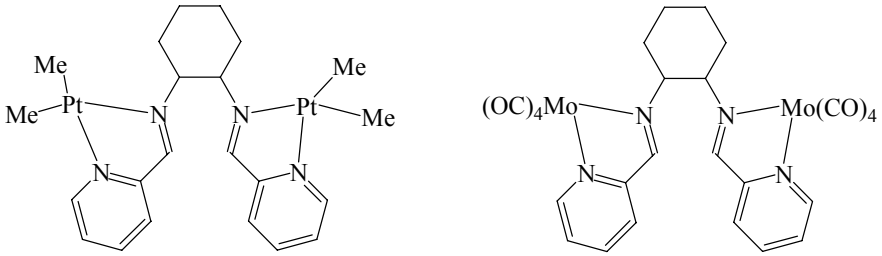

Puddephatt Perez

Figure 3.16 Dinuclear complexes from bis(imine-pyridine) ligands

In further structural characterization studies, single crystals were grown of (*R*,*R*)-**11** and (*R*,*R*)-**12**. Subsequent X-ray analysis revealed 5-coordinate nickel complexes (Figures 3.12 and 3.13 respectively). The thermal ellipsoid plot of (*R*,*R*)-**11** clearly shows how one of the side arms orients itself so as to twist outwards from the center of the complex (Figure 3.17). There is coordination to nickel from both imine donors, but from only one of the two pyridyl nitrogen donors. Both iodide anions also remain coordinated. This is likely due to the insufficient lability of the anion as well the metal favoring the anionic donors. It is likely there would be too much

steric congestion for the ligand to become a tetradentate donor with both iodide anions still coordinated, thus the molecule orients in this preferred trigonal bipyramidal geometry. Selected bond lengths and angles for (*R*,*R*)-**11** are provided in Table 3.4.

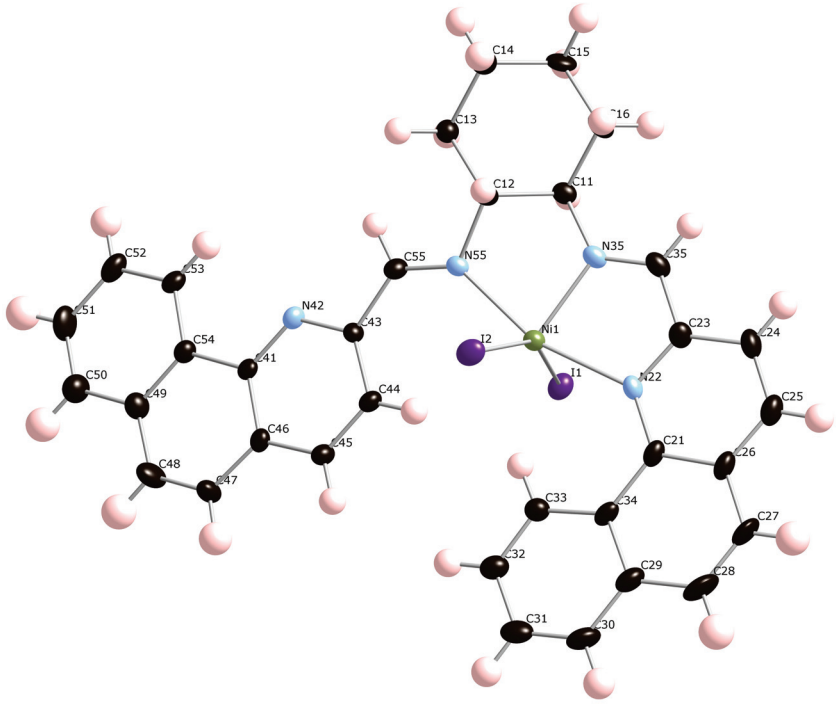

Figure 3.17 Thermal ellipsoid plot (50% probability) of (*R*,*R*)-**11**

Table 3.4 Selected bond lengths (Å) and bond angles (°) for (*R*,*R*)-**11**

Bond lengths	Ni_1-N_{55}	2.102(6)	Ni_1-I_1	2.633(10)
	Ni_1-N_{35}	1.954(6)	Ni_1-I_2	2.645(10)
	Ni_1-N_{22}	2.199(6)		
Bond angles	N_{35}-Ni_1-N_{55}	81.9(2)	N_{35}-Ni_1-I_1	97.9(16)
	N_{35}-Ni_1-N_{22}	80.5(2)	N_{35}-Ni_1-I_2	110.7(16)
	N_{55}-Ni_1-N_{22}	161.9(2)	I_1-Ni_1-I_2	151.4(4)

X-ray analysis indicated complex (*R*,*R*)-**12** is also 5-coordinate, adopting a similar geometry (Figure 3.18) to that of (*R*,*R*)-**11**. Again, there is N_3-coordination, and both iodo ligands remain intact, the result is a trigonal bypyramidal coordination geometry. There are two molecules in the unit cell (1 and 2), and as is evident from the data in table 3.5, there are only minimal differences in geometry between the two molecules. Furthermore each molecule lies upside down with respect to each other in the unit cell. This likely allows for favorable packing in the crystal lattice. For all the nickel complexes, Ni-I and Ni-N bond lengths are generally similar to those found in somewhat similar structures in the literature.[52]

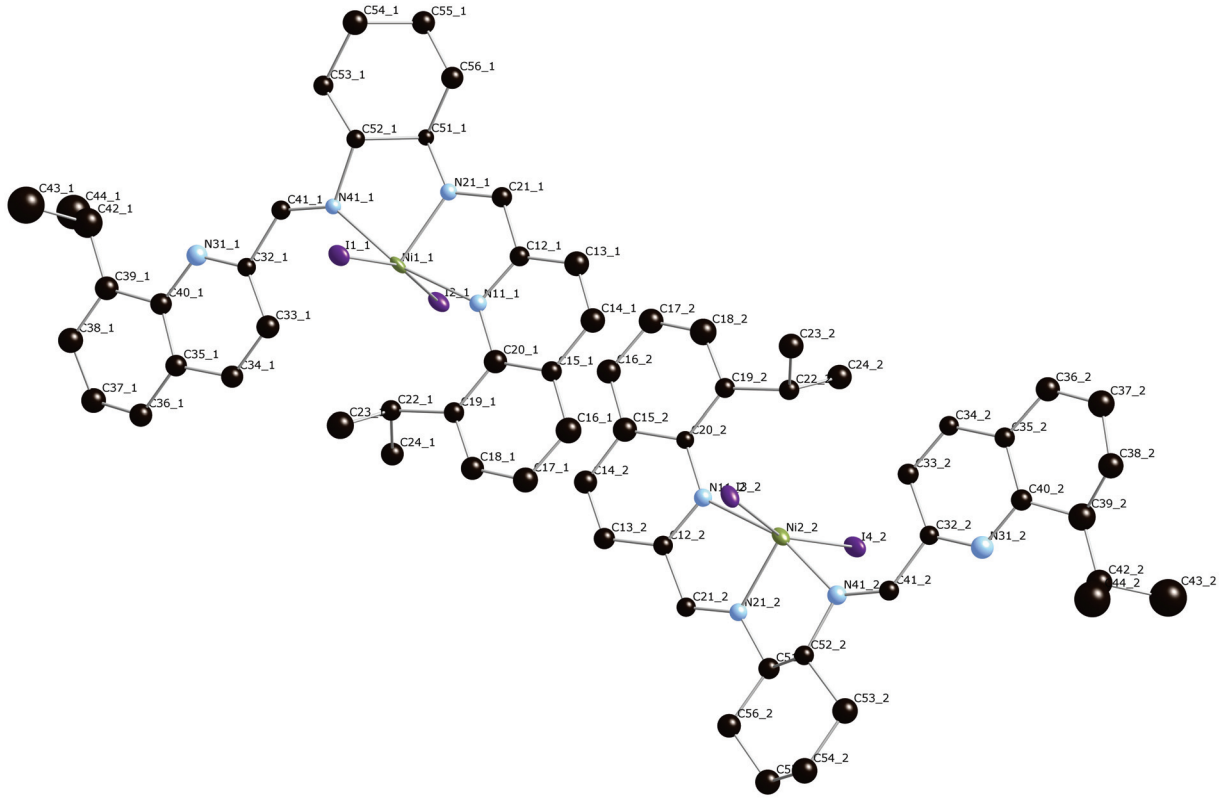

Figure 3.18 Thermal ellipsoid plots (50% probability) of (*R*,*R*)-**12**

Table 3.5 Selected bond lengths (Å) and bond angles (°) for (*R*,*R*)-**12**

	Molecule 1		Molecule 2	
Bond lengths	Ni_1-N_{41}	2.045(16)	Ni_2-N_{41}	2.079(19)
	Ni_1-N_{21}	1.913(18)	Ni_2-N_{21}	1.907(19)
	Ni_1-N_{11}	2.147(16)	Ni_2-N_{11}	2.175(16)
	Ni_1-I_1	2.638(3)	Ni_2-I_3	2.614(3)
	Ni_1-I_2	2.650(3)	Ni_2-I_4	2.637(3)
Bond angles	N_{21}-Ni_1-N_{41}	83.5(7)	N_{21}-Ni_2-N_{41}	82.3(7)
	N_{21}-Ni_1-N_{11}	81.6(6)	N_{21}-Ni_2-N_{11}	81.9(6)
	N_{41}-Ni_1-N_{11}	164.5(6)	N_{41}-Ni_2-N_{11}	163.2(7)
	N_{21}-Ni_1-I_1	101.4(6)	N_{21}-Ni_2-I_3	104.4(6)
	N_{21}-Ni_1-I_2	93.7(5)	N_{21}-Ni_2-I_4	93.5(6)
	I_1-Ni_1-I_2	164.4(12)	I_1-Ni_2-I_2	161.97(14)

Crystals of (*R*,*R*)-**14** grown from chloroform over which was layered toluene. The anticipated monohelix was not formed; instead a dinuclear complex with bridging iodides was the result (Figure 3.19). Each metal is coordinated via one imine nitrogen and one pyridyl nitrogen. Furthermore, iodide anions remain coordinated, two are bridging and two are non-bridging. The dinuclear core of the complex acts as a wedge pushing each sidearm outward. This has the effect of creating a butterfly shaped complex, which is clearly seen in the space filling model (Figure 3.20). The distance between the two metal centers is 3.305 Å. Some selected bond distances and bond lengths are included in Table 3.5. This is not the only dinuclear complex with bridging iodides to be synthesized in this work, similarly ligands derived from the binaphthyl backbone also form analogous nickel complexes. These are discussed further in chapter 4.

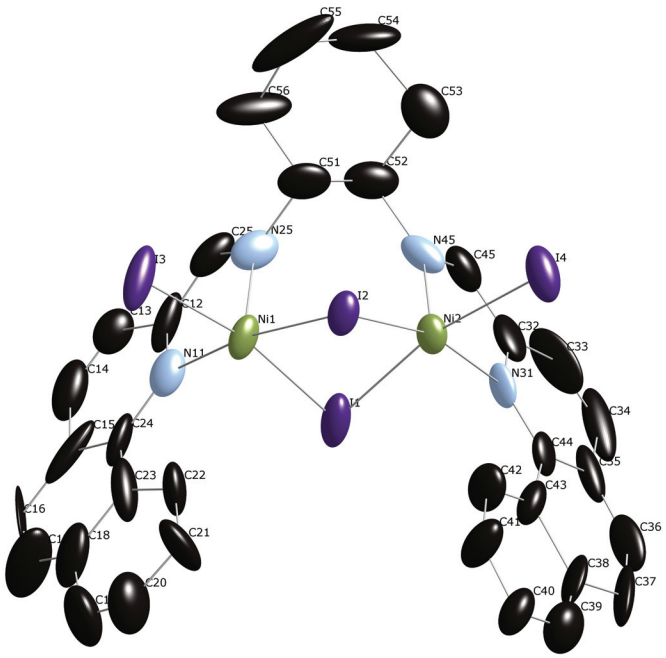

Figure 3.19 Thermal ellipsoid plot (50% probability) of (*R*,*R*)-**14**

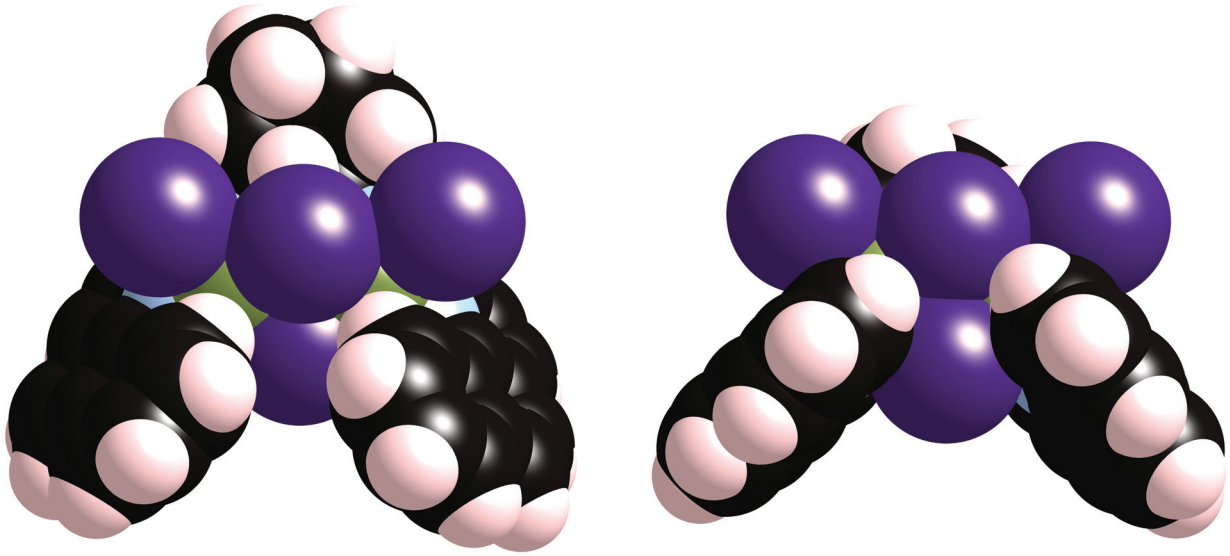

Figure 3.20 Space filling models of (*R*,*R*)-**14**

Table 3.5 Selected bond lengths (Å) and bond angles (°) for (*R*,*R*)-**14**

Bond lengths	Ni_1-N_{25}	1.958(13)	Ni_2-N_{45}	1.976(11)
	Ni_1-N_{11}	2.027(14)	Ni_2-N_{31}	2.044(11)
	Ni_1-I_1	2.466(13)	Ni_2-I_1	2.467(14)
	Ni_1-I_2	2.359(12)	Ni_2-I_2	2.328(12)
	Ni_1-I_3	2.635(13)	Ni_2-I_4	2.660(14)
Bond angles	N_{25}-Ni_1-N_{11}	83.1(6)	N_{45}-Ni_2-N_{31}	84.1(5)
	I_2-Ni_1-I_1	85.8(4)	I_2-Ni_2-I_1	86.4(4)
	I_2-Ni_1-I_3	93.1(4)	I_2-Ni_2-I_4	91.1(4)

Crystals of (*R*,*R*)-**16** were grown from chloroform over which was layered diethyl ether. The complex is 5-coordinate, with one of the positions having half occupation by I/OH (Figure 3.21). Furthermore the complex is coordinated to only three of the four nitrogen donors from the ligand. There are two molecules in the unit cell, each with only minimal differences in geometry with respect to the other. Selected bond lengths and angles are shown in Table 3.6.

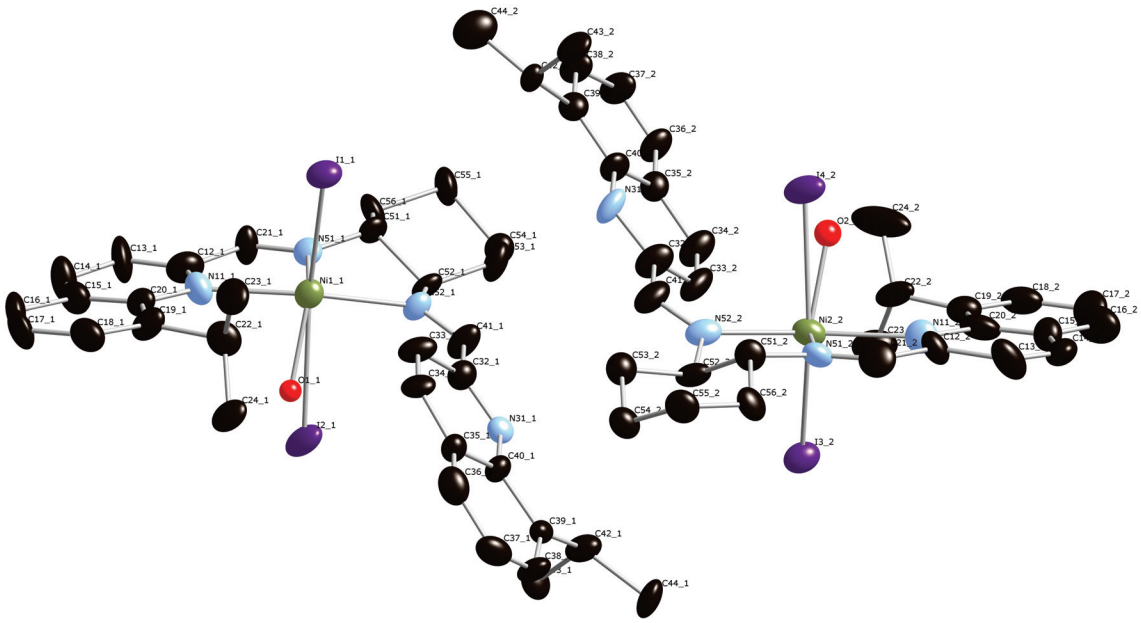

Figure 3.21 Thermal ellipsoid plots (50% probability) of (*R*,*R*)-**16**

Table 3.6 Selected bond lengths (Å) and bond angles (°) for (*R*,*R*)-**16**

	Molecule 1		Molecule 2	
Bond lengths	Ni_1-N_{51}	1.892(16)	Ni_2-N_{41}	1.929(16)
	Ni_1-N_{52}	2.142(18)	Ni_2-N_{21}	2.075(16)
	Ni_1-N_{11}	2.129(16)	Ni_2-N_{11}	2.160(16)
	Ni_1-O_1	1.892(18)	Ni_2-O_2	1.930(4)
	Ni_1-I_1	2.628(3)	Ni_2-I_3	2.643 (3)
	Ni_1-I_2	2.897(4)	Ni_2-I_4	2.759(3)
Bond angles	N_{51}-Ni_1-N_{11}	81.7(6)	N_{51}-Ni_2-N_{11}	79.7(7)
	N_{51}-Ni_1-N_{52}	80.7(5)	N_{51}-Ni_2-N_{52}	81.8(6)

So far we have seen a number of different coordination geometries for the two ligands; (*R*,*R*)-**5** and (*R*,*R*)-**11**, and in each case the ligand remains intact. A completely different structure is produced upon reaction of (*R*,*R*)-**5** with nickel(II) triflate (**17**): a double stranded helix ((*R*,*R*,*R*,*R*)-**18**) is the result (Figure 3.22). The two molecules in the unit cell are a 1:1 mixture of *M* and *P* helices and therefore diastereomers. Two tridentate ligands coordinate to one metal to create an octahedral complex, where both of the labile triflate anions have left the coordination sphere. The present ligand is the result of hydrolysis of the tetradentate ligand (*R*,*R*)-**5**. The new ligand has pyridine, imine and amine donors. The ammine moieties are cis to each other in the complex and each tridentate ligand orients in such a way as to lie almost perpendicular to each other. Due to this, and the twisted nature of the ligand, each behaves as if to wrap around each other in a helical fashion. This can be clearly seen in the space filling and stick model shown in Figure 3.23. Some selected bond lengths and angles are shown in table 3.7. Leznoff has reported a similar structure with his binaphthyl derived bis-imine ligand[39] (Figure 1.21). In this case, ligand hydrolysis to give the helical product also occurred.

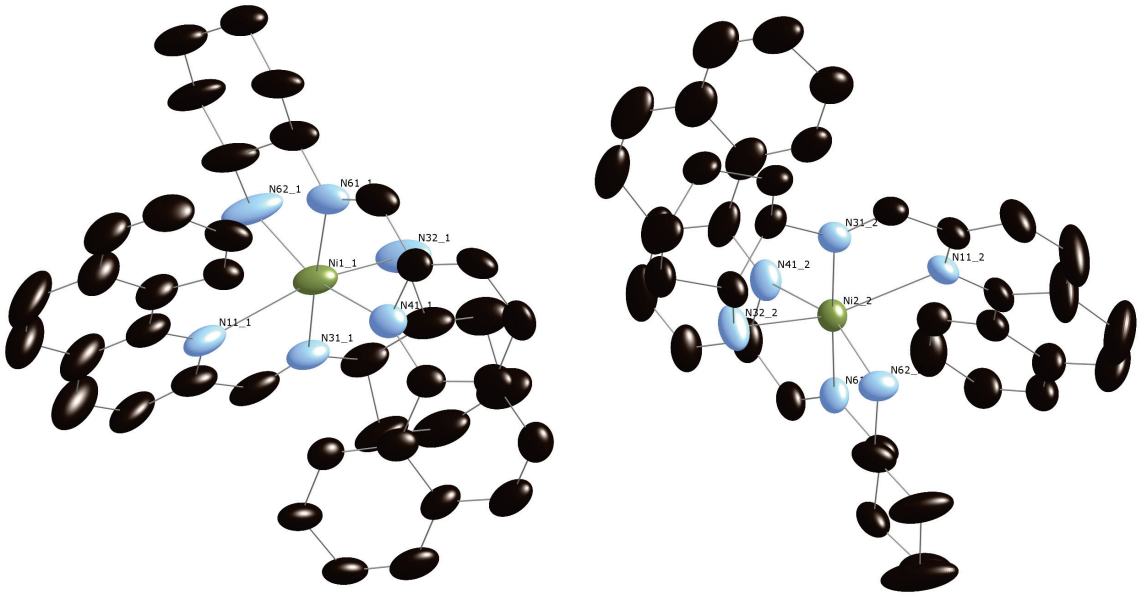

Figure 3.22 Thermal elipsoid plots (50% probability) of (*R*,*R*,*R*,*R*)-**18**, *M* (right) and *P* (left)

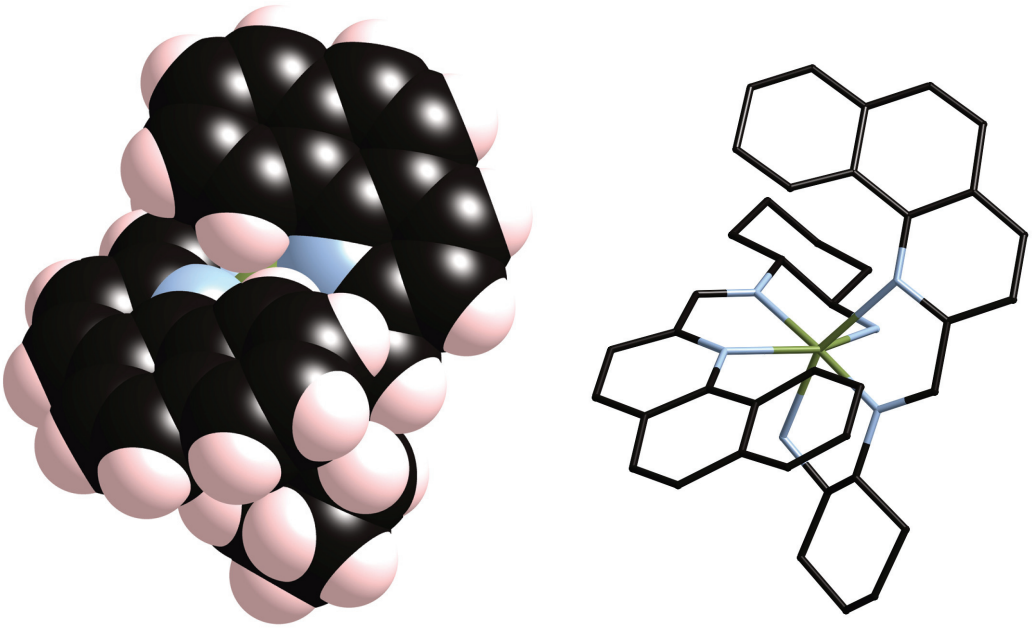

Figure 3.23 Space filling (left) and stick (right) model of (*R*,*R*,*R*,*R*)-**18**

(only the *P* form is shown)

Table 3.7 Selected bond lengths (Å) and bond angles (°) for (*R*,*R*,*R*,*R*)-**18**

	Molecule 1		Molecule 2	
Bond lengths	Ni_1-N_{31}	1.978(6)	Ni_2-N_{31}	1.978(5)
	Ni_1-N_{61}	1.994(6)	Ni_2-N_{61}	1.996(5)
	Ni_1-N_{62}	2.092(7)	Ni_2-N_{62}	2.096(5)
	Ni_1-N_{32}	2.096(7)	Ni_2-N_{32}	2.127(5)
	Ni_1-N_{11}	2.504(7)	Ni_2-N_{11}	2.349(5)
	Ni_1-N_{41}	2.300(6)	Ni_2-N_{41}	2.356(5)
Bond angles	N_{31}-Ni_1-N_{61}	174.3(2)	N_{31}-Ni_2-N_{61}	176.8(2)
	N_{61}-Ni_1-N_{62}	81.6(3)	N_{61}-Ni_2-N_{62}	82.3(2)
	N_{62}-Ni_1-N_{32}	94.8(3)	N_{31}-Ni_2-N_{61}	93.1(2)
	N_{31}-Ni_1-N_{41}	105.3(2)	N_{31}-Ni_2-N_{41}	107.4(2)

Bond distances for Ni-N bonds in the complexes; (*R*,*R*)-**11**, (*R*,*R*)-**12**, (*R*,*R*)-**14** (*R*,*R*)-**16** and (*R*,*R*,*R*,*R*)-**18** range between 1.892 and 2.504 Å. These bonds are of similar length to those observed in other Ni(II) complexes, with nitrogen donor ligands. For example typical bond distances for $[Ni(bipy)_3]^{2+}$ are between 2.08 and 2.10 Å,[53] and for $Ni(en)_3^{2+}$, between 2.13 to 2.14 Å.[54] Both Ni-N and Ni-I bond lengths are typical to those found in Ni(II) complexes with imine type donor ligands reported by Wieghardt[55] and Endres[56] (Figure 3.24).

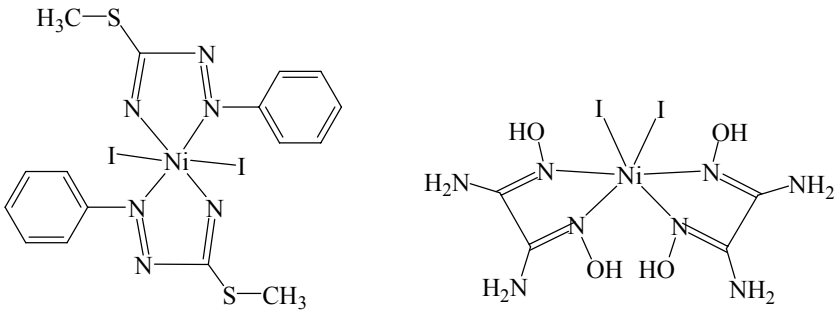

Wieghardt Endres

Figure 3.24 Nickel complexes of Wieghardt and Endres

In summary, ligands derived from the cyclohexyl backbone were found to afford complexes that exhibit many different coordination geometries. As discussed, often the reasons can be attributed to steric constraints of the ligand framework and the low lability of counterions (Cl^- and I^-). On the other hand the triflate anion was shown to be sufficiently labile, so as to leave the coordination sphere. In this case, hydrolysis of one imine bond in the ligand resulted in the formation of a double stranded complex. The different types of coordination geometries exhibited by some of these complexes are also observed in the literature.

Chapter 4

Syntheisis, characterization and study of complexes with the binaphthyldiamine backbone

4.1 Introduction

The previous chapter presented complexes formed with the cyclohexyl backbone. This chapter focuses on complexes containing the binaphthyl backbone. The binaphthyl unit is structurally more rigid than its cyclohexyl counterpart. This allows for a ligand that has less conformational mobility. Furthermore the binaphthyl moiety provides a greater twist, this could lead to complexes with deeply stepped structures.

4.2 Synthesis

The ligand (*R*)-**6** was metallated with zinc chloride to afford the dinuclear complex (*R*)-**19** (Figure 4.1). The yield is below 50% when a stoichiometric addition of zinc(II) chloride is employed. The underlying goal of this work is to produce single stranded mononuclear complexes, therefore initially a 1:1 mixture of ligand:metal was used. The presence of a large excess of unreacted ligand and the low yield pointed towards the formation of a dinuclear complex. From there on in, two equivalents of metal with respect to ligand was used in metallation reactions. Attempts to structurally characterize (*R*)-**19** were unsuccessful: even

though crystals were grown, they were too small and did not diffract well. However, there is sufficient evidence to suggest the desired compound was synthesized. Analysis by $^{1}H/^{13}C$ and 2D NMR revealed spectra that were suggestive of complex formation; these will be discussed further in the next chapter. The low yield and presence of unreacted ligand strongly indicate the formation of a dinuclear complex. Elemental data was consistent with calculated C, H, N values. Furthermore, the analogous dinuclear isopropylquinoline complex (*R*)-**20** (Figure 4.2) has been structurally characterized during previous work with these systems.

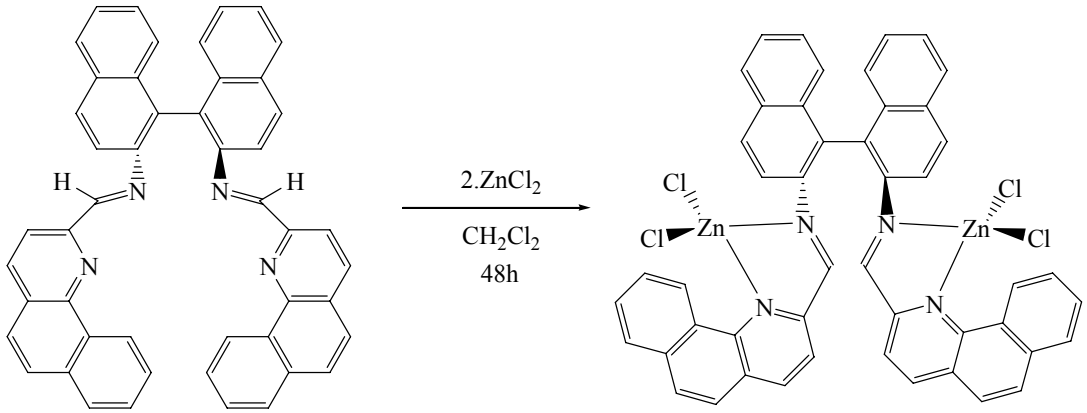

(*R*)-**6** (*R*)-**19**, 70%

Figure 4.1 Synthesis of dinuclear zinc complex (*R*)-**19**

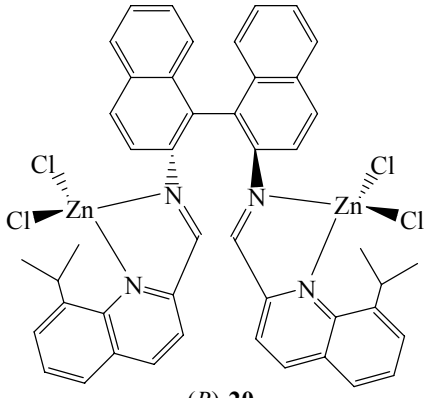

(*R*)-**20**

Figure 4.2 Dinuclear zinc complex (*R*)-**20**

Due to the relatively inert nature of the chloride anion it was sought to utilize the more labile triflate counterion to facilitate the formation of a monohelical complex. Ligand (*R*)-**6** was reacted with zinc trilfate in a two step procedure (Figure 4.3) to yield the reduced monohelical complex (*R*)-**21**. In the first step, the reaction mixture (ligand + metal) is heated to 55 °C in ethanol, the second step involves heating in toluene for 48 hours. During this procedure the ligand has undergone a reduction. It appears that ethanol has caused the reduction at one of the imine bonds by hydrogen transfer. There is precedence for this type of reduction in similar systems.[57] Reduction of the ligand leads to loss of C_2 symmetry, and this results in a C_1 symmetric complex. The number of signals observed by ^{1}H NMR is consistent with this loss of symmetry.

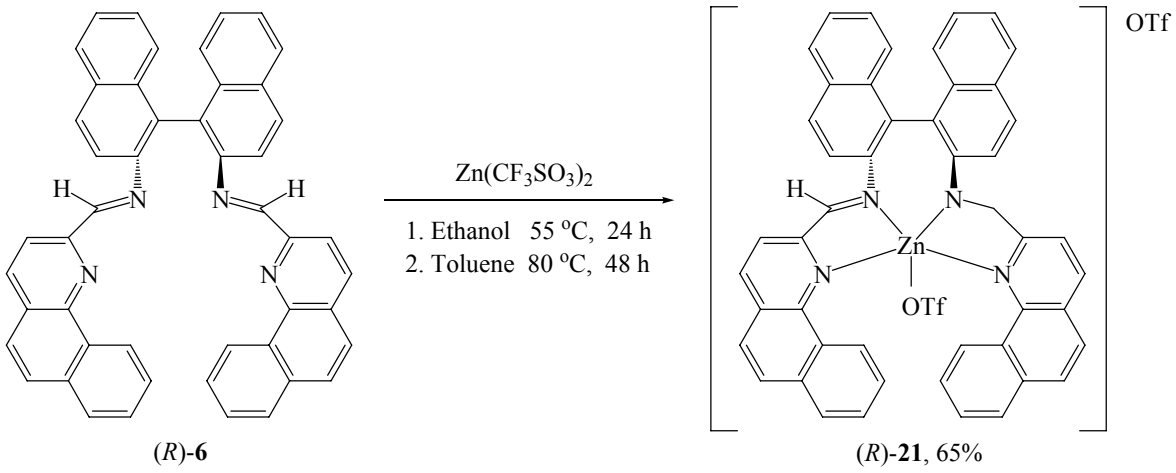

Figure 4.3 Synthesis of monohelical zinc complex (*R*)-**21**

In the case of (*R*)-**21**, there was sufficient lability in the triflte counterion to allow a monhelix to form. One triflate remains coordinated, while the other is in the outer coordination sphere. However, the reduction of one of the imine bonds, and therefore, the extra flexibility in

one of the side arms, is also a major contributing factor. Furthermore, due to the extra flexibility only the *P* helimer rather than the *M* is formed. In salen complexes, the (*R*)-binaphthyl backbone produces exclusively *M* helices. Unfortunately it was not possible to resynthesize (*R*)-**21**, repeated attempts only resulted in impure materials.

In further studies with ligands (*R*)-**6** and (*R*)-**22**, metallation reactions were carried out utilizing nickel iodide to afford the dinuclear complexes (*R*)-**23** and (*R*)-**24** respectively (Figure 4.4). Crystal structure analysis reveals that each nickel is 5-coordinate with two bridging

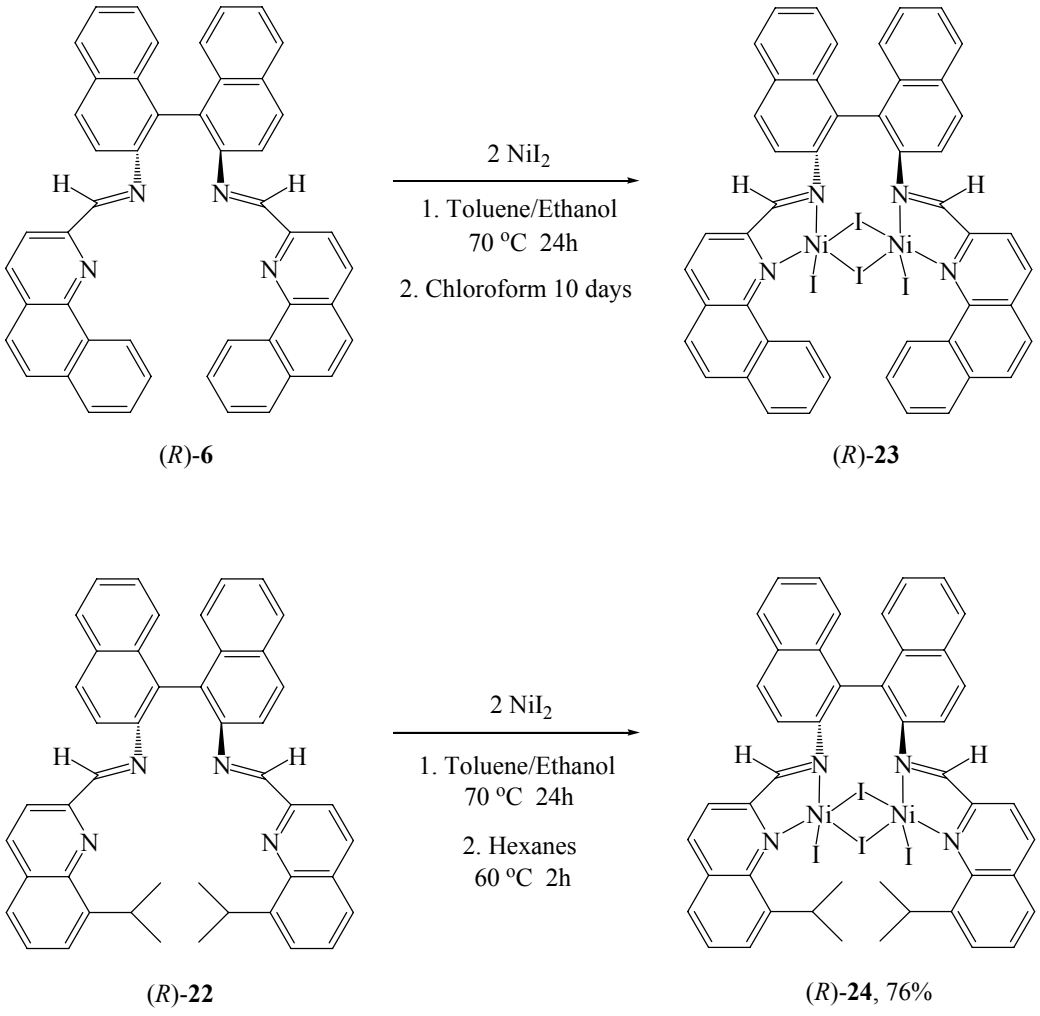

Figure 4.4 Synthesis of dinuclear nickel complexes (*R*)-**23** and (*R*)-**24**

iodides and one non-bridging iodide. In the case of (*R*)-**23**, the reaction was carried out in toluene and ethanol. Analysis by ^{1}H NMR, of the isolated solid after initial reaction in toluene and ethanol revealed the presence of impurities. These impurities are removed when by growing crystals from chloroform. Often a brown precipitate is also present: subsequent ^{1}H NMR analysis of this brown material indicated that it was the same as the crystalline material. In a similar sense, the synthesis of (*R*)-**24** also requires a two step procedure to remove unwanted impurities. After initial reaction in toluene and ethanol, the crude residue is heated to 60 °C in hexanes for 2 hours. Dinuclear complexes are formed regardless of either stoichiometric addition of nickel iodide, or the use of two equivalents. Therefore it is only obvious to use a 2:1 ratio of metal to ligand in order to maximize yields. Both complexes are sensitive to atmospheric oxygen and moisture; therefore NMR samples require the use of dry solvent. A complete NMR analysis was not possible due to the paramagnetic nature of complexes, however, they indicated compounds of high purity. Elemental analysis data confirmed this.

4.3 NMR spectroscopy of zinc and nickel complexes

The zinc and nickel complexes derived from the binaphthyl backbone were analyzed by NMR spectroscopy. Although solubility is generally low in organic solvents, reliable spectra could be collected. The 800 MHz ^{1}H NMR spectrum for (*R*)-**19** with assignment of protons is shown in Figure 4.5. The molecule is C_2 symmetric; there are fifteen resonances corresponding to the thirty hydrogens present in the molecule. It was not possible to grow crystals of (*R*)-**19** and so a full assignment of the proton signals helps us to provide further evidence for the

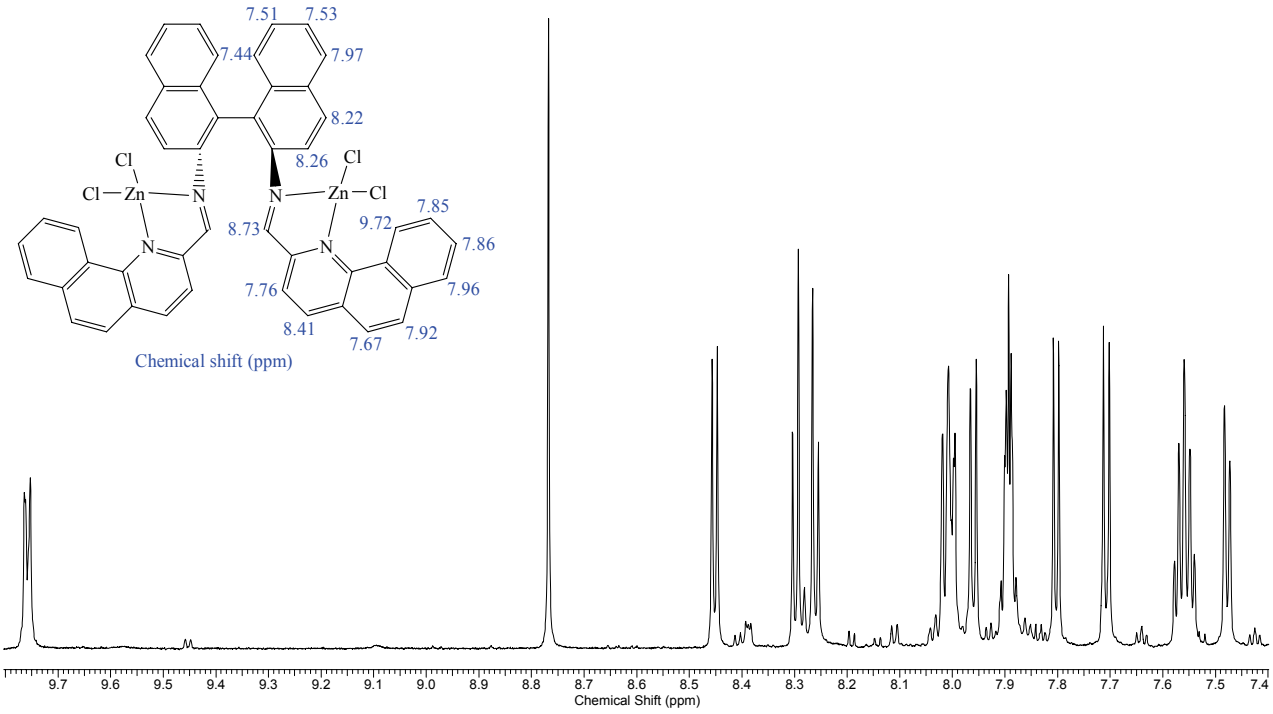

Figure 4.5 800 MHz ^{1}H NMR spectra of (*R*)-**19** (CD_2Cl_2) with assignments

formation of a dinuclear complex. As is expected with complex formation there are notable chemical shifts for the spectrum of (*R*)-**19** (Figure 4.5) compared to that of the ligand (Figure 2.9). For example, the peak at 8.80 ppm in the ligand spectrum now appears at 9.72 ppm, this proton experiences a greater shift than any other proton in the spectrum, likely due to the proximity to the metal. The peaks at 8.07 and 7.58 ppm in the ligand spectrum now appear at 8.41 and 7.58 ppm respectively. Interestingly, the singlet imine hydrogen experiences only a small chemical shift change on going from ligand to complex; 8.70 to 8.73 ppm. A comprehensive assignment of every proton was possible after analysis by COSY and NOESY (Figure 4.6). There are two adjacent pairs of triplet resonances in the spectra, each pair however, deceptively appears as a quintet due to overlap. The adjacent pair of triplet resonances from the backbone appear at 7.51 and 7.53 ppm, those from the sidearm resonate at 7.85 and 7.86 ppm.

This information could only be deciphered after using a combination of both COSY and NOESY experiments. As with the other ligands and complexes, the bay region hydrogen (9.72 ppm) appears at a higher chemical shift than the other hydrogens due to the ring current effect.

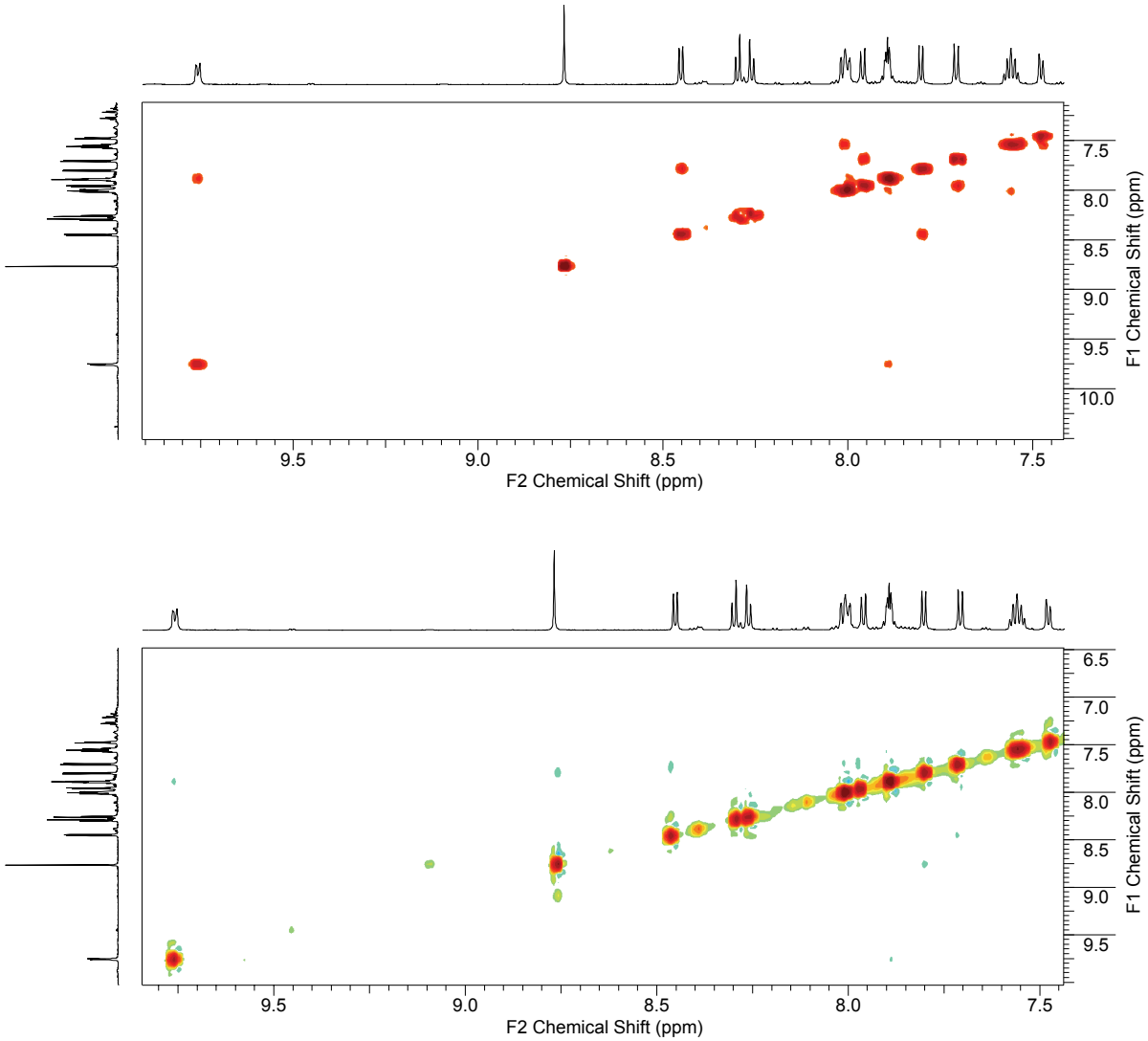

Figure 4.6 800 MHz COSY (top) and NOESY (bottom) NMR spectra for (*R*)-**19** (CD_2Cl_2)

In further analysis it is notable that there is a NOESY (through space) correlation between the imine hydrogen (8.70 ppm) and the one at 7.76 ppm of the sidearm. This correlation

was not seen in the NOESY spectra between the same two protons in the ligand spectrum (Figure 2.9). This is because these two protons are now closer to each other due to the ligand twist that results from complexation (Figure 4.7). In addition, the NOESY spectrum of (*R*)-**19** indicates no correlation between the imine hydrogen and the one at 8.26 ppm on the backbone. This correlation, however, is present in the NOESY spectrum of the ligand (*R*)-**6**. These two protons now lie far enough from each other that NOE is not experienced (Figure 4.7). This provides additional evidence for the formation of the dinuclear complex.

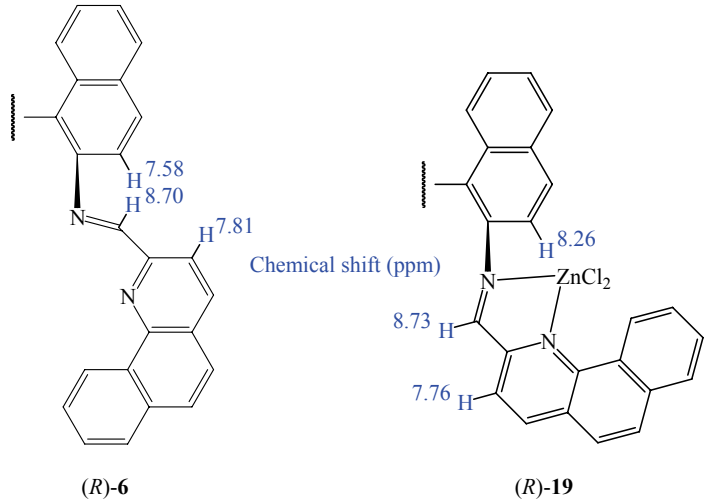

(*R*)-**6** (*R*)-**19**

Figure 4.7 Selected ^{1}H NMR data for (*R*)-**6** and (*R*)-**19**

The ^{1}H NMR spectrum for (*R*)-**21** is shown in Figure 4.8. Due to the reduction of one of the imine bonds, the molecule is no longer C_2 symmetric and the spectrum indicates the presence of 32 protons. This results in a ^{1}H NMR spectrum that is more complicated than previous spectra, with multiple resonances present over a relatively small chemical shift range. Coordination to zinc results in small changes in chemical shifts with respect to the ligand spectrum. The singlet peak at 9.74 ppm is likely due to the ammine hydrogen. This can often

appear highly shifted due to the proximity of the metal center and the conjugation present throughout the molecule. The presence of a number of multiplet peaks in the spectrum makes for difficult assignment of remaining protons, and sufficient sample to conduct 2D NMR experiments was not available. Chemical shifts are listed in listed in table 4.1.

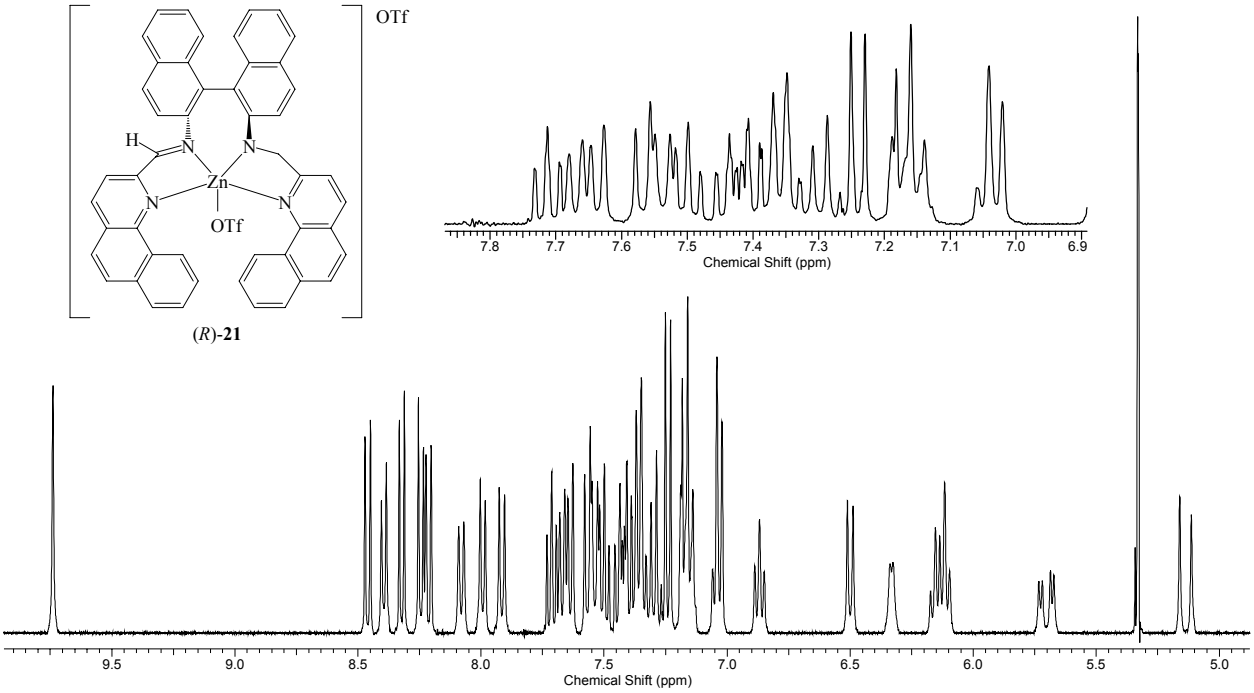

Figure 4.8 400 MHz ^{1}H NMR spectrum of (*R*)-**21** (CD_2Cl_2)

Table 4.1 400 MHz ^{1}H NMR (CD_2Cl_2) chemical shift data for (*R*,*R*)-**21** (multiplets)

	Chemical shifts, δ
(*R*,*R*)-**21**	(5.10-5.18), (5.66-5.75), (6.08-6.19), (6.30-6.36), 6.40, 6.87, 7.03, 7.05, (7.12-7.46), (7.47-7.59), (7.61-7.74), 7.92, 7.99, 8.08, 8.21, 8.24, 8.32, 8.39, 8.46, 9.74

The ^{1}H NMR spectra for (*R*,*R*)-**23** and (*R*,*R*)-**24** are shown in Figure 4.9. The spectral signals are broadened due to the presence of unpaired electrons on the nickel centers. The chemical shift data for (*R*,*R*)-**23** and (*R*,*R*)-**24** is listed in table 4.2. Peaks are often broadened and range between -3.94 to 46.20 ppm. Attempts to obtain ^{13}C NMR spectra for (*R*)-**23** and (*R*)-**24** were unsuccessful due to the paramagnetic nature of the complexes.

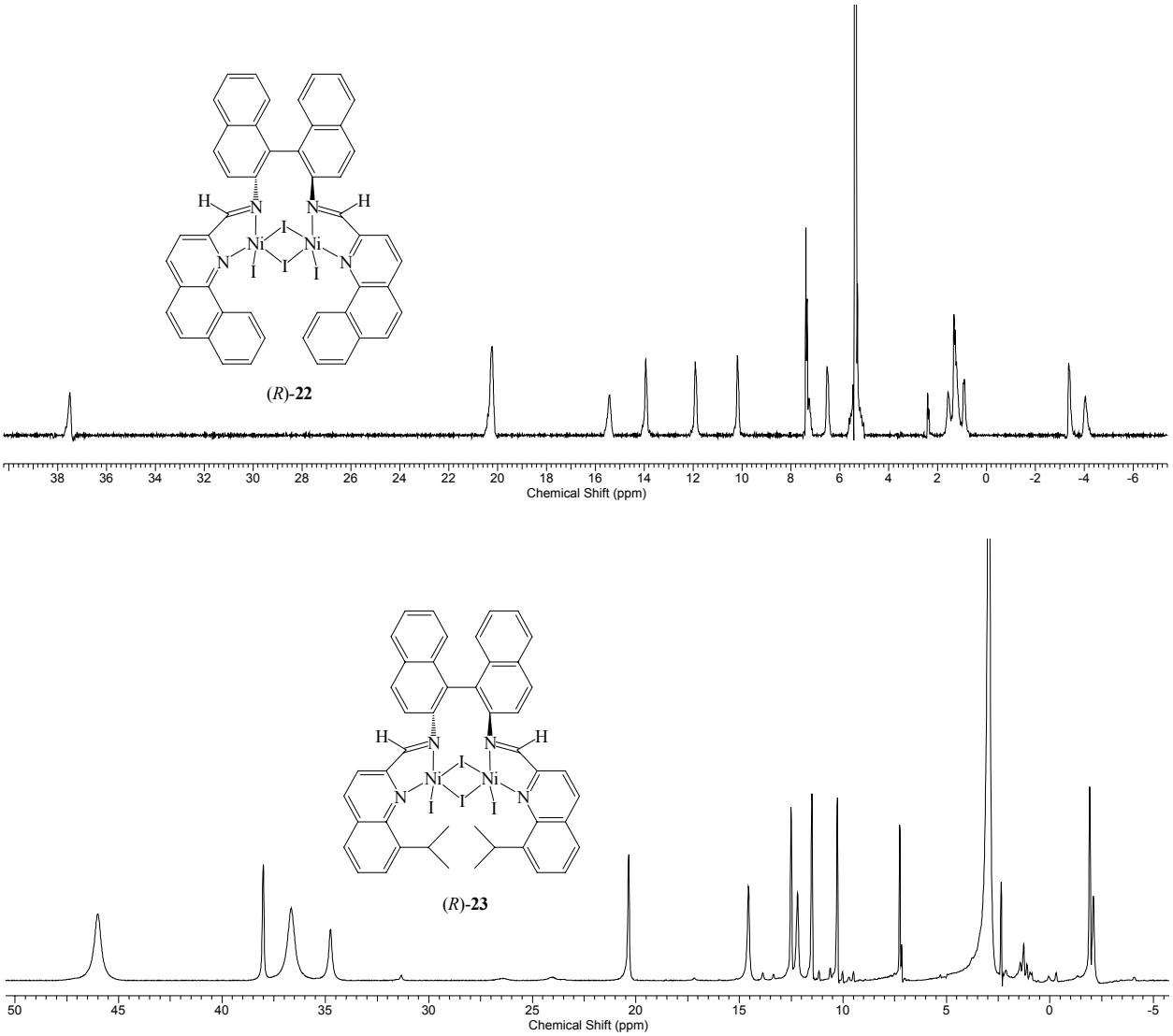

Figure 4.9 400 MHz ^{1}H NMR spectra ($CDCl_3$) of (*R*)-**23** and (*R*)-**24**

Table 4.2 400 MHz ^{1}H NMR ($CDCl_3$) chemical shift data for (*R*)-**23** and (*R*)-**24**

	Chemical shifts, δ
(*R*,*R*)-**23**	-3.94, -3.29, 6.46, 10.09, 11.80, 13.78, 15.28, 20.00, 23.80, 37.05, 37.80
(*R*,*R*)-**24**	-2.10, 10.29, 11.52, 12.20, 12.55, 14.60, 20.40, 34.85, 36.80, 46.20

4.4 Structural studies of zinc and nickel complexes

Several attempts to grow crystals of (*R*)-**19** only resulted in material that was not suitable for X-ray diffraction. Not only was the solvent diffusion method employed, but also vapor diffusion, slow cooling and evaporation methods. Often different solvent combinations were also used but with the same end result. Crystals of (*R*)-**21** were grown from methylene chloride over which was layered toluene. X-ray analysis revealed a monohelical complex, where one of the imine bonds has been reduced to an amine (Figure 4.10). The C-N bond length at the imine is 1.293 Å compared to the 1.473 Å at the amine. There is now an increased flexibility in one of the sidearms, and this is a major contributing factor in allowing the formation of a monohelix. The lability of the triflate counterion also plays a part. Furthermore, only the *P* helimer is produced: usually only the *M* helimer is produced when the (*R*)-backbone is utilized. This is likely due to the extra flexibility that has been introduced via the reduction. One indication of this, is the torsion angle on the ammine side (C_{23}-C_{35}-N_{35}-C_{13}) of the molecule which is -81.6°, compared to -161.3° near the imine (C_{53}-C_{65}-N_{65}-C_{43}).

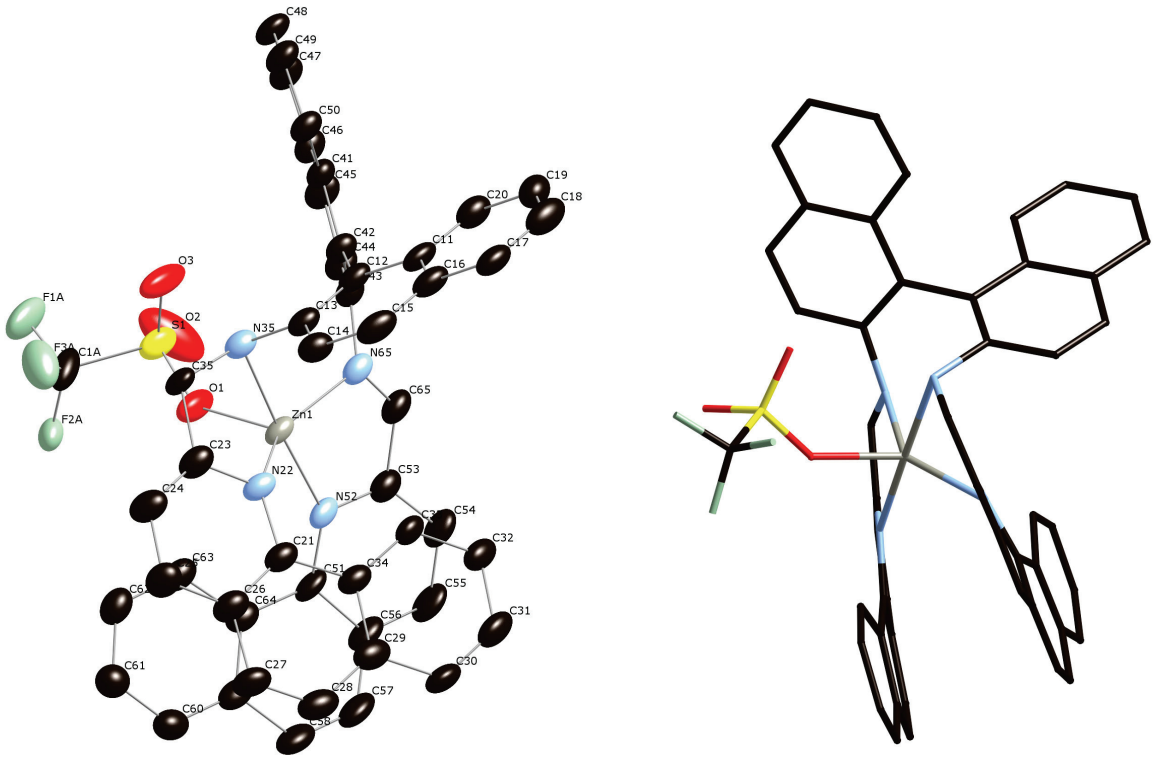

Figure 4.10 Thermal ellipsoid plot (50% probability) and stick model of (*R*)-**21**

The space filling model (Figure 4.11) indicates there are pi-pi interactions between the two arms of the ligand, the aromatic rings however do not lie directly on top of each other but are offset slightly. This creates an ideal face-to-face π-π interaction.[58] Distances between the two arms were calculated by measuring from the centroid of an aromatic ring in one arm to the closest carbon in the other arm (Table 4.3). The distances range from 3.278 to 3.533 Å. Typical distances for π-π interactions between aromatic rings are approximately 3.5 Å.[58] The degree of twist experienced by the binaphthyl backbone can be measured by the angle between the two napthyl planes, 76.54°. Other selected bond distances, bond angles, torsion angles interplanar angles are included in Table 4.3.

Table 4.3 Selected bond lengths (Å), bond angles (°) torsion angles (°), and interplanar angles (°) for (*R*,*R*)-**21**

Bond lengths	Zn_1-N_{65}	2.028(5)	*Cnt*1-C_{63}	3.278
	Zn_1-N_{22}	2.075(5)	*Cnt*2-C_{59}	3.469
	Zn_1-N_{52}	2.150(4)	*Cnt*3-C_{56}	3.533
	Zn_1-N_{35}	2.193(4)	*Cnt*4-C_{26}	3.391
	Zn_1-O_1	2.048(4)	*Cnt*5-C_{29}	3.442
	C_{35}-N_{35}	1.482(8)	*Cnt*6-C_{33}	3.323
	C_{65}-N_{65}	1.291(7)		
Bond angles	N_{65}-Zn_1-N_{22}	140.85(19)	N_{65}-Zn_1-N_{35}	95.7(2)
	N_{65}-Zn_1-N_{52}	81.8(2)	O_1-Zn_1-N_{52}	93.72(18)
	N_{22}-Zn_1-N_{52}	103.56(18)	O_1-Zn_1-N_{22}	120.0(2)
Torsion angles	C_{23}-C_{35}-N_{35}-C_{13}	-81.6(6)	C_{53}-C_{65}-N_{65}-C_{43}	-161.3(5)
Interplanar angles	($C_{41\text{-}50}$)-($C_{11\text{-}20}$)	76.54	($C_{11\text{-}20}$)-($C_{21\text{-}34}$)	71.94
	($C_{41\text{-}50}$)-($C_{51\text{-}64}$)	71.16	($C_{51\text{-}64}$)- ($C_{21\text{-}34}$)	10.41

Cnt = Centroid-1 = $C_{21\text{-}26}$, 2 = $C_{21,26,27,28,29,34}$, 3 = $C_{29\text{-}34}$, 4 = $C_{59\text{-}64}$, 5 = $C_{51,56,57,58,59,64}$, 6 = $C_{51\text{-}56}$

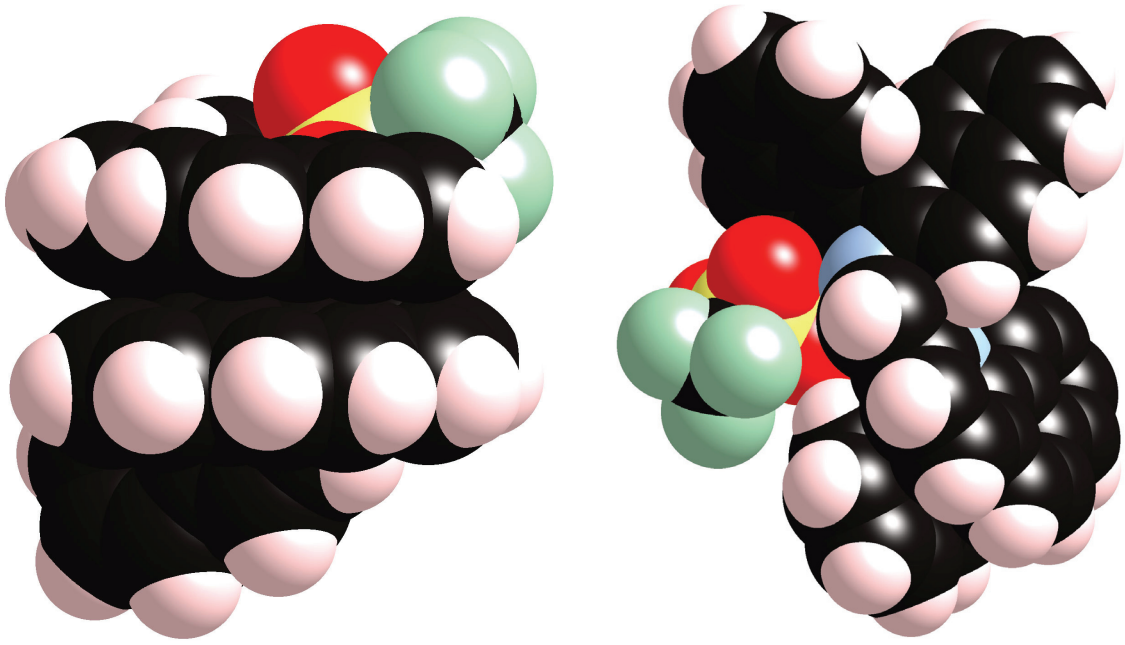

Figure 4.11 Space filling models of (*R*)-**21**; view from underneath (left) and from the side (right)

Crystals were grown of the nickel complex (*R*)-**23** from chloroform. Subsequent X-ray analysis revealed a dinucear nickel complex (Figure 4.12). Each metal is coordinated to one imine nitrogen and one pyridyl nitrogen. Of the four coordinated iodide anions, two are non-bridging and two are bridged between the two nickel atoms. The space filling model (Figure 4.13) shows a view looking at the molecule perpendicular to the Ni_2I_2 plane. It is clear that each

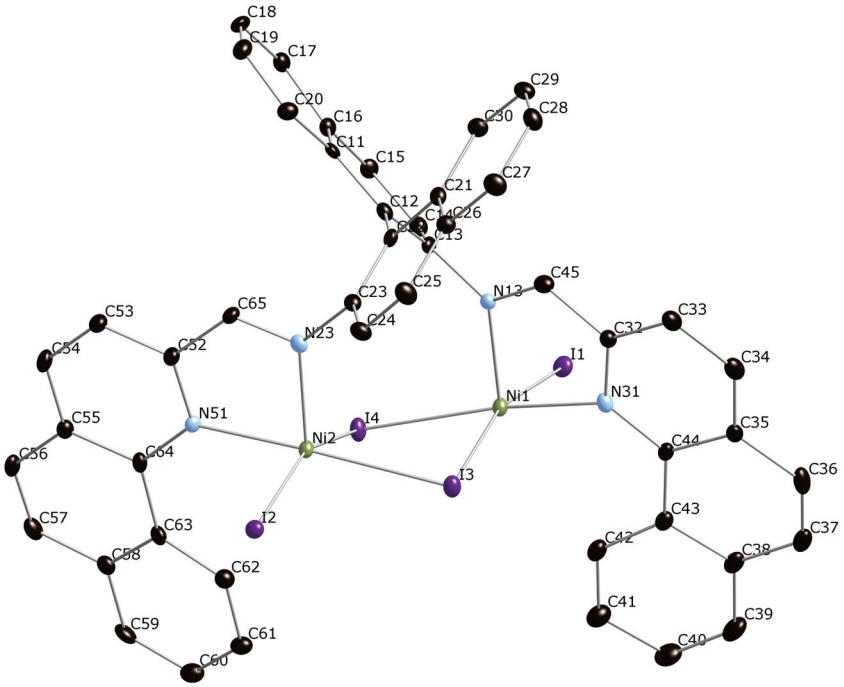

Figure 4.12 Thermal ellipsoid plot (50% probability) of (*R*)-**23**

arm wraps around the metal centers slightly offset from each other creating a stepped structure. This is the result of the chiral backbone being amplified through each arm. Furthermore the Ni_2I_4 moiety seems to act like a wedge, pushing each sidearm outwards. This effectively holds the arms in an offset fashion respective to each other as well as preventing any sidearm overlap.

Overall, the structure is very similar to that of a monohelix, except in this case there is a dinuclear core instead of a single metal and it exhibits solely *P* handedness.

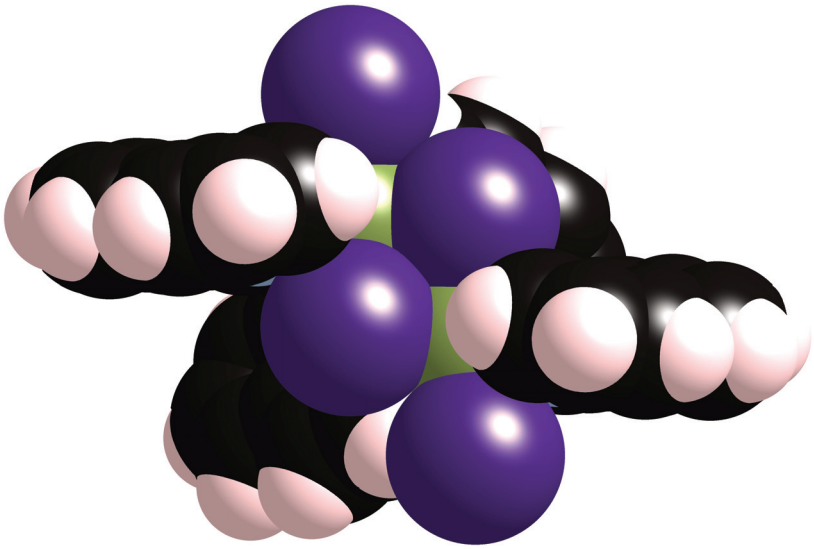

Figure 4.13 Space filling model (view perpendicular to Ni_2I_2 core) of (*R*)-**23**

An analogous complex to (*R*)-**23** is produced when ligand (*R*)-**7** is reacted with nickel iodide. The resulting dinuclear nickel complex (*R*)-**24** (Figure 4.14) has 5-cooordinate nickel centers with both bridging and non-bridging iodides present. It is clear from the space filling model (Figure 4.15) that a helical structure of solely *P* handedness is produced. The distance between the two Ni centers is 3.851 Å, compared with 3.812 Å for (*R*)-**23.** The dinuclear complex (*R*,*R*)-**14** has a much shorter Ni-Ni distance, 3.305 Å. Obviously this is due to the smaller "bite angle" of the cyclohexyl backbone, i.e. the two imine donors are closer to each other in the cyclohexyl backbone than in the binaphthyl. Usually there is also considerably less twist in the cyclohexyl backbone.

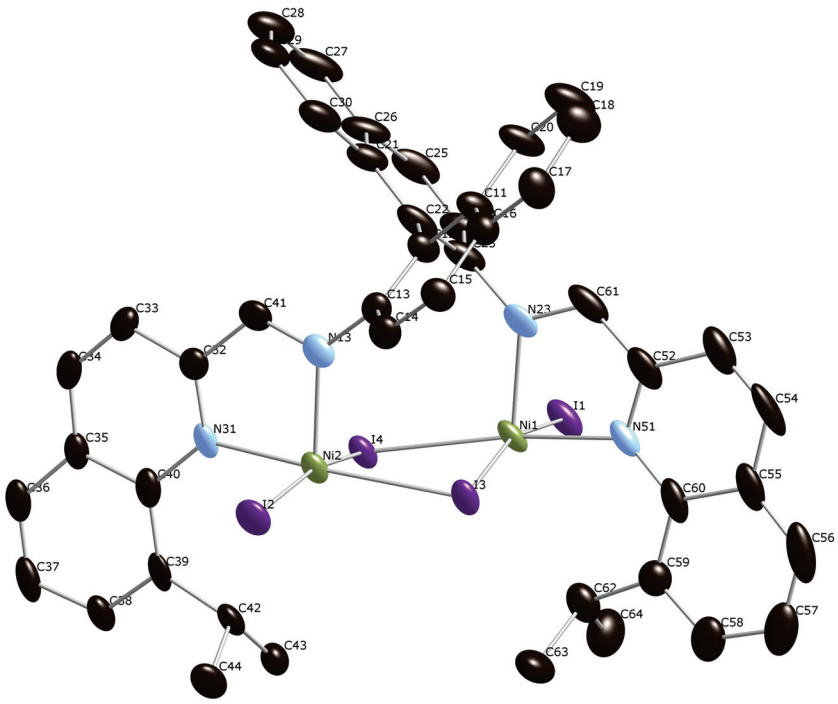

Figure 4.14 Thermal ellipsoid plots (50% probability) of (*R*)-**24**

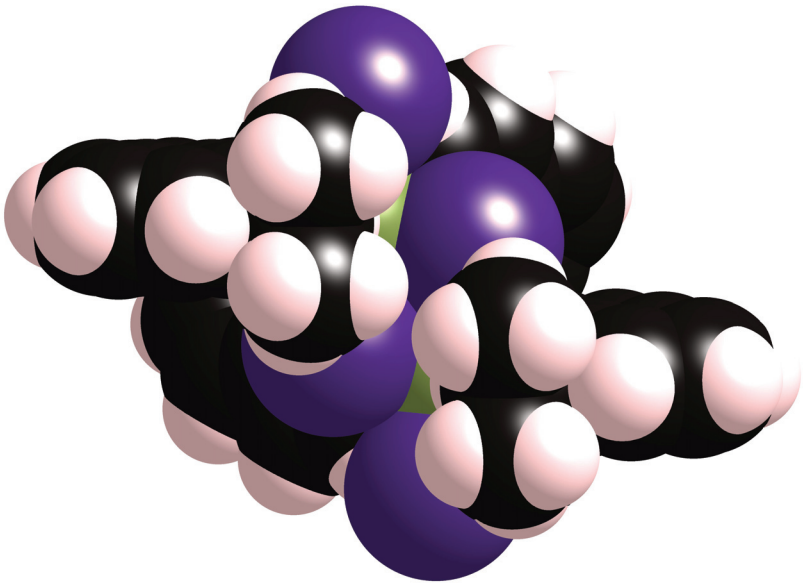

Figure 4.15 Space filling model (view perpendicular to Ni_2I_2 core) of (*R*)-**24**

A comparison of selected bond lengths and angles for the dinuclear complexes (*R*)-**23** and (*R*)-**24** is shown in table 4.4. In general, bond lengths around the metal center are similar for both complexes. For example, Ni-I bond lengths for the non-bridging iodides in (*R*)-**23** are 2.629 and 2.662 Å. For (*R*)-**24** the respective bond lengths are 2.673 and 2.675 Å. Similar comparisons can be made between Ni-N bonds and measured angles between napthyl and benzoquinoline planes. Furthermore, the degree of twist in the napthyl planes of the backbone is

Table 4.4 Selected bond lengths (Å), bond angles (°) and interplanar angles (°) for (*R*)-**24** and (*R*)-**25**

	(*R*)-**23**		(*R*)-**24**	
Bond lengths	Ni_1-N_{13}	1.992(3)	Ni_1-N_{23}	1.993(8)
	Ni_1-N_{31}	2.054(3)	Ni_1-N_{51}	2.030(8)
	Ni_1-I_1	2.629(5)	Ni_1-I_1	2.673(13)
	Ni_1-I_3	2.749(5)	Ni_1-I_3	2.777(12)
	Ni_1-I_4	2.652(5)	Ni_1-I_4	2.633(12)
	Ni_2-N_{23}	2.011(3)	Ni_2-N_{13}	2.007(8)
	Ni_2-N_{51}	2.093(3)	Ni_2-N_{31}	2.033(7)
	Ni_2-I_2	2.662(5)	Ni_2-I_2	2.675(12)
	Ni_2-I_3	2.677(6)	Ni_2-I_3	2.643(13)
	Ni_1-I_4	2.720(6)	Ni_2-I_4	2.751(13)
Bond angles	N_{13}-Ni_1-N_{31}	82.9(13)	N_{23}-Ni_1-N_{51}	82.7(4)
	N_{13}-Ni_1-I_1	98.3(9)	N_{23}-Ni_1-I_1	94.6(2)
	N_{31}-Ni_1-I_4	170.3(9)	N_{51}-Ni_1-I_4	171.5(2)
	I_3-Ni_1-I_4	85.5(16)	I_3-Ni_1-I_4	86.5(4)
	N_{23}-Ni_2-N_{51}	82.5(13)	N_{13}-Ni_2-N_{31}	83.7(3)
	N_{23}-Ni_2-I_2	96.7(9)	N_{13}-Ni_1-I_2	97.8(2)
	N_{51}-Ni_2-I_4	91.7(8)	N_{31}-Ni_1-I_4	83.3(2)
	I_3-Ni_2-I_4	85.6(15)	I_3-Ni_2-I_4	86.8(4)
Interplanar angles	($C_{11\text{-}20}$)-($C_{21\text{-}30}$)	78.71	($C_{11\text{-}20}$)-($C_{21\text{-}30}$)	84.82
	($C_{11\text{-}20}$)-(N_{31}-C_{44})	63.11	($C_{11\text{-}20}$)-(N_{31}-C_{40})	62.28
	($C_{21\text{-}30}$)-(N_{51}-C_{64})	75.06	($C_{21\text{-}30}$)-(N_{51}-C_{60})	75.53
	(N_{31}-C_{44}) -(N_{51}-C_{64})	7.88	(N_{31}-C_{40}) -(N_{51}-C_{60})	3.38

similar in each complex; 78.71° and 84.82° respectively for (*R*)-**23** and (*R*)-**24**. In the dinuclear complexes reported by Leznoff,[39] the Cu(μ-Cl_2) complex exhibits a napthyl-napthyl dihedral angle of 78.5° (Figure 1.22). Similar to the complexes studied in this work, the ligand adopts an open framework to accommodate the bridged metal species.

There are many examples of dinuclear nickel complexes with various bridging groups in the literature. For example, complexes with carbonyl,[59] chloride,[60] bromide,[61] and hydroxide bridges[62] have been reported previously. Dinuclear nickel complexes with bridging iodide anions are not as common, however there are some examples in the literature.[63] Typical bridging Ni-I bond distances range between approximately 2.5 and 2.8 Å. This concurs well with the data in Table 4.4 for complexes (*R*)-**23** and (*R*)-**24** (I_3 and I_4 are bridging). The Ni-N bond lengths range between 1.992 Å and 2.093 Å. These are of similar length to those observed in nickel complexes with nitrogen donor ligands.[53-56]

In summary, ligands derived from the binaphthyl backbone were found to afford both mononuclear and dinuclear complexes. Even though a crystal structure of (*R*)-**19** was not obtained, sufficient data was collected (NMR and elemental) to confirm its existence. A monohelical complex of exclusively *P* handedness was afforded, after ligand reduction at one of the imine bonds. In this case, the use of the triflate anion proved to be an important factor in determining the formation of a monohelix. Dinuclear complexes were formed when the less labile chloride and iodide anions were utilized. The dinuclear nickel complexes (*R*)-**23** and (*R*)-**24** were found to be helical with solely *P* handedness.

Chapter 5

Syntheisis, characterization and study of bis(quinolylcarboxamide) ligands and complexes

5.1 Introduction

In the previous two chapters it was shown that neutral imine-pyridine ligands generally lead to dinuclear complexes. One of the reasons for this is the inability of the neutral nitrogen donors to compete with and displace the anionic ligands of the metal. This led us to explore the use of dianionic bis-amide ligands. These ligands are attractive due to their ability to stabilize metals in high oxidation states, their resistance to oxidation and their facile synthesis. The synthesis of ligand (*R*,*R*)-**26** has been reported previously,[31] while ligand (*R*)-**27** is new.

5.2 Synthesis

Generally the synthesis of bis(amides) involves a condensation reaction between the appropriate carboxylic acid and amine in the presence of triphenyl phosphite (TPP).[64] TPP is required as a coupling agent[65] and reactions are often carried out in pyridine. For the synthesis of the amide ligands (Figure 5.1) quinaldic acid **25** is first required. Quinaldic acid is readily available commercially, however due to the expense and amount needed, it was synthesized according to literature procedures.[66] Reaction of quinaldic acid and the appropriate diamine backbone in the presence of TPP affords the ligands (*R*,*R*)-**26** and (*R*)-**27** (Figure 5.1). The

reactions are carried out by refluxing in pyridine. In the case of (*R*,*R*)-**26** purification of the crude product was achieved through several washes with toluene. For (*R*)-**27** the crude product was redissolved into methylene chloride, and the pure compound was then precipitated out by adding ethanol. These simple purification techniques yield pure products and removed residual pyridine. The yields are good for both ligands and they are isolated in high purity as indicated by ^{1}H NMR and elemental analysis. The syntheses were carried out without the use of inert conditions and the ligands are stable to atmospheric oxygen and moisture. The same methodology was employed to synthesize (*rac*)-**26**: this time *trans*-1,2-cyclohexanediamine was utilized rather than the *R*,*R* enantiomer.

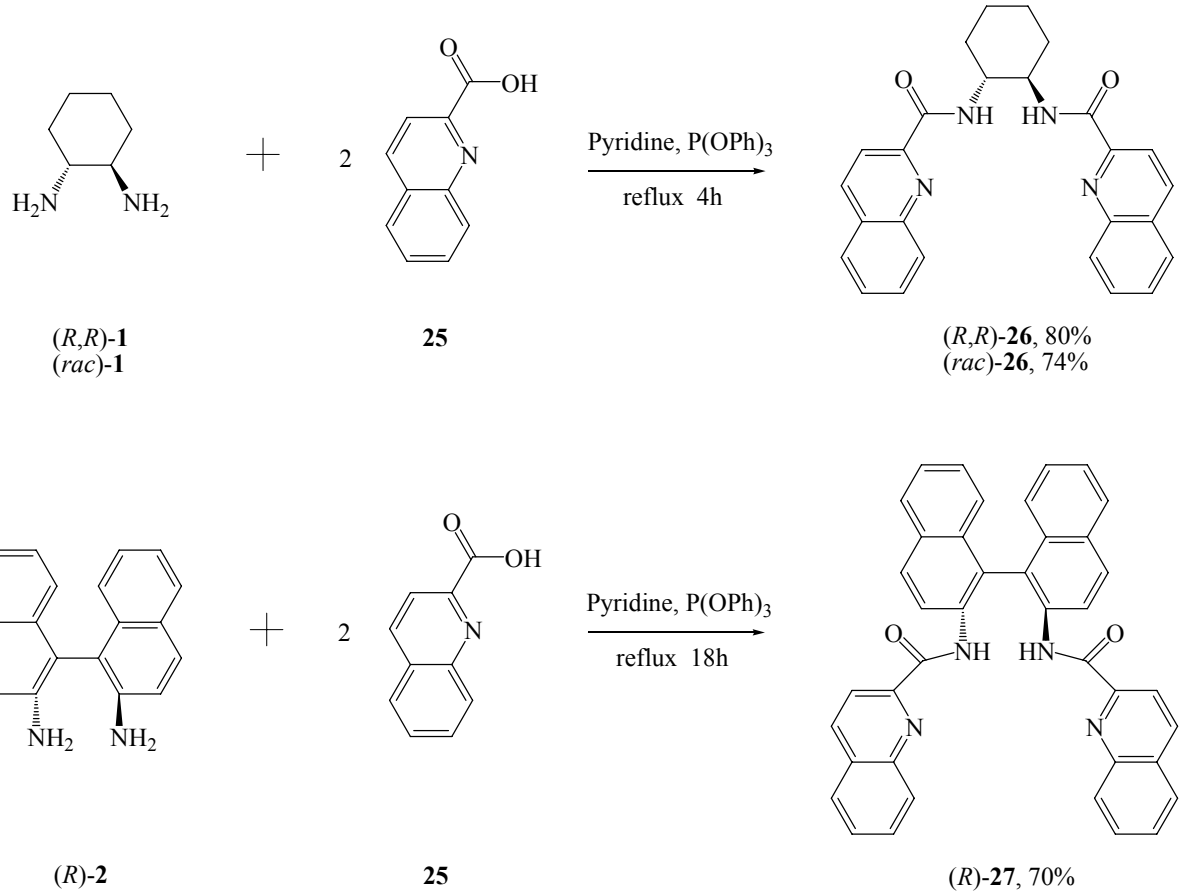

Figure 5.1 Synthesis of ligands (*R*,*R*)-**26** and (*R*)-**27**

The ligands (*R*,*R*)-**26** and (*R*)-**27** were subsequently used to carry out metallation reactions, typically under rigorously inert and dry conditions. Ligand (*R*,*R*)-**26** was reacted with both iron(II) chloride and iron(II) triflate, with and without base (NEt_3) respectively (Figure 5.2). In both cases, dramatic changes in the color of the reaction suggested complex formation. This was confirmed by ^1H NMR spectra indicating paramagnetic compounds. Complexes (*R*,*R*)-**28** and (*R*,*R*)-**29** were purple and red/orange respectively.

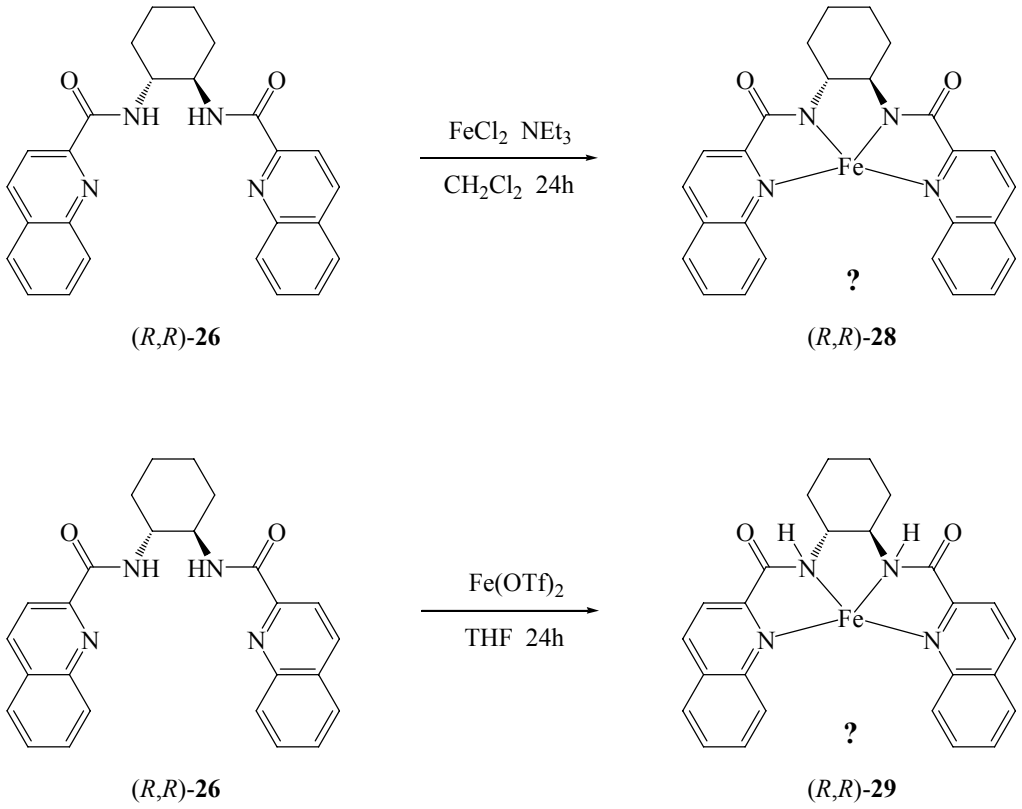

(*R*,*R*)-**26** (*R*,*R*)-**28**

(*R*,*R*)-**26** (*R*,*R*)-**29**

Figure 5.2 Synthesis of iron complexes (*R*,*R*)-**28** and (*R*,*R*)-**29** (CD_2Cl_2/pyridine-d^5)

It is anticipated that the complexes formed are monohelices, however, due to lack of structural data no definitive conclusion can be made here. Attempts to grow suitable crystals were unsuccessful. Purple crystalline needles were grown for (*R*,*R*)-**28**, however they did not

diffract well enough to produce a reliable data set. Twinned orange crystals were obtained for (*R*,*R*)-**29**, however attempts to cut these crystals resulted only in shattering the crystal. Consequently no structural data was obtained and therefore yields are not reported. The ligand (*R*)-**27** was metallated with iron(II) chloride in the presence of sodium methoxide (base) to form the double stranded dihelicate complex, (*R*,*R*)-**30** (Figure 5.3). Suitable crystals were grown of this compound.

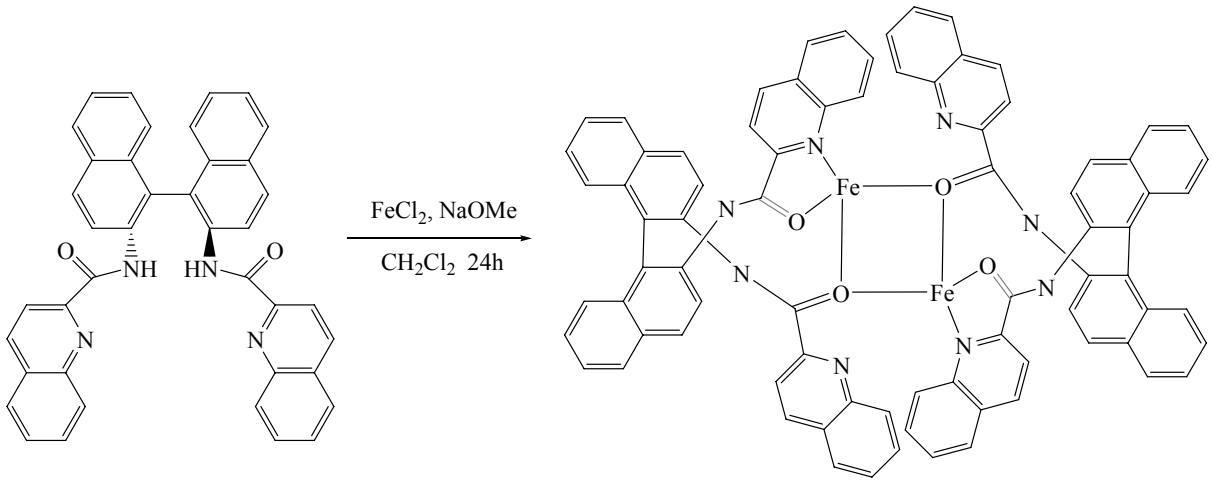

Figure 5.3 Synthesis of double stranded iron complex (*R*,*R*)-**30**

Structural analysis revealed a complex that has two ligands and two iron atoms. Furthermore two of the four pyridyl nitrogens are coordinated to the metal, while amide nitrogens do not coordinate despite being deprotonated. Instead, amide oxygens are coordinated. It was anticipated that the ligands (*R*,*R*)-**26** and (*R*)-**27** would form mononuclear complexes through coordination by the four nitrogen donors of the ligand. However, it seems there are competitive nitrogen and oxygen donors in the amide ligands. The resulting complex in this case is a double stranded complex that can be classed as a helicate. Interestingly the ^{1}H NMR spectra

for the complex does not appear to be paramagnetic, thus indicating that a low-spin Fe(II) complex is formed. ^{1}H NMR spectroscopy studies are discussed further in section 5.2.

The coordination behaviour of the (*R*)-**27** is not the first example of competitive oxygen/nitrogen donors in bis-amide ligands. Yamasaki[33] and Vagg[34] have discussed this phenomenon, typically the type of coordination is dependant on the synthetic conditions employed. N_4-tetradentate coordination of the ligand usually requires that the amide moiety be deprotonated. An example reported by Vagg, where deprotonated ligand coordinates to copper is shown in Figure 5.4.[67] An example of a ruthenium complex formed via N_4-coordination of a similar bis-amide ligand (deprotonated) was shown in Figure 1.17.

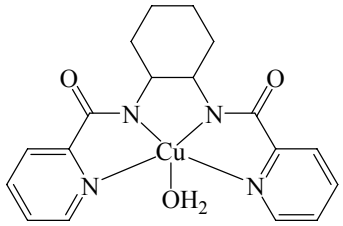

Vagg

Figure 5.4 Vagg's copper complex

In general, it has been shown that, coordination will occur through the carbonyl oxygen when the amide nitrogen is protonated. The molybdenum and palladium complexes of Perez[51] and Lloyd-Jones[68] respectively (Figure 5.5) were derived from protonated ligands. Reported crystal structures displayed coordination through amide oxygen atoms. The complex (*R*,*R*)-**30**, synthesized in this work exhibits coordination through amide oxygens, even though amine nitrogens are deprotonated.

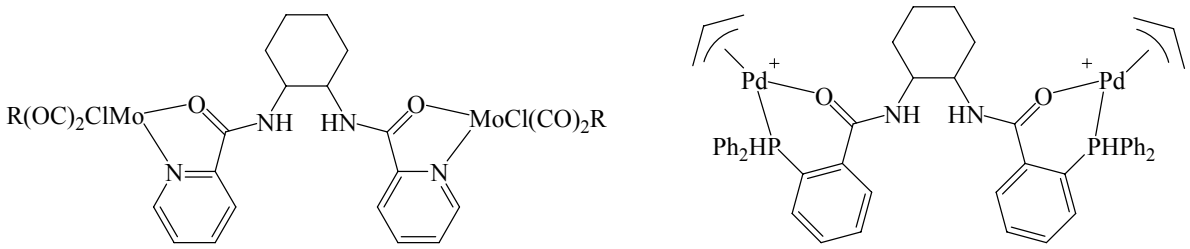

Perez Lloyd-Jones

Figure 5.5 Amide oxygen coordination (R = η^3-C_3H_5)

Numerous attempts to incorporate different metal salts into (*R*,*R*)-**26** and (*R*)-**27** and were unsuccessful. Iron(II) triflate, zinc(II) chloride, zinc(II) acetate nickel(II) chloride and manganese(II) triflate, were all utilized. Often, low solubility of these metal salts in organic solvents ruled out their use. For those where solubility was not an issue, initial characterization attempts with ^{1}H NMR spectroscopy resulted in only impure and often broadened spectra. Several attempts to grow suitable crystals were also unsuccessful.

5.3 NMR spectroscopy of ligands and complexes

The ligands and iron complexes were characterized by ^{1}H NMR spectroscopy. The 400 MHz ^{1}H NMR spectrum of (*R*,*R*)-**26** is shown in Figure 5.6. The number of resonances is half of that possible since the molecule is C_2 symmetric. Slightly broadened peaks in the aliphatic region of the spectrum correspond to the cyclohexyl backbone. This line broadening is a result of minor ring fluctuations. The broadened singlet peak at 8.52 ppm resonates from the amide protons.

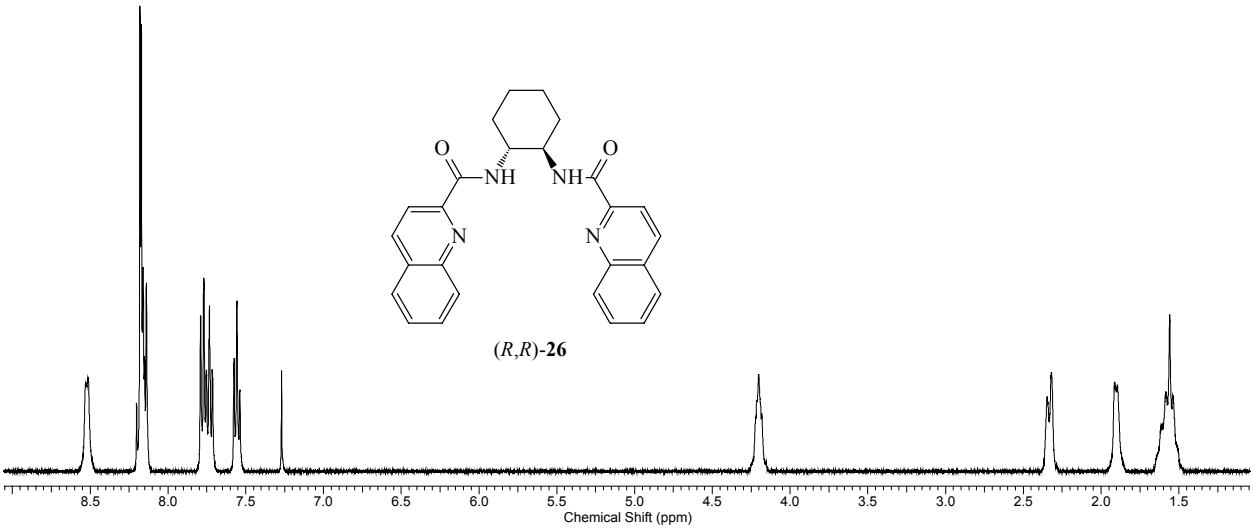

Figure 5.6 400 MHz ^{1}H NMR spectra of (*R*,*R*)-**26** ($CDCl_3$)

The ^{1}H NMR spectrum for (*R*)-**27** is shown in Figure 5.7. The molecule is C_2 symmetric: there are 13 resonances corresponding to 26 hydrogens. Of the 26 aromatic hydrogens, 14 reside as multiplet peaks in the region between 7.25 and 7.75 ppm. The amide hydrogen appears as a broadened singlet peak at 10.50 ppm. The particularly low field shift of the amine hydrogen is

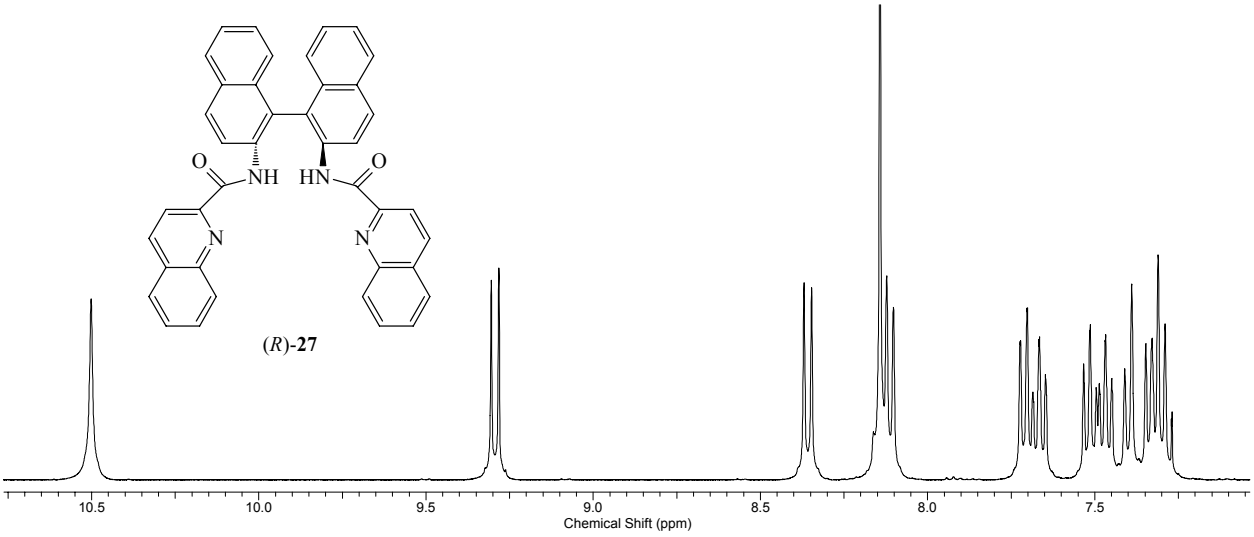

Figure 5.7 400 MHz ^{1}H NMR spectra of (*R*)-**27** ($CDCl_3$)

attributed in part to the increased electron withdrawing character of the bianphthyl backbone. Compared to the cyclohexyl backbone, the amide proton in the binaphthyl backbone is more acidic and more deshielded, therefore it appears at a higher chemical shift.

^{1}H NMR studies were also carried out for the iron(II) complexes (*R*,*R*)-**28**, (*R*,*R*)-**29** and (*R*,*R*)-**30**. Iron(II) has a $3d^6$ electronic configuration and often forms high spin complexes that are paramagnetic. Low spin iron complexes are able to form diamagnetic complexes. The ^{1}H NMR spectra for (*R*,*R*)-**28** and (*R*,*R*)-**29** are shown in Figure 5.8. Extensive line broadening

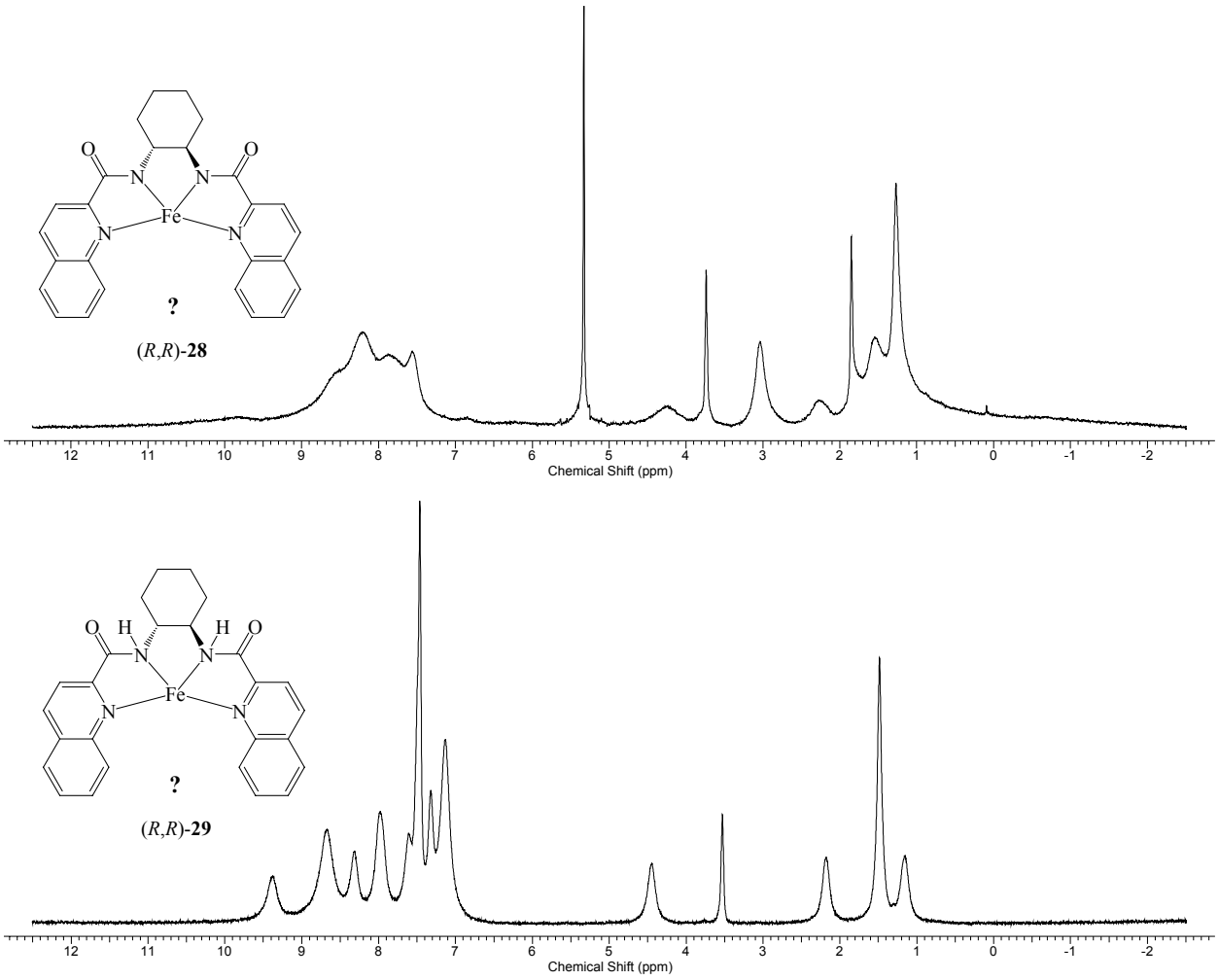

Figure 5.8 400 MHz ^{1}H NMR spectra of (*R*,*R*)-**28** (CD_2Cl_2) and (*R*,*R*)-**29** (pyridine-d^5)

clearly indicates the possibility of paramagnetic complexes, although the chemical shift range appears normal. When the two spectra (Figure 5.6) are compared to the ligand spectrum, (Figure 5.4) it is clear that no significant shifts have occurred from the normal diamagnetic range. Thus exchange broadening of fluxional complexes may also explain the spectral appearance. A complete NMR analysis is therefore difficult. In any case, a variable temperature study was undertaken with (*R*,*R*)-**29** to determine if any fluxional processes were at play.

Several spectra, each taken at different temperatures ranging from 25 °C to -60 °C are shown in Figure 5.9. A mixture of dueterated solvents is used for the analysis. Pyridine-d^5 is used for facile solubility of (*R*,*R*)-**29** and a few drops of CD_2Cl_2 are added as an internal reference between spectra at different temperature. The spectrum taken at 25 °C is broadened significantly, upon cooling there is a gradual increase in the sharpness of spectra in the aromatic region. Peaks in the aliphatic region are generally broad at room temperature due to ring fluctuations of the cyclohexyl backbone. The exact nature of the fluxional process is unclear and further studies are required to determine this. The presence of competitive nitrogen and oxygen donors in the ligand has been discussed earlier, thus coordination exchange between oxygen and nitrogen is a possibility. Monomer to dimer transitions and ion hopping within the dihelicate pocket are also possibilities. The latter is evident considering the partial occupancy of four iron centers in the crystal structure. Each is only 50% occupied and therefore only two are present at any one time. This is discussed further in the next Section 5.4.

No definitive conclusions can be made as to whether the desired compounds, (*R*,*R*)-**28** and (*R*,*R*)-**29** were synthesized due to the inherent difficulty in assigning highly broadened spectra and the lack of structural data.

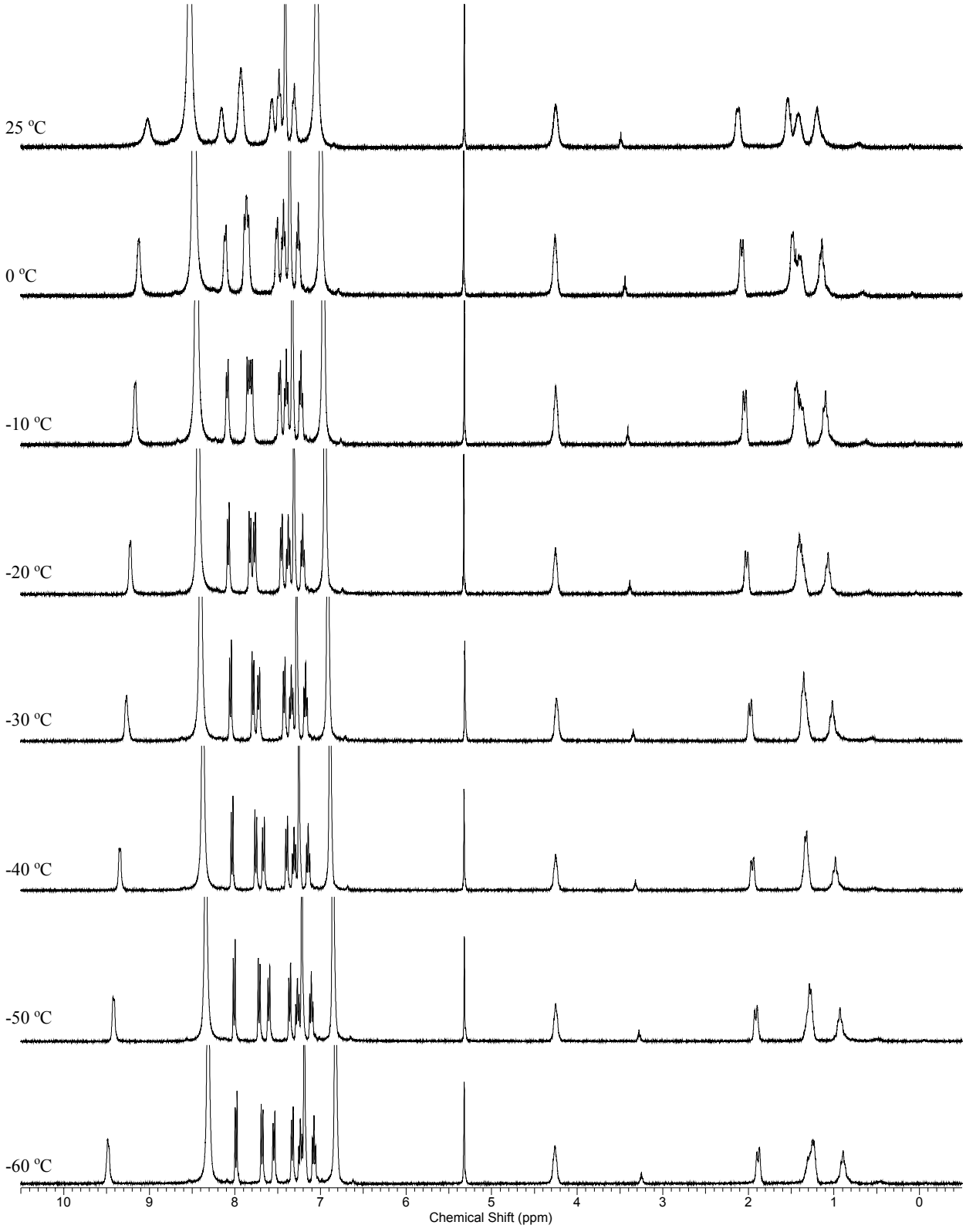

Figure 5.9 400 MHz VT ^{1}H NMR spectra for (*R*,*R*)-**29** (Pyridine-d^5/CD_2Cl_2)

The ^{1}H NMR spectrum for the dihelicate iron complex (*R*,*R*)-**30** is shown in Figure 5.9. Contrary to previous iron complexes, the spectrum for (*R*,*R*)-**30** shows sharp signals corresponding to a diamagnetic species with no significant exchange on the NMR time scale. It is therefore likely that a low spin iron(II) complex is produced. The ^{1}H NMR spectrum indicates a molecule that is C_2 symmetric: only half the total number of possible resonances is seen. The crystal structure indicates there are four different iron positions in the complex, each is only 50% occupied, therefore only two are present at any one time. This indicates there is likely some fluxional process at play. Deprotonation of the ligand results in the disappearance of the signal resonating from the amine hydrogen. This signal appears at 10.50 ppm in the ligand spectrum (Figure 5.7).

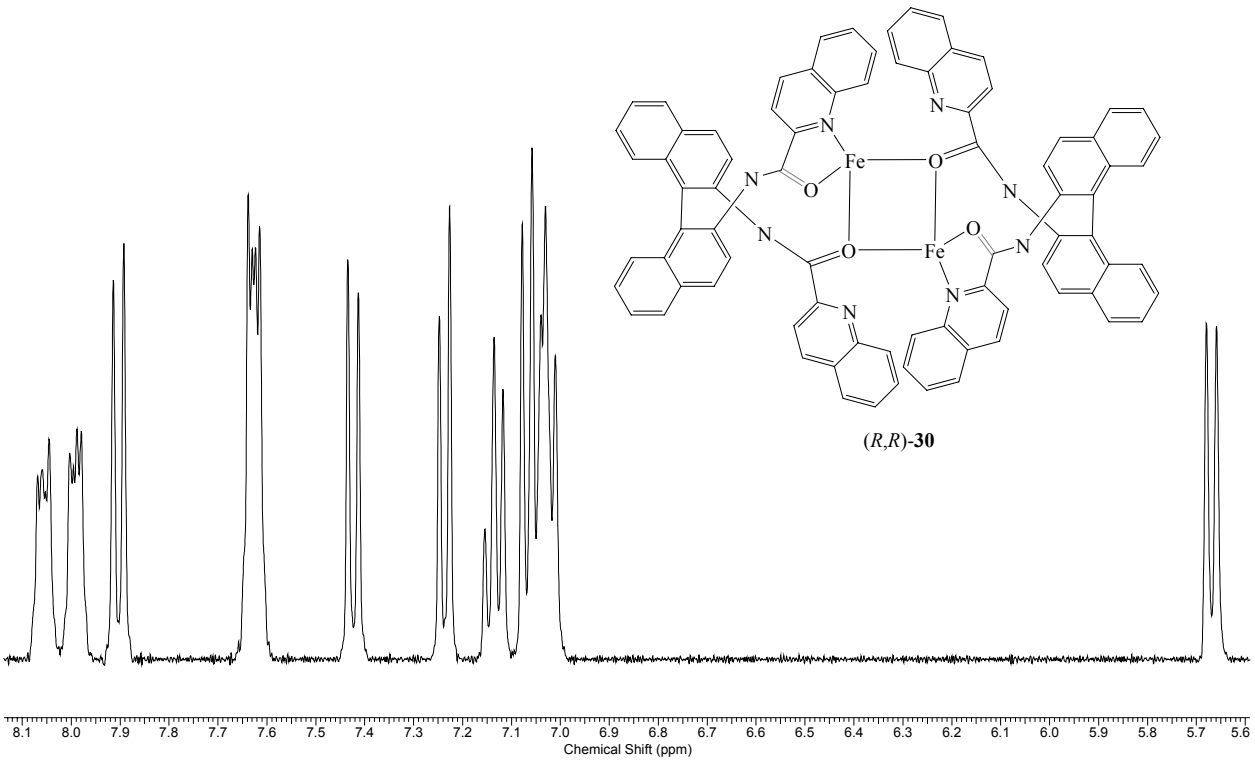

Figure 5.10 400 MHz ^{1}H NMR spectra of (*R*,*R*)-**30** (CD_2Cl_2)

5.4 Structural studies of ligands and complexes

Structural studies were undertaken for the ligand (*R*,*R*)-**27** and the iron complex (*R*,*R*)-**30**. Crystals were grown of (*R*,*R*)-**27** from methylene chloride over which was layered hexanes. X-ray analysis of the crystals revealed the expected structure; with two amide linkers present (Figure 5.10). The ligand can be roughly divided into two halves, bridged by a naphthyl-naphthyl bond. Each of these halves is comprised of a naphthyl moiety (backbone) and a quinolyl moiety (sidearm) that are almost co-planar; thus there is significant conjugation present throughout the π system. In one half of the molecule the dihedral angle between the naphthyl and quinolyl plane is 13.80° (Table 5.1), in the other half it is only 2.36°. Some other selected structural data is also shown in Table 5.1.

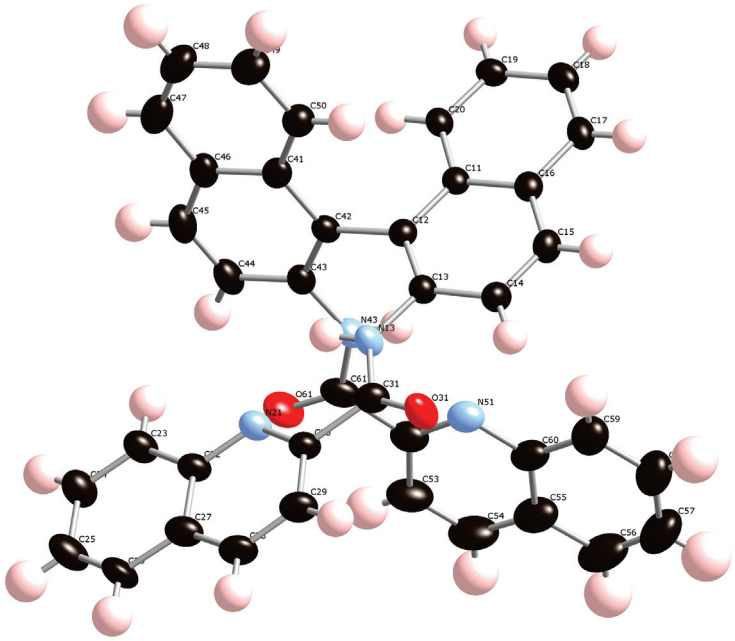

Figure 5.11 Thermal ellipsoid plot (50% probability) of (*R*)-**27**

Table 5.1 Selected bond lengths (Å) and interplanar angles (°) for (*R*)-**27**

Bond lengths	C_{31}-N_{13}	1.356(4)
	C_{61}-N_{43}	1.356(4)
	C_{31}-O_{31}	1.207(4)
	C_{61}-O_{61}	1.215(4)
Interplnar angles	($C_{11\text{-}20}$)-($C_{41\text{-}50}$)	71.35
	($C_{11\text{-}20}$)-(N_{21}-C_{30})	13.80
	($C_{41\text{-}50}$)-(N_{51}-C_{60})	2.36

The thermal ellipsoid plot for (*R*,*R*)-**30** is shown in Figure 5.11. Crystals were grown from methylene chloride over which was layered diethyl ether. The structure reveals a double stranded, dihelicate with *P* helicity. There are four iron positions in the structure, each with

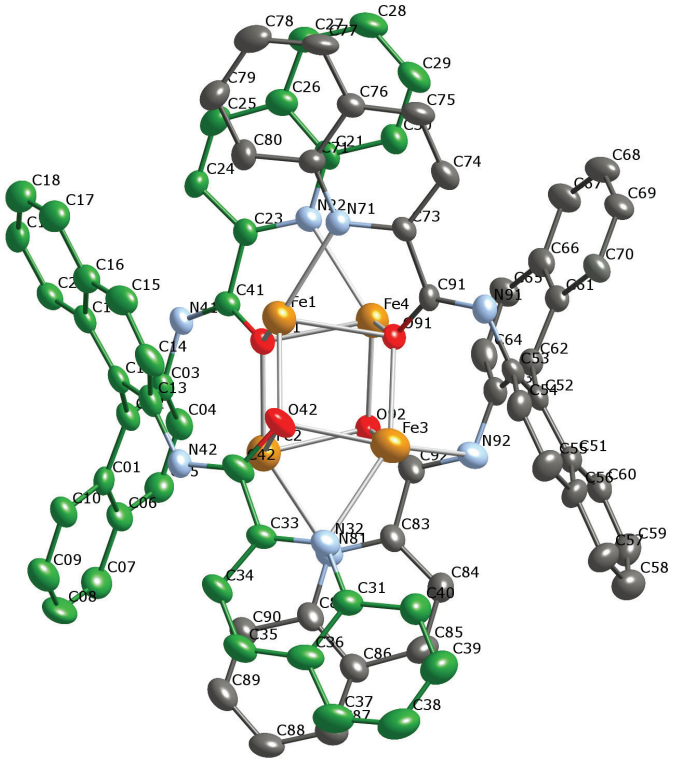

Figure 5.12 Thermal ellipsoid plot (50% probability) of (*R*,*R*)-**30**

50% occupancy. Each ligand coordinates to iron through both amide oxygens and pyridyl nitrogens. The ligands wrap around the four metal centers and each other. Each of the binaphthyl backbones is severely twisted and therefore the result is the formation of a dihelical structure. A space filling model is shown in Figure 5.12.

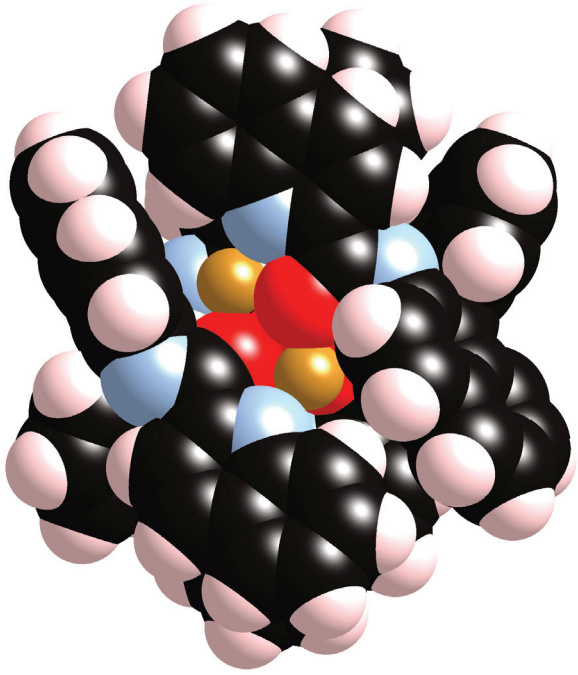

Figure 5.13 Space filling model of (*R*,*R*)-**30**

It is evident there is a competition between amide nitrogens and oxygens for metal binding. The amide nitrogens have been deprotonated, even then they remain uncoordinated. The competition can be explained after analysis of some bond lengths of (*R*,*R*)-**30** (Table 5.2) and comparison to those of (*R*)-**27** (Table 5.1). Typical C-O bond lengths in the complex (*R*,*R*)-**30** are at the least 0.5 Å longer than in the ligand (*R*)-**27**. Longer bond lengths strongly suggest there is reduced double bond character, and therefore the oxygens must be somewhat anionic.

Amide C-N bond lengths in the complex are typically shorter than in the ligand (see tables 5.1 and 5.3). The shorter bond lengths imply that there is increased double bond character and ultimately less anionic character for the nitrogens than for the oxygens. Generally anionic donors are more likely to coordinate to metals than neutral donors.

Table 5.2 Selected bond lengths (Å), bond angles (°) and interplanar angles (°) for (*R*,*R*)-**30**

Bond lengths	Fe_1-O_{42}	2.193(4)	C_{41}-N_{41}	1.284(5)
	Fe_1-O_{41}	2.278(3)	C_{42}-N_{42}	1.293(6)
	Fe_1-O_{91}	2.377(3)	C_{91}-N_{91}	1.304(5)
	Fe_1-N_{71}	2.388(4)	C_{92}-N_{92}	1.319(6)
	Fe_2-O_{92}	2.226(4)	C_{41}-O_{41}	1.302(5)
	Fe_2-O_{41}	2.310(4)	C_{42}-O_{42}	1.289(6)
	Fe_3-O_{91}	2.264(4)	C_{91}-O_{91}	1.267(5)
	Fe_3-O_{42}	2.301(4)	C_{92}-N_{92}	1.268(6)
	Fe_4-O_{92}	2.278(4)		
	Fe_4-O_{41}	2.289(3)		
	Fe_4-O_{91}	2.337(3)		
Bond angles	O_{42}-Fe_1-O_{41}	89.9(14)	O_{92}-Fe_4-O_{41}	78.2(14)
	O_{41}-Fe_1-O_{91}	94.4(12)	O_{42}-Fe_1-N_{71}	137.9(15)
	O_{92}-Fe_2-O_{41}	78.8(14)	O_{41}-Fe_1-N_{71}	120.6(14)
	O_{91}-Fe_3-O_{42}	81.2(13)	O_{91}-Fe_1-N_{71}	69. 3(12)
Interplanar angles	($C_{1\text{-}10}$)-($C_{11\text{-}20}$)	67.16		
	($C_{51\text{-}60}$)-($C_{61\text{-}70}$)	60.47		
	($C_{1\text{-}10}$)-($C_{21\text{-}30}$)	69.31		
	($C_{11\text{-}20}$)-($C_{31\text{-}40}$)	67.53		
	($C_{51\text{-}60}$)-($C_{71\text{-}80}$)	84.90		
	($C_{61\text{-}70}$)-($C_{81\text{-}90}$)	55.66		

In summary bis-amide ligands were synthesized and characterized by ^{1}H NMR and X-ray crystallography. Attempts to structurally characterize Fe(II) complexes synthesized from ligand (*R*,*R*)-**26** were unsuccessful and it is evident that there are fluxional processes at play. This is

one reason for the inherent difficulty in growing crystals. Upon reaction of ligand (*R*)-**27** with $FeCl_2$ a double stranded helicate was formed. It was found that coordination occurs through carbonyl oxygens rather than deprotonated amide nitrogens. Amide oxygen coordination of similar ligands have been reported in the literature, however generally this only occurs with protonated ligands. The competitive nature of the different donors provides further indications that fluxional processes are taking place.

Chapter 6

Conclusions and future work

6.1 Conclusions

A number of unique chiral transition metal complexes have been synthesized and characterized from some new tetradentate nitrogen donor ligands. In the process we have learned much about the formation of a monohelix. Below is a discussion in response to the research objectives stated in the introduction.

1. To synthesize single-stranded mononuclear helical transition metal complexes with chiral bis(imine-pyridine) and bis(quinaldinecarboxamide) ligands.

   Bis(imine-pyridine) and bis(quinaldinecarboxamide) ligands were successfully synthesized and thoroughly characterized using $^{1}H/^{13}C$ and 2D NMR, X-ray crystallography, UV and ECD. Upon metallation with Zn(II), Ni(II) and Fe(II), it has been shown the ligands form complexes with different coordination modes. A single-stranded monohelix was synthesized in one case ((*R*)-**21**). The binaphthyl ligand wraps around the metal (Zn) in a helical fashion via tetradentate coordination of four nitrogens. The result is a helical complex that exhibits π-π stacking interactions between the overlapping aromatic sidearms. It was found that the ligand had undergone reduction at one imine bond. The extra flexibility introduced via this reduction and the use of a labile

triflate anion, are believed to be critical in formation of the single-stranded monohelix (*R*)-**21**.

2. To produce helical complexes of one 'hand'. Upon complexation the overlapping sidearms will produce a conformation that is 'locked' in either the *M* or the *P* form, hence there will be no inter-conversion between the two forms.

A variety of helical complexes were successfully synthesized and characterized in this work. In all but one case, helical complexes of exclusively one 'hand' were afforded (*M* or *P*). The following is a brief summary of the different types of helices encountered in this work:

(a) Single-stranded dinuclear helicates: (*R*,*R*)-**8** and (*R*)-**19**. In the case of *R*-**19**, a crystal structure was not obtained, therefore the handedness of the molecule in the solid state is not certain. For (*R*,*R*)-**8**, both molecules in the unit cell were found to exhibit exclusively *M*,*M* helicity. A space filling model is shown in Figure 6.1.

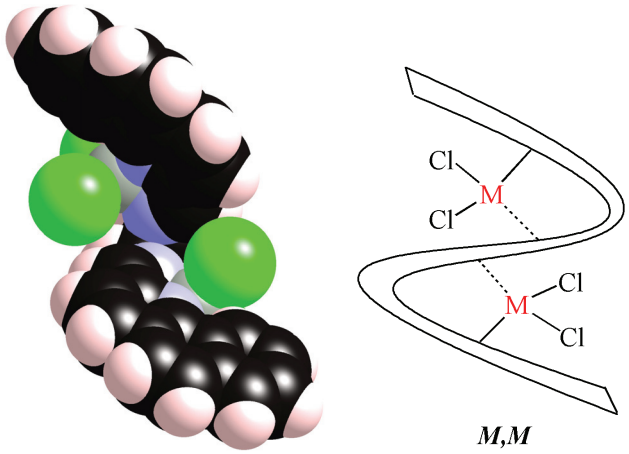

Figure 6.1 Space filling model of (*R*,*R*)-**8** and its illustration of helicity

(b) Double-stranded monohelix: (*R*,*R*,*R*,*R*)-**18**. In this case a 1:1 mixture of *M* and *P* helices is afforded (Figure 6.2). The cyclohexyl backbone this time doesn't produce a large enough energy difference between the two helical diastereomeric forms.

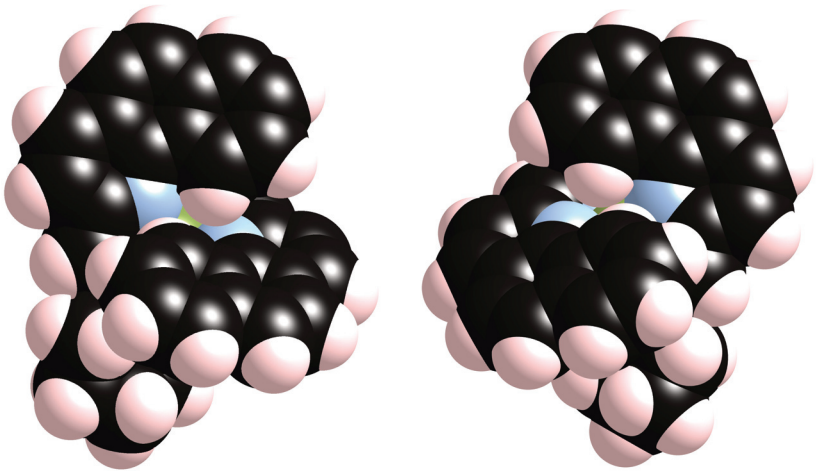

Figure 6.2 Space filling models, *M* (left) and *P* (right) of (*R*,*R*,*R*,*R*)-**18**

(c) Single-stranded monohelix: *R*-**21**. The complex has overlapping sidearms that produce a 'locked' conformation of exclusively *P* helicity.

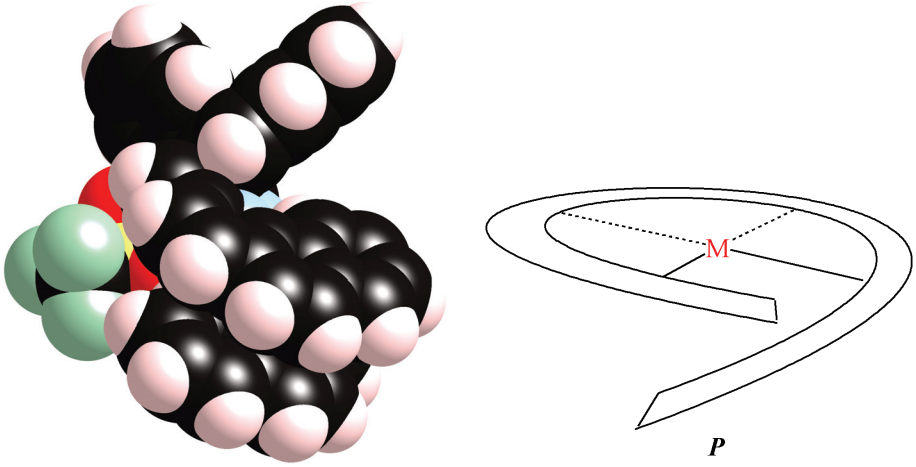

Figure 6.3 Space filling model of *R*-**21** and illustration of helicity

(d) Single-stranded dinuclear pseudo-helices: *R*-**22**, and *R*-**23**. Both of these complexes exhibit helices of solely *P* handedness in the solid state.

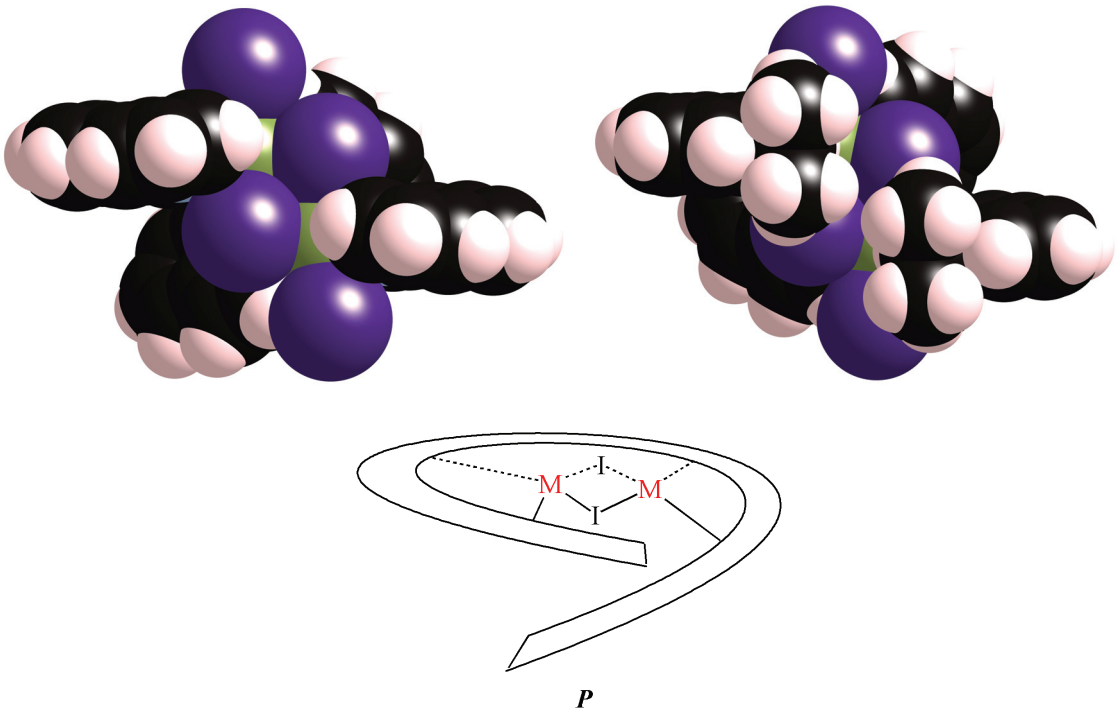

Figure 6.4 Space filling models of *R*-**22** (top left), *R*-**23** (top right) and illustration of helicity (bottom)

(e) Double-stranded dihelicate: (*R*,*R*)-**30**. There are two ligands and two metals in this complex, the four iron positions in the crystal structure are 50% occupied. Both ligands in the resulting double stranded helix are exclusively of *P*,*P* helicity (Figure 6.5).

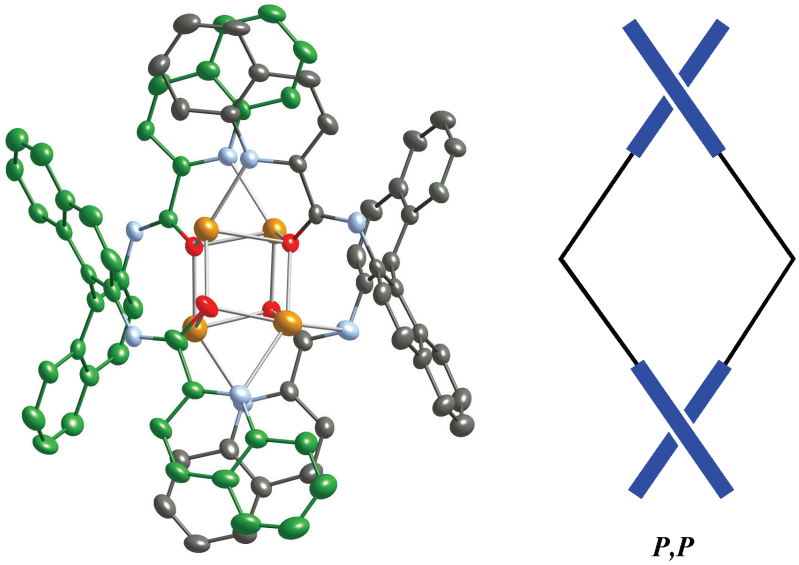

Figure 6.5 Crystal structure of *R*-**30** and illustration of ligand helicity

3. Use the new systems to understand the nature of helix formation. Looking at the effect of the chiral backbone, donor groups, and metal centers. Can we control helix/helicate formation?

The work presented in this thesis clearly implies that it is more difficult to form helices with neutral donors then with anionic donors. It is apparent that the ligand donors are not able to compete the anionic halides of the metals. The use of bis-amide ligands to form monohelices was found to be unreliable. Even though these have anionic nitrogen donors, there is competitive binding with carbonyl oxygens. In addition, the complexes formed with these ligands were shown to exhibit fluxional processes. Both of the ligand systems studied in this work have donor groups incorporated in the aromatic sidearm of the ligand. This severely reduces the ligand flexibility with respect to salen ligands and therefore disfavors helix formation. When extra flexibility is introduced via reduction of

an imine bond, a monohelix is formed (*R*-**21**). The metal salt is also very important, it has been shown that the anion determines the product of metallation. The insufficient labilty of the chloride and iodide anions were found to disfavor the monohelix formation. On the other hand, in the two cases where a monohelix was afforded, the triflate anion proved to be sufficiently labile, so as to leave the coordination sphere. This aided monohelix formation. Monohelices in this work were formed when Zn(II) ((*R*)-**21**) and Ni(II) ((*R*,*R*,*R*,*R*))-**18**) were used as metals. One of the reasons for using Ni(II) as the metal is its preference for square planar geometries, obviously this would aid monohelix formation rather than if a metal that prefers tetrahedral geometry was used. However the monohelix afforded is an octahedral one. Zn(II) was used because it does not have a strong preference for one coordination geometry over another. Therefore it can readily adapt to geometric preferences of the ligand.

4. Examine the scope of coordination chemistry of new ligand designs. As will be seen, the ligands developed in this work can form monohelices, but also have a number of other interesting coordination modes.

A general summary of the different coordination modes exhibited by each complex is shown in Figure 6.6. In the case of the dinuclear zinc complexes (*R*,*R*)-**8** and (*R*)-**19**, each metal is in a tetrahedral coordination geometry. The monohelix (*R*)-**21**, is penta-coordinate with N_4-coordination of the ligand and a triflate anion completes the coordination sphere. Complexes (*R*,*R*)-**11** and (*R*,*R*)-**12** are trigonal bypyramidal with

N_3-coordination of the ligand, two iodide anions also remain coordinated. The monohelix (*R*,*R*,*R*,*R*)-**18** is octahedral via tridenate coordination of two ligands. The dinuclear nickel complexes (*R*,*R*)-**14**, (*R*)-**22** and (*R*)-**23** have bridging and non-bridging iodo ligands. In these cases each nickel is 5-coordinate. The dinuclear iron complex (*R*,*R*)-**30** is coordinated via carbonyl oxygens and pyridyl nitrogens of two ligands to form a helicate. Each iron is coordinated via three oxygens and one nitrogen.

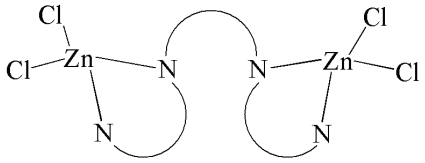

(*R*,*R*)-**8**, (*R*)-**19**

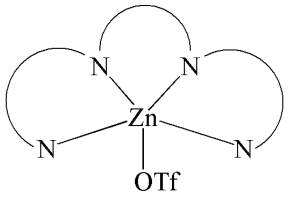

(*R*)-**21**

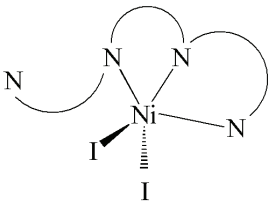

(*R*,*R*)-**11**, (*R*,*R*)-**12**

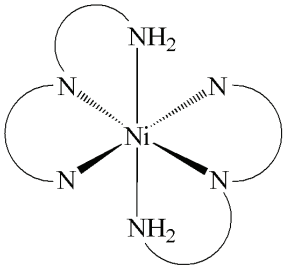

(*R*,*R*)-**18**

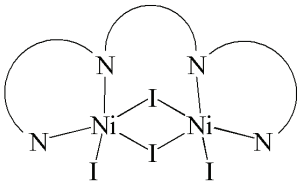

(*R*,*R*)-**14**, (*R*)-**22**, (*R*)-**23**

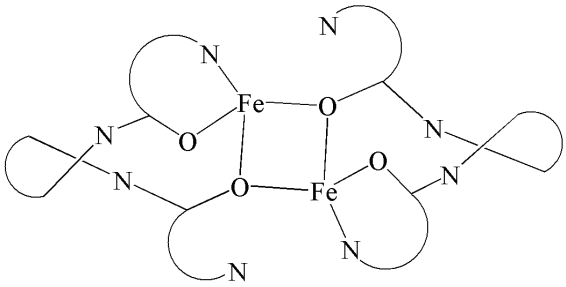

(*R*,*R*)-**30**

Figure 6.6 Different coordination modes of ligands

5. Examine some of the reaction chemistry of the new ligands and helical complexes.

Halide abstractions were attempted with nickel complexes (*R*,*R*)-**11** and (*R*,*R*)-**12**. It was believed a successful abstraction would yield monohelices. Instead, a dinuclear complex ((*R*,*R*)-**14**) and one with a coordinated oxygen were afforded ((*R*,*R*)-**16**). The mechanism of these transformations are unclear as of yet. Hydrolysis of the ligand during the synthesis of complex (*R*,*R*,*R*,*R*)-**18**, resulted in loss of one sidearm and ultimately a tridentate ligand. The cause of hydrolysis is unknown, however the most likely scenario is via moisture contamination. Variable temperature ^{1}H NMR studies of the iron complex (*R*,*R*)-**12**, indicated fluxional processes were likely at play in complexes derived from bis-amide ligands. This is not surprising considering the ambivalent nature of donors in these ligands and the partial occupancy of iron centers in (*R*,*R*)-**30**. Due to fluxional processes, isolation and characterization of complexes is difficult.

6.2 Future work

It is clearly evident from this work, that the formation of a monohelix requires the use of a ligand that is more flexible and less sterically congested upon coordination. The obvious solution for the benzoquinoline sidearms is to use a ligand that has a reduced imine bond. Thus a bis(amine-pyridine) ligand is produced. Another approach is to use an asymmetric ligand: for example if one sidearm has a benzoquinoline sidearm and the other a quinoline, (**A** in Figure 6.7). Yet another approach is to use a ligand that has one salen type sidearm and one pyridine-

imine type sidearm (**B**). This could lead to complexes that have a much a greater asymmetric nature and stronger binding. The use of more labile counterions such as PF_6^- and BAr_f^- may aid in the formation of monohelical structures, thus avoiding dinucleation.

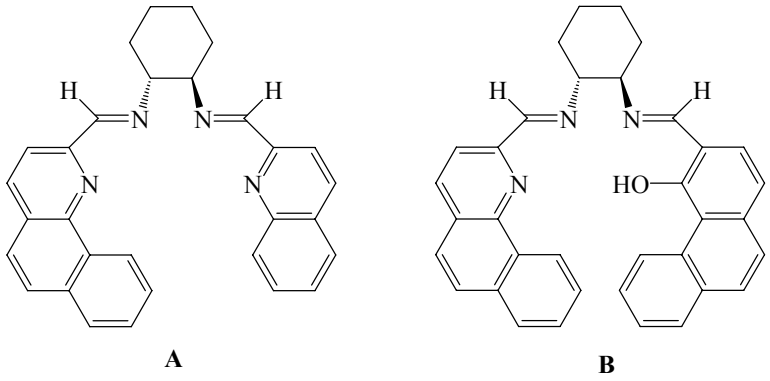

Figure 6.7 Asymmetric ligands

Some of these new approaches are currently being investigated in our group. The underlying goal of this project was to synthesize monohelical complexes that would act as catalysts for asymmetric reactions such as hydroxylation and epoxidation. Even though in most cases, monohelices were not afforded, there remains the potential these new systems can be used as catalysts albeit not in the manner that was first anticipated. For example, mono and dinuclear nickel complexes could potentially be attractive as catalysts for olefin polymerization. There is a great deal of interest in the use of late transition metal catalysts for olefin polymerization and the use of diimine nickel catalysts has been explored previously. Other metals could also be used; manganese and chromium are appealing since they have been shown to have advantageous catalytic properties.

Experimental Section

General Methods

All of the metallation reactions were carried out under an inert atmosphere. Solvents were pre-dried with calcium hydride, sodium benzophenone ketyl or magnesium alkoxide and degassed before use. Inert gases were passed through 4A molecular sieves and a Englehard Q5 catalyst bed before use.

Elemental analyses were carried out by Desert Analytics of Tucson, Arizona. Elemental analyses were carried out by Desert Analytics of Tucson, Arizona. UV-vis spectra were acquired on a Varian Cary 500 spectrometer, and CD spectra on a JASCO 720 spectropolarimeter. Solution samples for both CD and UV were prepared using spectroscopic grade THF dried using calcium hydride, concentrations were typically between 1.5 and 2.5 $\times$ 10^{-5} M. A 1 cm path length quartz cell was employed for the analysis. ^{1}H, ^{13}C and 2D NMR spectra were acquired on either a Varian Unity 400 MHz, or a Bruker 800 MHz spectrometer equipped with a TCI cryprobe. Residual solvent protons were used as the internal standard. Crystallographic data was collected using either a Bruker SMART 1000 CCD or a Bruker-AXS SMART APEX CCD.

2-Formylbenzoquinoline (3). A solution of **4** (4.0 g, 20 mmol) in dioxane (4.4 mL) was added to a solution of selenium dioxide (2.28 g, 20 mmol) in dioxane (21 mL) and H_2O (1.2 mL). The reaction mixture was refluxed for 26 hours, and after cooling, filtered to remove precipitated selenium. The solution was then concentrated to a red/orange solid. This was redissolved in a

4:1 mixture of hexanes/ethyl acetate (30 mL) and subsequently filtered through a silica gel plug to remove selenium byproduct. Concentration of the solution yielded **3** (1.5 g, 38% yield) as a white solid. ^{1}H NMR ($CDCl_3$, 800 MHz): δ 7.75 (d, 1 H, *J* = 8.56 Hz, CH), 7.78 (t, 1 H, *J* = 7.05 Hz, CH), 7.82 (t, 1 H, *J* = 7.55 Hz, CH), 7.95 (d, 1 H, *J* = 8.56 Hz, CH), 7.96 (d, 1 H, *J* = 8.06 Hz, CH), 8.16 (d, 1 H, *J* = 8.06 Hz, CH), 8.31 (d, 1 H, *J* = 8.06 Hz, CH), 9.43 (d, 1 H, *J* = 8.56 Hz, CH), 10.36 (s, 1 H, CH). ^{13}C NMR ($CDCl_3$, 200 MHz): δ 118.50, 124.51, 124.88, 127.77, 128.00, 128.88, 128.95, 130.67, 133.73, 133.76, 137.76, 146.38, 151.08, 194.07. Anal. Calcd for $C_{14}H_9NO$: C 81.14, H 4.38, N 6.76. Found: C 80.63, H 4.55, 6.71. Crystals suitable for X-ray analysis were grown from chloroform over which was layered petroleum ether.

2-Methylbenzoquinoline (4). Synthesis was carried out using literature procedures except purification the crude material was achieved through a silica gel plug using toluene as the eluent. ^{1}H NMR data collected for the pure material was consistent with literature.

(1*R*,2*R*)-*N*,*N*'-Bis[(2-benzoquinolyl)methylene]-1,2-cyclohexanediamine) ((*R*,*R*)-5). (1*R*,2*R*)-1,2-cyclohexanediamine (0.2 g, 1.8 mmol) and **3** (0.75 g, 3.6 mmol) were refluxed in ethanol (25 mL) for 2 hours. The white precipitate was filtered and washed twice with ethanol (5 mL) to afford (*R*,*R*)-**5** (0.63 g, 73% yield). ^{1}H NMR ($CDCl_3$, 800 MHz): δ 1.57-1.66 (m, 2 H, CH), 1.91-2.02 (m, 6 H, CH), 3.71-3.76 (m, 2 H, CH), 7.57 (d, 2 H, *J* = 8.56 Hz, CH), 7.66 (t, 2 H, *J* = 7.05 Hz, CH), 7.70 (t, 2 H, *J* = 7.55 Hz, CH), 7.72 (d, 2 H, *J* = 8.56 Hz, CH), 7.84 (d, 2 H, *J* = 7.55 Hz, CH), 8.07 (d, 2 H, *J* = 8.06 Hz, CH), 8.22 (d, 2 H, *J* = 8.56 Hz, CH), 8.69 (s, 2 H, CH), 9.26

(d, 2H, J = 8.06 Hz, CH). ^{13}C NMR ($CDCl_3$, 200 MHz): δ 24.48, 32.84, 73.92, 119.02, 124.24, 125.09, 126.82, 126.98, 127.72, 128.06, 128.25, 131.40, 133.55, 136.06, 145.74, 153.51, 162.68. Anal. Calcd for $C_{34}H_{28}N_4$: C 82.9, H 5.73, N 11.37. Found C 82.20, H 5.75, N 11.31. Crystals suitable for X-ray analysis were grown from methylene chloride over which was layered diethyl ether.

(1*R*)-*N*,*N*'-Bis[(2-benzoquinolyl)methylene]-[1,1'-Binapthalene]-2,2'-diamine ((*R*)-6). (*R*)-[1,1'-binapthalene]-2,2'-diamine (0.52 g, 1.8 mmol) and **3** (0.75 g, 3.6 mmol) were refluxed in ethanol (25 mL) for 2 hours. The off yellow precipitate was filtered and washed twice with ethanol (5 mL) to afford (*R*)-**6** (1.11 g, 92% yield). ^{1}H NMR (CD_2Cl_2, 800 MHz): 7.32 (t, 2 H, J = 8.00 Hz, CH), 7.35 (d, 2 H, J = 8.06 Hz, CH), 7.40 (t, 2 H, J = 7.05 Hz, CH), 7.46 (t, 2 H, J = 7.00 Hz, CH), 7.55 (t, 2 H, J = 7.00 Hz, CH), 7.58 (d, 2 H, J = 8.56 Hz, CH), 7.63 (d, 2 H, J = 9.06 Hz, CH), 7.72 (d, 2 H, J = 8.56 Hz, CH), 7.77 (d, 2 H, J = 7.55 Hz, CH), 7.81 (d, 2 H, J = 8.06 Hz, CH), 8.01 (d, 2 H, J = 8.06 Hz, CH), 8.07 (d, 2 H, J = 8.06 Hz, CH), 8.10 (d, 2 H, J = 8.56 Hz, CH), 8.70 (s, 2 H, CH), 8.80 (d, 2 H, J = 8.06 Hz, CH). ^{13}C NMR (CD_2Cl_2, 200 MHz): δ 119.16, 119.33, 124.39, 125.54, 125.76, 127.05, 127.35, 127.46, 127.62, 128.19, 128.34, 128.56, 128.67, 129.23, 130.04, 131.68, 132.76, 134.01, 134.04, 136.67, 146.35, 148.72, 153.89, 162.82. Anal. Calcd for $C_{48}H_{30}N_4$: C 86.98, H 4.56, N 8.45. Found C 86.97, H 4.85, N 8.45.

(*rac*)-*N*,*N*'-Bis[(2-benzoquinolyl)methylene]-[1,1'-Binapthalene]-2,2'-diamine ((*rac*)-6). The procedure for (*R*)-**6** was followed using (*rac*)-[1,1'-binapthalene]-2,2'-diamine in place of the *R*-

enantiomer to afford (*rac*)-**6** (0.395 g, 85% yield). ^{1}H NMR spectra were identical to that of compound (*R*)-**6**.

Zn_2Cl_4-(*R*,*R*)-5 complex ((*R*,*R*)-8). Zinc chloride (0.026 g, 0.2 mmol) and (*R*,*R*)-**5** (0.1 g, 0.2 mmol) were suspended in toluene (25 mL) and stirred at 80 °C for 4 hours. The resulting pale yellow precipitate was filtered and washed with toluene (5 mL) to afford (*R*,*R*)-**8** (0.048 g, 31% yield). ^{1}H NMR (CD_2Cl_2, 800 MHz): δ 1.71 (m, 2 H, CH), 2.09 (m, 2 H, CH), 2.17 (m, 2 H, CH), 2.57 (m, 2 H, CH), 4.69 (m, 2 H, CH), 7.74 (d, 2 H, *J* = 8.56 Hz, CH), 7.94 (t, 2 H, *J* = 7.05 Hz, CH), 7.99 (t, 2 H, *J* = 7.05 Hz, CH), 8.01 (d, 2 H, *J* = 9.06 Hz, CH), 8.03 (d, 2 H, *J* = 8.56 Hz, CH), 8.05 (d, 2 H, *J* = 8.06 Hz, CH), 8.53 (d, 2 H, *J* = 8.06 Hz, CH), 9.35 (s, 2 H, CH), 9.89 (d, 2H, *J* = 8.06 Hz, CH). ^{13}C NMR (CD_2Cl_2, 200 MHz): δ 24.31, 33.50, 72.94, 125.35, 126.40, 126.61, 127.89, 128.80, 129.74, 131.36, 132.33, 132.73, 135.70, 141.98, 146.56, 146.84, 167.39. Anal. Calcd for $C_{34}H_{28}N_4Zn_2Cl_4$: C 53.37, H 3.69, N 7.32. Found C 53.70, H 4.22, N 8.59. Crystals suitable for X-ray analysis were grown from methylene chloride over which was layered diethyl ether.

Zn_2Cl_4-(*R*,*R*)-10 complex ((*R*,*R*)-9). The synthesis and assignments have been previously reported except for the following data. Anal. Calcd for $C_{32}H_{36}N_4Zn_2Cl_4$: C 51.30, H 4.84, N 7.48. Found C 51.61, H 4.71, N 7.18.

(1*R*,2*R*)-*N*,*N*'-Bis[(8-isopropyl-2-quinolinyl)methylene]-1,2-cyclohexanediamine ((*R*,*R*)-10). The synthesis and assignments have been previously reported except for the following data. Anal. Calcd for $C_{32}H_{36}N_4$: C 80.63, H 7.61, N 11.75. Found C 80.41, H 7.76, N 12.01.

Ni(II)I_2-(*R*,*R*)-5 complex ((*R*,*R*)-11). Nickel iodide (0.063 g, 0.2 mmol) and (*R*,*R*)-**5** (0.1 g, 0.2 mmol) were suspended in a mixture of toluene (15 mL) and ethanol (10 mL) then stirred at 70 °C for 24 hours. The resulting brown precipitate was filtered and washed with 5 mL of the toluene/ethanol mixture to afford (*R*,*R*)-**11** (0.09 g, 55% yield). ^{1}H NMR ($CDCl_3$, 400 MHz): δ -7.15 (br, 2 H, CH), -5.70 (br, 2 H, CH), 7.91 (br, 2 H, CH), 10.87 (br, 2 H, CH), 11.34 (br, 2 H, CH), 11.95 (br, 2 H, CH), 13.50 (br, 2 H, CH), 17.57 (br, 2 H, CH), 24.66 (br, 2 H, CH). Anal. Calcd for $C_{34}H_{28}N_4Ni_2I_4$: C 50.72, H 3.51, N 6.96. Found C 49.50, H 3.59, N 6.82. Crystals suitable for X-ray analysis were grown from methylene chloride over which was layered toluene.

Ni(II)I_2-(*R*,*R*)-10 complex ((*R*,*R*)-12). Nickel iodide (0.096 g, 0.3 mmol) and (*R*,*R*)-**10** (0.1 g, 0.15 mmol) were suspended in a mixture of toluene (15 mL) and ethanol (10 mL) and then stirred at 100 °C for 24 hours. The mixture was then cooled to room temperature and about a third of the solvent was then removed. The resulting brown precipitate was filtered and washed with 5 mL of the toluene/ethanol mixture to afford (*R*,*R*)-**12** (0.11 g, 66% yield). ^{1}H NMR ($CDCl_3$, 400 MHz): δ -6.05 (br, CH), 0.90 (br, CH), 1.28 (br, CH), 8.83 (br, CH), 10.74 (br, CH), 13.00 (br, CH), 24.15 (br, CH). Anal. Calcd for $C_{32}H_{36}N_4NiI_2$: C 48.70, H 4.60, N 7.10. Found

C 50.14, H 4.58, N 6.68. Crystals suitable for X-ray analysis were grown from methylene chloride over which was layered diethyl ether.

Ni_2I_4-(*R*,*R*)-3 complex ((*R*,*R*)-14). Silver triflate (0.016 g, 0.062 mmol) and (*R*,*R*)-**11** (0.05 g, 0.062 mmol) were suspended in methylene chloride and stirred for 30 minutes at room temperature. The precipitate that had developed was filtered. Solvent was removed from the filtrate to leave a brown colored residue. Analysis by ^{1}H NMR resulted in rather complicated spectra, multiple broad peaks were observed, indicating the presence of more than one species in solution. Several of these peaks were consistent with starting material. Crystals suitable for analysis were grown from the residual brown material using $CDCl_3$ over which was layered toluene.

NiI_2O-(*R*,*R*)-5 complex ((*R*,*R*)-16). Silver triflate (0.016 g, 0.063 mmol) and (*R*,*R*)-**12** (0.05 g, 0.063 mmol) were suspended in methylene chloride and stirred at room temperature for 30 minutes. The precipitate that had developed was filtered. Solvent was removed from the filtrate leaving a brown colored residue. Analysis by ^{1}H NMR resulted in rather complicated spectra, multiple broad peaks were observed indicating the presence of more than one species in solution. Several of these peaks were consistent with starting material. Crystals suitable for analysis were grown from the residual brown material using $CDCl_3$ over which was layered diethyl ether.

Nickel(II)triflate (17). Synthesis was carried out according to literature procedures except methanol was used as solvent during the addition of triflouromethanesulfonic acid to the guaranteed grade of basic nickel carbonate. Purification was achieved by stirring in ethanol for 30 minutes after which the desired compound was filtered, washed twice with ethanol and dried on a high vacuum line for 72 hours at 120 °C.

Ni(II)triflate-(*R*,*R*)-3 complex ((*R*,*R*,*R*,*R*)-18). Nickel triflate (0.072 g, 0.2 mmol) and (*R*,*R*)-**3** (0.1 g, 0.2 mmol) were suspended in a mixture of toluene (15 mL) and methanol (10 mL) and stirred for 24 hours at 60 °C. After cooling to room temperature, two thirds of the solvent was removed and hexanes (10 mL) was added and the reaction was allowed to stir for 2 hours. The resulting yellow precipitate was filtered and washed twice with 2 mL of the toluene/methanol mixture to afford (*R*,*R*,*R*,*R*)-**18**. Crystals suitable for analysis were grown from methylene chloride over which was layered hexanes.

Zn_2Cl_4-(*R*)-6 complex ((*R*)-19). Zinc chloride (0.04 g, 0.30 mmol) and (*R*)-**6** (0.1 g, 0.15 mmol) were suspended in methylene chloride (30 mL) and stirred at room temperature for 48 hours. After concentrating the solution down to 2 mL, the reaction mixture was quenched with toluene (15 mL) and stirred at room temperature for 30 minutes. The resulting orange precipitate was filtered and washed with toluene (5 mL) to afford (*R*)-**19** (0.1 g, 70% yield). ^{1}H NMR (CD_2Cl_2, 800 MHz): 7.44 (d, 2 H, *J* = 8.06 Hz, CH), 7.51 (t, 2 H, *J* = 6.55 Hz, CH), 7.53 (t, 2 H, *J* = 6.55 Hz, CH), 7.67 (d, 2 H, *J* = 9.06 Hz, CH), 7.76 (d, 2 H, *J* = 8.06 Hz, CH), 7.85 (t, 2 H, *J* = 7.55

Hz, CH), 7.86 (t, 2 H, *J* = 8.06 Hz, CH), 7.92 (d, 2 H, *J* = 9.06 Hz, CH), 7.96 (d, 2 H, *J* = 8.06 Hz, CH), 7.97 (d, 2 H, *J* = 8.56 Hz, CH), 8.22 (d, 2 H, *J* = 8.56 Hz, CH), 8.26 (d, 2 H, *J* = 9.06 Hz, CH), 8.41 (d, 2 H, *J* = 8.06 Hz, CH), 8.73 (s, 2 H, CH), 9.72 (d, 2 H, *J* = 7.05 Hz, CH). ^{13}C NMR (CD_2Cl_2, 200 MHz): δ 124.44, 125.25, 125.78, 126.15, 126.91, 127.53, 127.83, 128.18, 128.70, 128.96, 129.22, 129.43, 129.82, 131.51, 131.93, 132.55, 133.09, 133.13, 133.76, 135.70, 141.83, 143.47, 146.66, 164.03. Anal. Calcd for $C_{48}H_{30}N_4Zn_2Cl_4$: C 61.64, H 3.24, N 5.99. Found C 61.51, H 3.56, N 6.14.

Zn_2Cl_4-(*R*)-22 complex ((*R*)-20). The Synthesis and assignments have been previously reported except for the following data. Anal. Calcd for $C_{46}H_{38}N_4Zn_2Cl_4$: C 60.09, H 4.17, N 6.09. Found C 58.81, H 4.44, N 5.94.

Zn(II)triflate-(*R*)-6 complex ((*R*)-21). Zinc triflouromethanesulfonate (0.05 g, 0.15 mmol) and (*R*)-**6** (0.1 g, 0.15 mmol) were suspended in ethanol (15 mL) then stirred at 55 °C for 24 hours. After removal of ethanol, toluene (20 mL) was added and the reaction was heated to 80 °C and stirred for a further 24 hours. The resulting yellow precipitate was filtered and washed with toluene (5 mL) to afford (*R*)-**21** (0.1 g, 65% yield). ^{1}H NMR ($CDCl_3$, 400 MHz): δ 5.10-5.18 (m, 1 H, CH), 5.66-5.75 (m, 1 H, CH), 6.08-6.19 (m, 1 H, CH), 6.30-6.36 (m, 1 H, CH), 6.40 (d, 1 H, *J* = 9.16 Hz, CH), 6.87 (t, 1 H, *J* = 7.60 Hz, CH), 7.03 (d, 1 H, *J* = 8.24 Hz, CH), 7.05 (d, 1 H, *J* = 7.14 Hz, CH), 7.12-7.46 (m, 8 H, CH), 7.47-7.59 (m, 3 H, CH), 7.61-7.74 (m, 3 H, CH), 7.92 (d, 1 H, *J* = 8.61 Hz, CH), 7.99 (d, 1 H, *J* = 8.24 Hz, CH), 8.08 (d, 1 H, *J* = 8.42 Hz, CH), 8.21

(d, 1 H, *J* = 8.42 Hz, CH), 8.24 (d, 1 H, *J* = 8.06 Hz, CH), 8.32 (d, 1 H, *J* = 8.24 Hz, CH), 8.39 (d, 1 H, *J* = 8.06 Hz, CH), 8.46 (d, 1 H, *J* = 8.79 Hz, CH), 9.74 (s, 1 H, CH). Crystals suitable for X-ray analysis were grown from chloroform over which was layered toluene.

(1*R*)-*N*,*N*'-Bis[(8-isopropyl-2-quinolinyl)methylene]-[1,1'-Binapthalene]-2,2'-diamine ((*R*)-22). The Synthesis and assignments have been previously reported except for the following data. Anal. Calcd for $C_{46}H_{38}N_4$: C 85.42, H 5.92, N 8.66. Found C 85.76, H 5.89, N 8.72.

Ni_2I_4-(*R*)-4 complex ((*R*)-23). Nickel iodide (0.09 g, 0.3 mmol) and (*R*)-**6** (0.1 g, 0.15 mmol) were suspended in a mixture of toluene (15 mL) and ethanol (10 mL) then stirred at 70 °C for 24 hours. After cooling to room temperature the reaction mixture was filtered and the filtrate was concentrated down to a brown solid. This was redissolved into chloroform and filtered to remove unwanted precipitate. The filtrate was then left to stand for 10 days after which crystals of the desired compound had grown. These crystals were then filtered, washed with chloroform (2 mL) to afford (*R*)-**23**. ^{1}H NMR ($CDCl_3$, 400 MHz): δ -3.94 (br, 2 H, CH), -3.29 (br, 2 H, CH), 6.46 (br, 1 H, CH), 10.09 (br, 2 H, CH), 11.80 (br, 2 H, CH), 13.78 (br, 2 H, CH), 15.28 (br, 2 H, CH), 20.00 (br, 4 H, CH), 23.80 (br, 2 H, CH), 37.05 (br, 1 H, CH), 37.80 (br, 1 H, CH). Anal. Calcd for $C_{48}H_{30}N_4Ni_2I_4$: C 44.70, H 2.35, N 4.35. Found C 44.32, H 2.53, N 4.25.

Ni_2I_4-(*R*)-6 complex ((*R*)-24). Nickel iodide (0.065 g, 0.2 mmol) and (*R*)-**6** (0.1 g, 0.2 mmol) were suspended in a mixture of toluene (15 mL) and ethanol (10 mL) and then stirred at 75 °C for 24 hours, cooled to room temperature and filtered. The filtrate was then concentrated down to 5 mL and hexanes, (15 ml) was added. This was allowed to stir at 65 °C for 2 hours after which there was a brown precipitate in solution. The resulting brown precipitate was filtered and washed with 2 mL of the toluene/ethanol/hexanes mixture to afford (*R*)-**24** (0.15 g, 76% yield). ^{1}H NMR ($CDCl_3$, 400 MHz): δ -2.10 (br, 4 H, CH), 10.29 (br, 2 H, CH), 11.52 (br, 2 H, CH), 12.20 (br, 2 H, CH), 12.55, 3 H, CH), 14.60 (br, 2 H, CH), 20.40 (br, 2 H, CH), 34.85 (br, 1 H, CH), 36.80 (br, 3 H, CH), 38.09 (br, 2 H, CH), 46.20 (br, 2 H, CH). Anal. Calcd for $C_{46}H_{38}N_4Ni_2I_4$: C 43.44, H 3.01, N 4.41. Found C 43.36, H 3.16, N 4.34. Crystals suitable for X-ray analysis were grown from methylene chloride over which was layered diethyl ether.

(1*R*,2*R*)-*N*,*N*'-Bis[(2-quinolylcarboxamide]-1,2-cyclohexane) ((*R*,*R*)-26). To a solution of quinaldic acid (5.195 g, 0.03 mol) in pyridine (12 mL) was added a solution of (1*R*,2*R*)-1,2-cyclohexanediamine (1.71 g, 0.015 mol) in pyridine and triphenylphosphite (9.3 g , 0.03 mol). The mixture was heated under reflux for for 4 hours after which the solution was allowed to cool for 24 hours. The resultant white precipitate was filtered and washed first with pyridine (5 mL) and then twice with toluene (5 mL) to afford (*R*,*R*)-**26** (5.08 g, 80%). ^{1}H NMR ($CDCl_3$, 400 MHz): δ 1.47-1.67 (m, 4 H, CH), 1.84-1.97 (m, 2 H, CH), 2.27-2.39 (m, 2 H, CH), 4.20 (br, s, 2 H, CH), 7.56 (t, 2 H, J = 7.42 Hz, CH), 7.73 (t, 2 H, J = 8.16 Hz, CH), 7.78 (d, 2 H, J = 8.24 Hz, CH), 8.12-8.21 (m, 6 H, CH), 8.52 (d, 2 H, J = 6.96 Hz, CH). Anal. Calcd for $C_{26}H_{24}N_4O_2$: C 73.57, H 5.70, N 13.20. Found C 72.60, H 5.69, N 12.99.

(*rac*)-*N*,*N*'-Bis[(2-quinolylcarboxamide]-1,2-cyclohexane) ((*rac*)-26). The procedure for (*R*,*R*)-**26** was followed using *rac*-1,2-cyclohexanediamine in place of the *R*,*R* enantiomer to afford (*rac*)-**26** (0.95 g, 74%). ^{1}H NMR spectra were identical to that of compound (*R*,*R*)-**26**.

(1*R*)-*N*,*N*'-Bis[(2-quinolylcarboxamide]-[1,1'-Binapthalene] ((*R*)-27). To a solution of quinaldic acid (5.195 g , 0.03 mol) in pyridine (12 mL) was added a solution of (*R*)-[1,1'-Binapthalene]-2,2'-diamine (4.25 g, 0.015 mol) in pyridine (5 mL) and triphenylphosphite (9.3 g, 0.03 mol). The mixture was heated under reflux for 18 hours, after cooling to room temperature the solution was left at -15 °C for 24 hours. The resulting white precipitate was filtered washed twice with pyridine (5 mL) and then redissolved into methylene chloride (100 mL) and filtered to remove unwanted impurity. Ethanol (250 mL) was then added to the filtrate untill precipitation of the desired compound was complete. The off white precipitate was filtered and washed twice with ethanol (5 mL) to afford (*R*)-**27** (6.2 g, 70%). ^{1}H NMR ($CDCl_3$, 400 MHz): δ 7.28-7.36 (m, 4 H, CH), 7.40 (d, 2 H, *J* = 8.42 Hz, CH), 7.43-7.55 (m, 4 H, CH), 7.64-7.74 (m, 4 H, CH), 8.08-8.17 (m, 6 H, CH), 8.36 (d, 2 H, *J* = 8.97 Hz, CH), 9.29 (d, 2 H, *J* = 9.16 Hz, CH), 10.50 (s, 2 H, CH). Anal. Calcd for $C_{40}H_{26}N_4O_2$: C 80.79, H 4.41, N 9.42. Found C 80.82, H 4.64, N 9.71. Crystals suitable for analysis were grown from methylene chloride over which was layered hexanes.

Fe(II)Cl_2-(*R*)-27 complex ((*R*)-30). Iron (II) chloride (0.043 g , 0.34 mmol), (*R*)-**27** (0.2 g, 0.34 mmol) and sodium methoxide (0.036 g , 0.067 mmol) were suspended in a mixture of methylene

chloride (20 mL) and stirred for 24 hours at room temperature. The reaction mixture was then filtered to remove a small amount of impurity, and the filtrate was concentrated down to approximately 5 mL. The reaction was the quenched with diethyl ether (20 mL) to precipitate out the desired compound. This was filtered and subsequently washed with 5 mL of the methylene chloride/diethyl ether mixture to afford (*R*)-**30** (0.09 g, 37%). ^{1}H NMR (CD_2Cl_2, 400 MHz): δ 5.65 (d, 2 H, *J* = 8.24 Hz, CH), 6.97-7.08 (m, 6 H, CH), 7.12 (t, 2 H, *J* = 7.42 Hz, CH), 7.21 (d, 2 H, *J* = 8.42 Hz, CH), 7.40 (d, 2 H, *J* = 8.61 Hz, CH), 7.57-7.64 (m, 4 H, CH), 7.88 (d, 2 H, *J* = 8.42 Hz, CH), 7.94-8.00 (m, 2 H, CH), 8.01-8.07 (m, 2 H CH). Crystals suitable for analysis were grown from methylene chloride over which was layered diethyl ether.

References

1. Aspinall, H. C. *Chem. Rev.* **2002**, *102*, 1807.
2. Constable, E. C.; Chotalia, R.; Tocher, T. A. *J. Chem. Soc. Chem. Commun.* **1992**, 771.
3. Cornioley, C. D.; Stoeckli-Evans, H.; Zelewsky, A. *J. Chem. Soc. Chem. Commun.* **1990**, 121.
4. Gillard, R. D. *Prog. Inorg. Chem.* **1966***, 7*, 215.
5. Albrecht, M. *Chem. Rev.* **2001**, *101*, 3457.
6. Lehn, J. M.; Rigault, A.; Siegel, J.; Harrowfield, J.;Chevrier, B.; Moras, D. *Proc. Natl. Acad. Sci. U.S.A.* **1987**, *84*, 2565.
7. (a) Van Stein, C.G.; Van Koten, G.; Passeinier, H.; Steinebach, O.; Vrieze, K. *Inorg. Chim. Acta.* **1984**, *89*, 79. (b) Van Stein, C.G.; Van Koten, G.; Vrieze, K.; Brevard, C. *J. Am. Chem. Soc.* **1984**, *106*, 4486.
8. Pallavicini, P.; Amendola, V.; Fernandez, Y. D.; Ghisalberti, M.; Linati, L.; Mangano, C.; Lanfredi, A. M.; Massera, C. *J. Chem. Soc. Dalton Trans.* **2003**, 575.
9. Vázquez, M.; Bermejo, M. R.; Fondo, M.; García-Deibe, A.; Sanmartin, J.; Pedrido, R.; Sorace, L.; Gatteschi, D. *Eur. J. Inorg. Chem.* **2003**, 1128-1135.
10. Fleming, J. S.; Mann, K. L. V.; Couchman, S. M.; Jeffery, J. C.; McCleverty, J. A.; Ward, M. D. *J. Chem. Soc. Dalton Trans.* **1998**, 2047.
11. Amendola, V.; Fabbrizzi, L.; M.; Linati, L.; Mangano, C.; Pallavicini, P.; Pedrazzini, V.; Zema, M. *Chem. Eur. J.* **1999**, *5*, 3679.
12. Miyasaka, H.; Okamura, S.; Nakashima, T.; Matsumoto. *Inorg. Chem.* **1997**, *36*, 4329.

13. Chen-jie, F.; Chun-ying, D.; Hong, M.; Cheng, H.; Qing-jin, M.; Yong-jiang, L.; Yuhua, M.; Zhe-ming, W. *Organometallic.* **2001**, *20*, 2525

14. Fu, Y.; Yang, H.; Wang, D.; Tang, W.; Wu, B.; Mak, T. C. W. *Polyhedron.* **1997**, *16*, 1505.

15. Vallina, A. T.; Stoeckli-Evans, H. *Polyhedron.* **2002**, *21*, 1177.

16. Shoner, S. C.; Nienstedt, A. M.; Ellison, J. J.; Kung, I, Y.; Barnhart, D. Kovacs, J. A. *Inorg. Chem.* **1998**, *37*, 5721.

17. End, N.; Macko, L.; Zehnder, M.; Pflaltz, A. *Chem. Eur. J.* **1998**, *4*, 818.

18. Zhu, Y.; Peng li, Z.; Ma, J.; Tang, F.; Kang, L.; Zhou, Q. *Tetrahedron: Asymmetry.* **2002**, 1396.

19. Yano, T.; Tanaka, R.; Nishioka, T.; Kinoshita, I.; Isobe, K.; Wright, L. J.; Collins, T. J. *Chem. Commun.* **2002**, 1396.

20. Seitz, M.; Kaiser, A.; Stempfhumber, S.; Zabel, M.; Reiser, O. *Inorg. Chem.* **2005**, *44*, 4630.

21. Wiznycia, A. V.; Desper, J.; Levy, C. J. *J. Chem. Soc. Chem. Commun.* **2005**, 4693.

22. Ettling, C. *Liebigs Ann. Chem.* **1840**, *35*, 241.

23. (a) Calligaris, M.; Randacio, L.; Wilkinson, G.; Gillard, R. D.; McCleverty, J. A. *Comprehensive Coordination Chemistry*; Pergamon, Oxford, 1987. (b) Larson, E. J.; Pecoraro, V. L. *J. Am. Chem. Soc.* **1991**, *113*, 3810. (c) Wohre, D. *Adv. Polym. Sci.* **1983**, *50*, 45. (d) Khan, M. M. T.; Srinivas, D.; Kureshi, R. I.; Khan, N. H.; *Inorg. Chem.* **1990**, *29*, 2320. (e) Costamagma, J.; Vargas, J.; Latorre, R.; Alvarado, A.; Mena, G. *Coord. Chem. Rev.* **1992**, *119*, 67. (f) Atkins, A. J.; Black, D.; Blake, A. J.; Marin-

Becerra, A.; Parson, S.; Ruiz-Ramirez, L.; Schroder, M. *J. Chem. Soc. Chem. Commun.* **1996**, 457. (g) Ramade, I.; Kahn, O.; Jeannin, Y.; Robert, F. *Inorg. Chem.* **1997**, *36*, 930.

24. Zhang, W.; Loebach, J. L.; Wilson, S. R.; Jacobsen, E. N. *J. Am. Chem. Soc.* **1990**, *112*, 2801.

25. Piguet, C.; Bernardinelli, G.; Hopfgartner, G. *Chem. Rev.* **1997**, *97*, 2005.

26. White, C. M.; Doyle, A. G.; Jacobsen, E. N. *J. Am. Chem. Soc.* **2001**, *123*, 7194.

27. (a) Murphy, A.; Dubois, G.; Stack, T. D. P. *J. Am. Chem. Soc.* **2003**, *125*, 5250. (b) Murphy, A.; Dubois, G.; Stack, T. D. P. *Org. Lett.* **2003**, *5*, 2469.

28. (a) Chen, K.; Que, L. *J. Am. Chem. Soc.* **2001**, *123*, 6327. (b) Kim, C.; Chen, K.; Kim, J.; Que, L. *J. Am. Chem. Soc.* **1997**, *119*, 5964. (c) Chen, K.; Que, L. *J. Chem. Soc. Chem. Commun.* **1999**, 1357.

29. Collins, T. J.; Powell, R. D.; Slebodnick, C.; Uffelman, E.S. *J. Am. Chem. Soc.* **1990**, *112*, 899. (b) Collins, T. J. *Acc. Chem. Res.* **1994**, *27*, 279. (c) Cheng, W. K.; Wong, K. Y.; Tong, W. F.; Lai, T. F.; Che, C. M. *J. Chem. Soc. Dalton Trans.* **1992**, 91. (d) Che, C. M.; Cheng, W. K.; Mak, T. C. W. *J. Chem. Soc. Chem. Commun.* **1986**, 200. (e) Diaddario, L. L.; Robinson, W. R.; Margerum, D. W. *Inorg. Chem.* **1983**, *22*, 1021.

30. (a) Mak, T. S.; Yam, V. W. W.; Che, C. M. *J. Chem. Soc. Dalton Trans.* **1990**, 2555. (b) Che, C. M.; Cheng, W. K.; Mak, T. C. W. *J. Chem. Soc. Chem. Commun.* **1986**, 200. (c) Chapman, R. L.; Stephens, S. F.; Vagg, R. S. *Inorg. Chim. Acta.* **1981**, *52*, 161. (d) Chapman, R. L.; Vagg, R. S. *Inorg. Chim. Acta.* **1981**, *33*, 227. (e) Sung, J. L.; Lee, J. Y.; Kim, C.; Nam, W.; Kim, Y. *Acta. Cryst. 58*, 191.

31. (a) Trost, B. M.; Hildbrand, S.; Dogra, K. *J. Am. Chem. Soc.* **1999**, *121*. (b) Trost, B. M.; Dogra, K.; Hachiya, I.; Emura, T.; Hughes, D. L.; Krska, S.; Reamer, R. A.; Palucki, M. P.; Yasuda, N.; Reider, P. J. *Angew. Chem. Int. Ed.* **2002**, *41*, 1929. (c) Krska, S. W.; Hughes, D. L.; Reamer, R. A.; Mathre, D. J.; Sun, Y.; Trost, B. M. *J. Am. Chem. Soc.* **2002**, *1241*.

32. Moberg, C.; Belda, O. *Acc. Chem. Res.* **2004**, *37*, 159.

33. Nonoyama, M.; Tomita, S.; Yamakasi. *Inorg. Chim. Acta.* **1975**, *12*, 33.

34. (a) Barnes, D. J.; Chapman, R. L.; Stephens, S. F.; Vagg, R. S. *Inorg. Chim. Acta.* **1981**, *51*, 155. (b) Mulqi, W.; R. L.; Stephens, S. F.; Vagg, R. S. *Inorg. Chim. Acta.* **1982**, *63*, 197. (c) Stephens, S. F.; Vagg, R. S. *Inorg. Chim. Acta.* **1988**, *142*, 43.

35. Che, C.-M.; Huang, J.-S. *Coord. Chem. Rev.* **2003**, *242*, 97 and references cited therein.

36. Bari, L. D.; Pescitelli G.; Salvadori, P. *J. Am. Chem. Soc.* **1999**, *121*, 7998.

37. (a) Che, C.-M.; Kwong, H.-L.; Chu, W.-C.; Cheng, K.-F.; Lee, W.-S.; Yu, H.-S.; Yeung, C.-T.; Cheung, K.-K. *Eur. J. Inorg. Chem.* **2002**, 1456. (b) Wang, Y.; Stack, T. D. P. *J. Am. Chem. Soc.* **1996**, *118*, 13097. (c) Zhou, X.-G.; Huang, J.-S.; Yu, X.-Q.; Zhou, Z.-Y.; Che, C.-M. *J. Chem. Soc. Dalton Trans.* **2000**, 1075. (d) Cheng, M.-C.; Chan, M.C.-W; Peng, S.-M.; Cheung, K.-K.; Che, C.-M. *J. Chem. Soc. Dalton Trans.* **1997**, 3479. (e) Zhou, X.-G.; Huang, J.-S.; Ko, P.-H.; Cheung, K.-K.; Che, C.-M. *J. Chem. Soc. Dalton Trans.* **1999**, 3303.

38. Hamblin, J.; Childs, L. J.; Alcock, N. W.; Hannon, M. J. *J. Chem. Soc. Dalton Trans.* **2002**, 164.

39. Telfer, S. G.; Sato, T.; Haradi, T.; Kuroda, R.; Lefebvre, J.; Leznoff, D .B. *Inorg. Chem.* **2004**, *43*, 6168.

40. Lin, J-H.; Che, C-H.; Lai, T-F.; Poon, C-K.; Cui, Y-X. *J. Chem. Soc. Chem. Ccommun.* **1991**, 468.

41. (a) Larrow, J. F.; Jacobsen, E. N. *J. Org. Chem.* **1994**, *59*, 1939. (b) Brown, K. J.; Berry, M. S.; Murdoch, J. R. *J. Org. Chem.* **1985**, *50*, 4345.

42. Hamada, Y.; Takeuchi, I. *J. Org. Chem.* **1977**, *42*, 4209.

43. Köppl, A.; Alt, H. G. *J. Mol. Catal. A.* **2000**, *154*, 45.

44. Platt, K. L.; Oesch, F. *J. Org. Chem.* **1982**, *47*, 5321, and references therein.

45. Letcher, R. M. *Organic Magnetic Resonance.* **1981**.

46. (a) Takei, T. *Surface Technology.* **1984**, *23*, 73. (b) Takei, T. *Surface and Coatings Technology.* **1987**, *31*, 163. (c) Jansky, M. T.; Yoke, J. T. *Inorg. Nucl. Chem.* **1979**, *41*, 1707.

47. Bertini, I.; Luchinat, C. *NMR of Paramagnetic Molecules in Biological Systems*; Benjamin/Cummings: Menlo Park, CA, 1986.

. (a) Chen, J.; Chinn, M. S. *Inorg. Chem.* **1995**, *34*, 6080. (b) Hlavinka, M. L.; Hagadorn, J. R. *J. Chem. Soc. Chem. Commun.* **2003**, 2686.

49. Goodwin, H. A.; Lions, F. *J. Am. Chem. Soc.* **1960**, *82*, 5013.

44. Baar, C. R.; Jennings, M. C.; Puddephatt, R. J.; Muir, K. W. *Organometallics.* **1999**, *18*, 4373.

51. Morales, D.; Perez, M.; Riera, L.; Suarez, R. C.; Garcia, S. G.; Miguel, D. *Organometallics.* **1999**, *21*, 1540.

45. (a) Hamm, D. J.; Bordner, J.; Schreiner, A. F. *Inorg. Chim. Acta.* **1973**, *7*, 637. (b) Endres, H. *Acta. Cryst.* **1985**, *C41*, 1423.

53. Wada, A.; Sakabe, N.; Tanaka, J. *Acta. Crystallogr. B.* **1976**, *32*, 1121.

54. Chestnut, D. J.; Haushalter, R. C.; Zubieta, J. *Inorg. Chim. Acta.* **1999**, *292*, 41.

55. Blanchard, S.; Neese, F.; Bothe, E.; Bill, E.; Weyhermuller, T.; Wieghardt, K. *Inorg. Chem.* **2005**, *44*, 3636.

56. Endres, H. *Acta. Cryst. C.* **1985**, *41*, 1423.

57. Lavery, A.; Nelson, M.S. *J. Chem. Soc. Dalton Trans.* **1985**, 1053.

58. Steed, J. W.; Atwood, J. L. *Supermolecular Chemistry*; Wiley, New York, 2000.

59. Simon-Manso, E.; Valderamma, M.; Arancibia, V.; Simon-Manso, Y. *Inorg. Chem.* **2000**, *39*, 1650.

60. (a) Kunrath, F. A.; Souza, R. F.; Casagrande, O. L.; Brooks, N. R.; Young, V. G. *Organometallics.* **2003**, *22*, 4739. (b) Speiser, F.; Braunstein, P. *Inorg. Chem.* **2004**, *43*, 4234.

61. Quisenberry, K. T.; Smith, J. D.; Voehler, M.; Stec, D. F.; Hanusa, T. P.; Brennessel, W. W. *J. Am. Chem. Soc.* **2005**, *127*, 4376.

62. Kryatov, S. V.; Nazarenko, A. Y.; Smith, M. B.; Rybak-Akimova, E. V. *J. Chem. Soc. Chem. Commun.* **2001**, 1174.

63. (a) Quisenberry, K. T.; Smith, J. D.; Voehler, M.; Stec, D. F.; Hanusa, T. P.; Brennessel, W. W. *J. Am. Chem. Soc.* **2005**, *127*, 4376. (b) Morgenstern, D. A.; Ferrence, G. M.; Washington, J.; Henderson, J. I.; Rosenhein, L.; Heise, J. D.; Fanwick, P. E.; Kubiak, C.

P. *J. Am. Chem. Soc.* **1996**, 118, 2198. (c) Ercoloni, C.; Quagliano, J. V.; Vallarino, L. M. *Inorg. Chim. Acta.* **1972**, *7*, 413.

64. Barnes, D. J.; Chapman, R. L.; Vagg, R. S.; Watton, E. C. *J. Chem. Eng. Data.* **1978**, 23, 349.

65. (a) Yamazaki, N.; Higashi, F. *Tetrahedron.* **1974**, *30*, 1323. Yamazaki, N.; Higashi, F. *Tetrahedron. Lett.* **1972**, *49*, 5047.

66. Campbell, K. N.; Helbing, H. C.; Kerwin, J. F. *J. Am. Chem. Soc.* **1946**, 68, 1840.

67. Stephens, S. F.; Vagg, R. S. *Inorg. Chim. Acta.* **1981**, *51*, 149.

68. Butts, C. P.; Crosby, J.; Lloyd-Jones, G. C.; Stephen, S. C. *J. Chem. Soc. Chem. Commun.* **1999**, 1707.

Appendix I

^{13}C NMR spectra

Acquisition Time (sec)	0.6802	***Date***	24 Nov 2006 18:37:52			***Date Stamp***	24 Nov 2006 18:37:52
File Name						***Frequency (MHz)***	201.22
Nucleus	13C	***Number of Transients***	1032	***Origin***	spect	***Original Points Count***	32701
Owner	nmrsu	***Points Count***	32768	***Pulse Sequence***	zgpg30	***Receiver Gain***	32768.00
SW(cyclical) (Hz)	48076.92	***Solvent***	CHLOROFORM-d			***Spectrum Offset (Hz)***	20121.3398
Sweep Width (Hz)	48075.45	***Temperature (degree C)***	25.000				

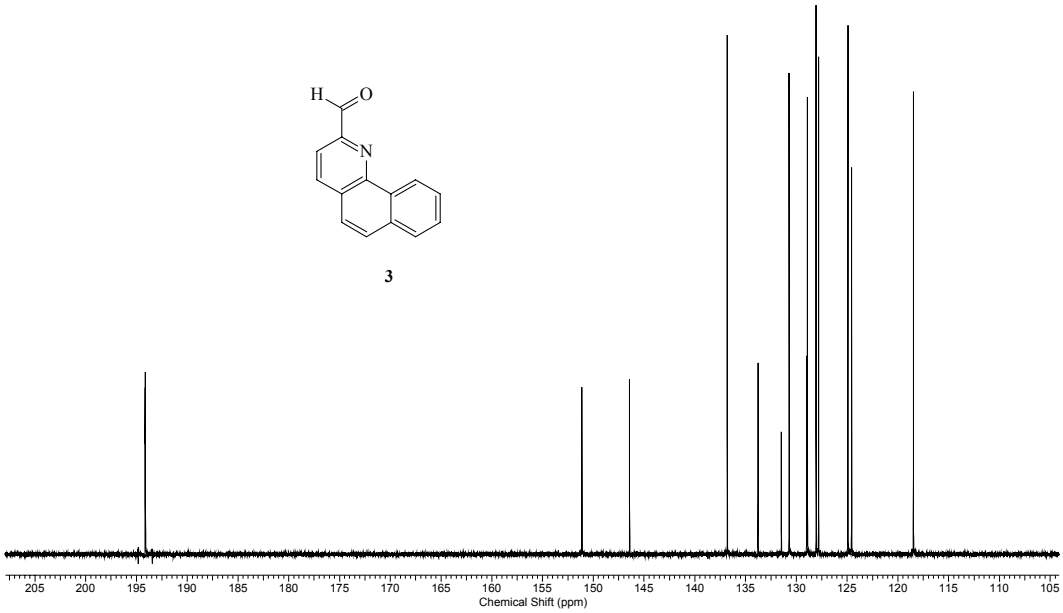

3

Acquisition Time (sec)	0.6802	***Date***	21 Nov 2006 21:20:00			***Date Stamp***	21 Nov 2006 21:20:00
File Name							
Frequency (MHz)	201.22	***Nucleus***	13C	***Number of Transients***	512	***Origin***	spect
Original Points Count	32701	***Owner***	nmrsu	***Points Count***	32768	***Pulse Sequence***	zgpg30
Receiver Gain	32768.00	***SW(cyclical) (Hz)***	48076.92	***Solvent***	CHLOROFORM-d		
Spectrum Offset (Hz)	20121.3398	***Sweep Width (Hz)***	48075.45	***Temperature (degree C)***	25.000		

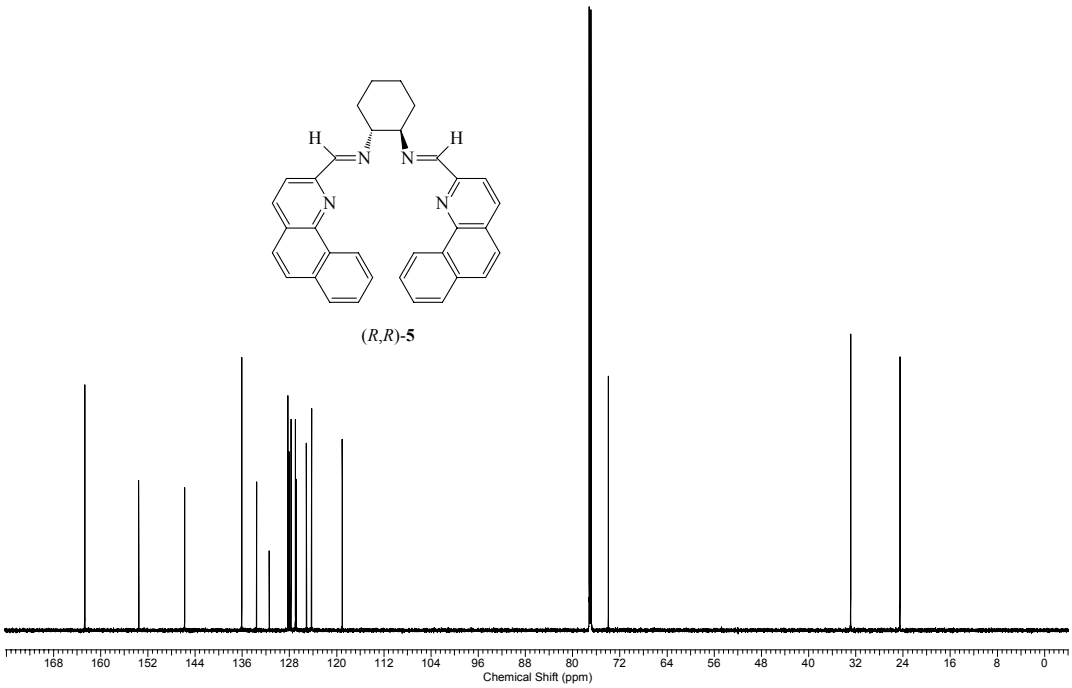

(*R*,*R*)-**5**

Acquisition Time (sec)	0.6802	***Date***	22 Nov 2006 20:35:12			***Date Stamp***	22 Nov 2006 20:35:12
File Name							
Frequency (MHz)	201.22	***Nucleus***	13C	***Number of Transients***	2000	***Origin***	spect
Original Points Count	32701	***Owner***	nmrsu	***Points Count***	32768	***Pulse Sequence***	zgpg30
Receiver Gain	32768.00	***SW(cyclical) (Hz)***	48076.92	***Solvent***	DICHLOROMETHANE-d2		
Spectrum Offset (Hz)	20121.3398	***Sweep Width (Hz)***	48075.45	***Temperature (degree C)***	25.000		

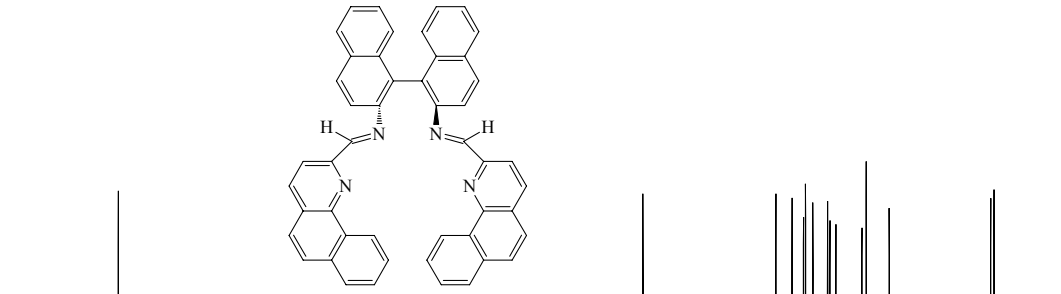

(*R*)-**6**

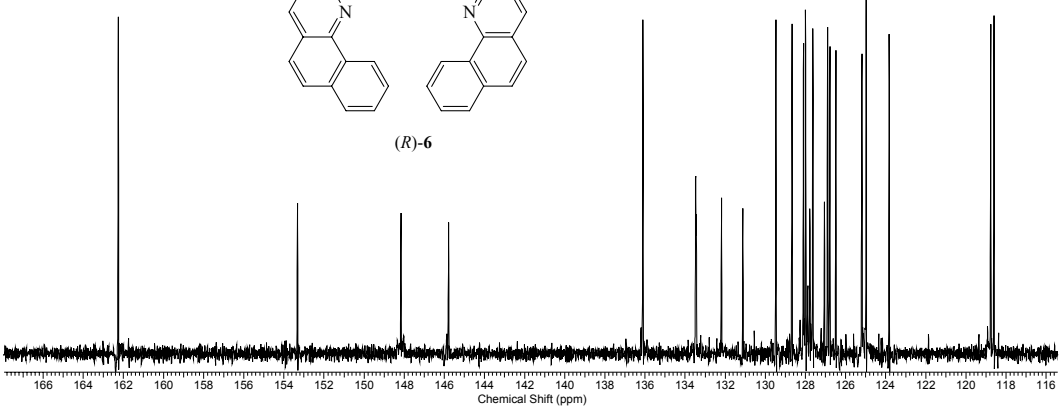

Acquisition Time (sec)	0.6802	***Date***	22 Nov 2006 17:10:24			***Date Stamp***	22 Nov 2006 17:10:24
File Name							
Frequency (MHz)	201.22	***Nucleus***	13C	***Number of Transients***	1024	***Origin***	spect
Original Points Count	32701	***Owner***	nmrsu	***Points Count***	32768	***Pulse Sequence***	zgpg30
Receiver Gain	32768.00	***SW(cyclical) (Hz)***	48076.92	***Solvent***	DICHLOROMETHANE-d2		
Spectrum Offset (Hz)	20121.3398	***Sweep Width (Hz)***	48075.45	***Temperature (degree C)***	25.000		

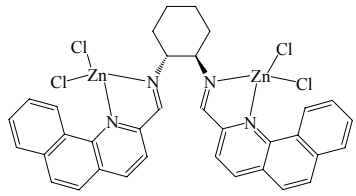

(*R*,*R*)-**8**

Acquisition Time (sec)	0.6802	***Date***	23 Nov 2006 18:05:52			***Date Stamp***	23 Nov 2006 18:05:52
File Name						***Frequency (MHz)***	201.22
Nucleus	13C	***Number of Transients***	1024	***Origin***	spect	***Original Points Count***	32701
Owner	nmrsu	***Points Count***	32768	***Pulse Sequence***	zgpg30	***Receiver Gain***	32768.00
SW(cyclical) (Hz)	48076.92	***Solvent***	DICHLOROMETHANE-d2			***Spectrum Offset (Hz)***	20121.3398
Sweep Width (Hz)	48075.45	***Temperature (degree C)***	25.000				

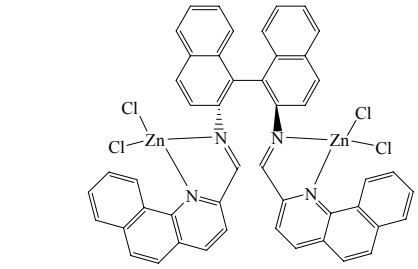

(*R*)-**19**

Appendix II

Crystal Data

Crystal data and structure refinement for **3**

Identification code	dp0503m	
Empirical formula	C14 H9 N O	
Formula weight	207.22	
Temperature	173(2) K	
Wavelength	0.71073 Å	
Crystal system	Monoclinic	
Space group	P2(1)/c	
Unit cell dimensions	a = 7.4691(10) Å	α = 90°.
	b = 19.748(3) Å	β = 105.028(9)°.
	c = 6.9392(11) Å	γ = 90°.
Volume	988.5(2) $Å^3$	
Z	4	
Density (calculated)	1.392 g/cm^3	
Absorption coefficient	0.089 mm^{-1}	
F(000)	432	
Crystal size	0.40 x 0.20 x 0.15 mm^3	
Theta range for data collection	2.06 to 28.24°.	
Index ranges	-9<=h<=9, -25<=k<=23, -9<=l<=9	
Reflections collected	7160	
Independent reflections	2304 [R(int) = 0.1563]	
Completeness to theta = 28.24°	94.4 %	
Absorption correction	None	
Refinement method	Full-matrix least-squares on F^2	
Data / restraints / parameters	2304 / 0 / 145	
Goodness-of-fit on F^2	1.084	
Final R indices [I>2sigma(I)]	R1 = 0.0771, wR2 = 0.1858	
R indices (all data)	R1 = 0.1114, wR2 = 0.2041	
Largest diff. peak and hole	0.461 and -0.365 $e.Å^{-3}$	

Crystal data and structure refinement for (*R*,*R*)-**5**

Identification code	dp0502m	
Empirical formula	C34 H28 N4	
Formula weight	492.60	
Temperature	173(2) K	
Wavelength	0.71073 Å	
Crystal system	Tetragonal	
Space group	P4(1)2(1)2	
Unit cell dimensions	a = 6.6519(2) Å	α = 90°.
	b = 6.6519(2) Å	β = 90°.
	c = 56.855(3) Å	γ = 90°.
Volume	2515.71(18) $Å^3$	
Z	4	
Density (calculated)	1.301 g/cm^3	
Absorption coefficient	0.077 mm^{-1}	
F(000)	1040	
Crystal size	0.40 x 0.30 x 0.25 mm^3	
Theta range for data collection	2.87 to 26.84°.	
Index ranges	-8<=h<=8, -8<=k<=7, -68<=l<=65	
Reflections collected	14701	
Independent reflections	1685 [R(int) = 0.1366]	
Completeness to theta = 26.84°	96.6 %	
Absorption correction	None	
Refinement method	Full-matrix least-squares on F^2	
Data / restraints / parameters	1685 / 0 / 173	
Goodness-of-fit on F^2	1.127	
Final R indices [I>2sigma(I)]	R1 = 0.0487, wR2 = 0.1130	
R indices (all data)	R1 = 0.0557, wR2 = 0.1178	
Absolute structure parameter	6(5)	
Extinction coefficient	0.025(3)	
Largest diff. peak and hole	0.198 and -0.264 e.$Å^{-3}$	

Crystal data and structure refinement for (*R*,*R*)-**8**

Identification code	dp0504m	
Empirical formula	C36 H32 Cl8 N4 Zn2	
Formula weight	935.00	
Temperature	203(2) K	
Wavelength	0.71073 Å	
Crystal system	Monoclinic	
Space group	P2(1)	
Unit cell dimensions	a = 15.0432(14) Å	α = 90°.
	b = 17.1668(17) Å	β = 111.564(4)°.
	c = 15.9752(14) Å	γ = 90°.
Volume	3836.7(6) $Å^3$	
Z	4	
Density (calculated)	1.619 g/cm^3	
Absorption coefficient	1.841 mm^{-1}	
F(000)	1888	
Crystal size	0.30 x 0.20 x 0.12 mm^3	
Theta range for data collection	1.37 to 28.35°.	
Index ranges	-19<=h<=19, -19<=k<=22, -20<=l<=21	
Reflections collected	25498	
Independent reflections	12493 [R(int) = 0.0868]	
Completeness to theta = 28.35°	89.4 %	
Absorption correction	Semi-empirical from equivalents α	
Max. and min. transmission	1.000 and 0.592	
Refinement method	Full-matrix least-squares on F^2	
Data / restraints / parameters	12493 / 1 / 896	
Goodness-of-fit on F^2	1.467	
Final R indices [I>2sigma(I)]	R1 = 0.1044, wR2 = 0.2516	
R indices (all data)	R1 = 0.1456, wR2 = 0.2640	
Absolute structure parameter	0.10(2)	
Largest diff. peak and hole	1.752 and -1.140 $e.Å^{-3}$	

Crystal data and structure refinement for (*R*,*R*)-**11**

Identification code	dp0506m	
Empirical formula	C35 H30 Cl2 I2 N4 Ni	
Formula weight	890.04	
Temperature	173(2) K	
Wavelength	0.71073 Å	
Crystal system	Monoclinic	
Space group	P2(1)	
Unit cell dimensions	a = 10.3909(6) Å	α = 90°.
	b = 24.3214(15) Å	β = 104.835(3)°.
	c = 13.5501(7) Å	γ = 90°.
Volume	3310.3(3) $Å^3$	
Z	4	
Density (calculated)	1.786 Mg/m^3	
Absorption coefficient	2.645 mm^{-1}	
F(000)	1744	
Crystal size	0.40 x 0.30 x 0.15 mm^3	
Theta range for data collection	1.55 to 28.27°.	
Index ranges	-13<=h<=13, -32<=k<=32, -17<=l<=17	
Reflections collected	41469	
Independent reflections	14798 [R(int) = 0.0505]	
Completeness to theta = 28.27°	95.7 %	
Absorption correction	Semi-empirical from equivalents	
Max. and min. transmission	1.000 and 0.634	
Refinement method	Full-matrix least-squares on F^2	
Data / restraints / parameters	14798 / 1 / 793	
Goodness-of-fit on F^2	1.072	
Final R indices [I>2sigma(I)]	R1 = 0.0415, wR2 = 0.0980	
R indices (all data)	R1 = 0.0621, wR2 = 0.1097	
Absolute structure parameter	0.00(2)	
Largest diff. peak and hole	1.316 and -1.370 $e.Å^{-3}$	

Crystal data and structure refinement for (*R*,*R*)-**12**

Identification code	dp0603m	
Empirical formula	C36.65 H33.30 Cl7.15 I2.15 N4 Ni2	
Formula weight	1173.50	
Temperature	173(2) K	
Wavelength	0.71073 Å	
Crystal system	Orthorhombic	
Space group	P2(1)2(1)2(1)	
Unit cell dimensions	a = 13.8504(14) Å	α = 90°.
	b = 14.2408(15) Å	β = 90°.
	c = 23.225(2) Å	γ = 90°.
Volume	4580.9(8) $Å^3$	
Z	4	
Density (calculated)	1.702 g/cm^3	
Absorption coefficient	2.718 mm^{-1}	
F(000)	2291	
Crystal size	0.20 x 0.10 x 0.10 mm^3	
Theta range for data collection	1.68 to 27.91°.	
Index ranges	-18<=h<=18, -16<=k<=18, -30<=l<=30	
Reflections collected	32516	
Independent reflections	10504 [R(int) = 0.1254]	
Completeness to theta = 27.91°	96.0 %	
Absorption correction	Semi-empirical from equivalents	
Max. and min. transmission	1.000 and 0.665	
Refinement method	Full-matrix least-squares on F^2	
Data / restraints / parameters	10504 / 21 / 476	
Goodness-of-fit on F^2	0.962	
Final R indices [I>2sigma(I)]	R1 = 0.0775, wR2 = 0.1848	
R indices (all data)	R1 = 0.1931, wR2 = 0.2261	
Absolute structure parameter	0.06(5)	
Largest diff. peak and hole	1.002 and -1.242 $e.Å^{-3}$	

Crystal data and structure refinement for (*R*,*R*)-**14**

Identification code	dp0605m	
Empirical formula	C32 H36 I2 N4 Ni	
Formula weight	789.16	
Temperature	173(2) K	
Wavelength	0.71073 Å	
Crystal system	Monoclinic	
Space group	P2(1)	
Unit cell dimensions	a = 14.9311(17) Å	α = 90°.
	b = 8.6427(9) Å	β = 103.466(8)°.
	c = 25.050(3) Å	γ = 90°.
Volume	3143.8(6) $Å^3$	
Z	4	
Density (calculated)	1.667 g/cm^3	
Absorption coefficient	2.608 mm^{-1}	
F(000)	1560	
Crystal size	0.40 x 0.25 x 0.08 mm^3	
Theta range for data collection	1.40 to 28.41°.	
Index ranges	-19<=h<=19, -10<=k<=11, -32<=l<=33	
Reflections collected	21125	
Independent reflections	12469 [R(int) = 0.0706]	
Completeness to theta = 28.41°	92.4 %	
Absorption correction	Semi-empirical from equivalents	
Max. and min. transmission	1.000 and 0.344	
Refinement method	Full-matrix least-squares on F^2	
Data / restraints / parameters	12469 / 78 / 343	
Goodness-of-fit on F^2	1.087	
Final R indices [I>2sigma(I)]	R1 = 0.1158, wR2 = 0.3006	
R indices (all data)	R1 = 0.1330, wR2 = 0.3104	
Absolute structure parameter	0.05(9)	
Largest diff. peak and hole	3.293 and -5.082 $e.Å^{-3}$	

Crystal data and structure refinement for (*R*,*R*)-**16**

Identification code	dp0607m	
Empirical formula	C64 H72 I3.20 N8 Ni2 O0.80	
Formula weight	1489.60	
Temperature	173(2) K	
Wavelength	0.71073 Å	
Crystal system	Rhombohedral	
Space group	R3	
Unit cell dimensions	a = 43.3113(17) Å	α = 90°.
	b = 43.3113(17) Å	β = 90°.
	c = 10.1110(8) Å	γ = 120°.
Volume	16425.8(16) $Å^3$	
Z	9	
Density (calculated)	1.355 g/cm^3	
Absorption coefficient	1.909 mm^{-1}	
F(000)	6696	
Crystal size	0.25 x 0.20 x 0.10 mm^3	
Theta range for data collection	1.63 to 28.38°.	
Index ranges	-57<=h<=57, -56<=k<=57, -13<=l<=12	
Reflections collected	40885	
Independent reflections	13549 [R(int) = 0.1204]	
Completeness to theta = 28.38°	94.4 %	
Absorption correction	None	
Refinement method	Full-matrix least-squares on F^2	
Data / restraints / parameters	13549 / 1 / 713	
Goodness-of-fit on F^2	0.941	
Final R indices [I>2sigma(I)]	R1 = 0.0883, wR2 = 0.2337	
R indices (all data)	R1 = 0.1615, wR2 = 0.2763	
Absolute structure parameter	0.01(5)	
Largest diff. peak and hole	2.237 and -1.528 e.$Å^{-3}$	

Crystal data and structure refinement for (*R*,*R*)-**18**

Identification code	dp0608	
Empirical formula	C44 H44 F6 N6 Ni O7 S2	
Formula weight	1005.68	
Temperature	100(2) K	
Wavelength	0.71073 Å	
Crystal system	Triclinic	
Space group	P1	
Unit cell dimensions	a = 12.3347(12) Å	α = 86.5080(10)°.
	b = 12.8896(13) Å	β = 73.8200(10)°.
	c = 17.0469(17) Å	γ = 62.9640(10)°.
Volume	2311.6(4) $Å^3$	
Z	2	
Density (calculated)	1.445 g/cm^3	
Absorption coefficient	0.590 mm^{-1}	
F(000)	1040	
Crystal size	0.12 x 0.24 x 0.46 mm^3	
Theta range for data collection	1.78 to 28.29°.	
Index ranges	-15<=h<=16, -16<=k<=17, -22<=l<=22	
Reflections collected	20473	
Independent reflections	17704 [R(int) = 0.0097]	
Completeness to theta = 28.29°	92.3 %	
Absorption correction	Semi-empirical from equivalents	
Max. and min. transmission	1.000 and 0.862	
Refinement method	Full-matrix least-squares on F^2	
Data / restraints / parameters	17704 / 53 / 1183	
Goodness-of-fit on F^2	1.454	
Final R indices [I>2sigma(I)]	R1 = 0.0866, wR2 = 0.2453	
R indices (all data)	R1 = 0.0918, wR2 = 0.2517	
Absolute structure parameter	0.054(14)	
Largest diff. peak and hole	1.690 and -0.696 $e.Å^{-3}$	

Crystal data and structure refinement for (*R*)-**21**

Identification code	dp0507	
Empirical formula	C54.50 H35 Cl3 F6 N4 O6 S2 Zn	
Formula weight	1191.70	
Temperature	100(2) K	
Wavelength	0.71073 Å	
Crystal system	Monoclinic	
Space group	C2	
Unit cell dimensions	a = 20.983(2) Å	α = 90°.
	b = 23.844(3) Å	β = 124.240(2)°.
	c = 12.1984(13) Å	γ = 90°.
Volume	5045.4(9) $Å^3$	
Z	4	
Density (calculated)	1.569 g/cm^3	
Absorption coefficient	0.808 mm^{-1}	
F(000)	2420	
Crystal size	0.08 x 0.14 x 0.24 mm^3	
Theta range for data collection	2.35 to 30.11°.	
Index ranges	-29<=h<=29, -33<=k<=33, -17<=l<=17	
Reflections collected	29354	
Independent reflections	14556 [R(int) = 0.0381]	
Completeness to theta = 30.11°	99.3 %	
Absorption correction	Semi-empirical from equivalents	
Max. and min. transmission	1.000 and 0.794	
Refinement method	Full-matrix least-squares on F^2	
Data / restraints / parameters	14556 / 34 / 781	
Goodness-of-fit on F^2	1.026	
Final R indices [I>2sigma(I)]	R1 = 0.0587, wR2 = 0.1340	
R indices (all data)	R1 = 0.0826, wR2 = 0.1463	
Absolute structure parameter	0.000(10)	
Largest diff. peak and hole	1.089 and -0.867 $e.Å^{-3}$	

Crystal data and structure refinement for (*R*)-**23**

Identification code	dp0604	
Empirical formula	C51 H33 Cl9 I4 N4 Ni2	
Formula weight	1645.88	
Temperature	100(2) K	
Wavelength	0.71073 Å	
Crystal system	Monoclinic	
Space group	P2(1)	
Unit cell dimensions	a = 11.6896(8) Å	α = 90°.
	b = 22.8266(16) Å	β = 118.9240(10)°.
	c = 11.9341(9) Å	γ = 90°.
Volume	2787.2(3) $Å^3$	
Z	2	
Density (calculated)	1.961 g/cm^3	
Absorption coefficient	3.362 mm^{-1}	
F(000)	1576	
Crystal size	0.40 x 0.12 x 0.07 mm^3	
Theta range for data collection	1.78 to 28.26°.	
Index ranges	-15<=h<=15, -30<=k<=30, -15<=l<=15	
Reflections collected	24886	
Independent reflections	12862 [R(int) = 0.0240]	
Completeness to theta = 28.26°	96.5 %	
Absorption correction	Semi-empirical from equivalents	
Max. and min. transmission	1.000 and 0.752	
Refinement method	Full-matrix least-squares on F^2	
Data / restraints / parameters	12862 / 1 / 631	
Goodness-of-fit on F^2	1.009	
Final R indices [I>2sigma(I)]	R1 = 0.0268, wR2 = 0.0606	
R indices (all data)	R1 = 0.0284, wR2 = 0.0613	
Absolute structure parameter	0.007(10)	
Largest diff. peak and hole	1.018 and -0.483 $e.Å^{-3}$	

Crystal data and structure refinement for (*R*)-**24**

Identification code	dp0601b	
Empirical formula	C47.60 H41.20 Cl3.20 I4 N4 Ni2 O	
Formula weight	1423.71	
Temperature	100(2) K	
Wavelength	0.71073 Å	
Crystal system	Orthorhombic	
Space group	P2(1)2(1)2(1)	
Unit cell dimensions	a = 12.1481(14) Å	α = 90°.
	b = 22.485(3) Å	β = 90°.
	c = 19.246(2) Å	γ = 90°.
Volume	5257.3(10) $Å^3$	
Z	4	
Density (calculated)	1.799 g/cm^3	
Absorption coefficient	3.265 mm^{-1}	
F(000)	2741	
Crystal size	0.38 x 0.16 x 0.09 mm^3	
Theta range for data collection	1.81 to 28.30°.	
Index ranges	-16<=h<=15, -29<=k<=26, -25<=l<=21	
Reflections collected	36142	
Independent reflections	12468 [R(int) = 0.0525]	
Completeness to theta = 28.30°	97.0 %	
Absorption correction	Semi-empirical from equivalents	
Max. and min. transmission	1.000 and 0.393	
Refinement method	Full-matrix least-squares on F^2	
Data / restraints / parameters	12468 / 6 / 582	
Goodness-of-fit on F^2	1.057	
Final R indices [I>2sigma(I)]	R1 = 0.0587, wR2 = 0.1440	
R indices (all data)	R1 = 0.0742, wR2 = 0.1521	
Absolute structure parameter	0.03(3)	
Largest diff. peak and hole	2.233 and -0.823 $e.Å^{-3}$	

Crystal data and structure refinement for (*R*)-**27**

Identification code	dp0401m	
Empirical formula	C41 H28 Cl2 N4 O2	
Formula weight	679.57	
Temperature	173(2) K	
Wavelength	0.71073 Å	
Crystal system	Orthorhombic	
Space group	P2(1)2(1)2(1)	
Unit cell dimensions	a = 10.2058(6) Å	α = 90°.
	b = 17.5392(10) Å	β = 90°.
	c = 18.2084(10) Å	γ = 90°.
Volume	3259.3(3) $Å^3$	
Z	4	
Density (calculated)	1.385 Mg/m^3	
Absorption coefficient	0.244 mm^{-1}	
F(000)	1408	
Crystal size	0.40 x 0.35 x 0.30 mm^3	
Theta range for data collection	1.61 to 28.29°.	
Index ranges	-12<=h<=13, -22<=k<=23, -24<=l<=23	
Reflections collected	23355	
Independent reflections	4265 [R(int) = 0.1087]	
Completeness to theta = 28.29°	94.5 %	
Absorption correction	None	
Refinement method	Full-matrix least-squares on F^2	
Data / restraints / parameters	4265 / 0 / 453	
Goodness-of-fit on F^2	1.046	
Final R indices [I>2sigma(I)]	R1 = 0.0539, wR2 = 0.1388	
R indices (all data)	R1 = 0.0739, wR2 = 0.1518	
Absolute structure parameter	0.42(11)	
Extinction coefficient	0.0051(12)	
Largest diff. peak and hole	0.394 and -0.333 $e.Å^{-3}$	

Crystal data and structure refinement for (*R*,*R*)-**30**

Identification code	dp0303m	
Empirical formula	C40.48 H24 Cl0.97 Fe N4 O2	
Formula weight	688.69	
Temperature	173(2) K	
Wavelength	0.71073 Å	
Crystal system	Monoclinic	
Space group	P2(1)	
Unit cell dimensions	a = 7.8385(8) Å	α = 90°.
	b = 19.8211(16) Å	β = 91.809(4)°.
	c = 21.611(2) Å	γ = 90°.
Volume	3356.1(6) $Å^3$	
Z	4	
Density (calculated)	1.363 g/cm^3	
Absorption coefficient	0.569 mm^{-1}	
F(000)	1414	
Crystal size	0.40 x 0.20 x 0.10 mm^3	
Theta range for data collection	1.89 to 28.27°.	
Index ranges	-9<=h<=9, -26<=k<=26, -26<=l<=28	
Reflections collected	39068	
Independent reflections	13943 [R(int) = 0.0715]	
Completeness to theta = 28.27°	93.7 %	
Absorption correction	None	
Refinement method	Full-matrix least-squares on F^2	
Data / restraints / parameters	13943 / 13 / 906	
Goodness-of-fit on F^2	0.939	
Final R indices [I>2sigma(I)]	R1 = 0.0660, wR2 = 0.1670	
R indices (all data)	R1 = 0.1341, wR2 = 0.1910	
Absolute structure parameter	0.51(2)	
Largest diff. peak and hole	0.848 and -0.606 e.$Å^{-3}$	

Appendix III

UV & ECD spectra

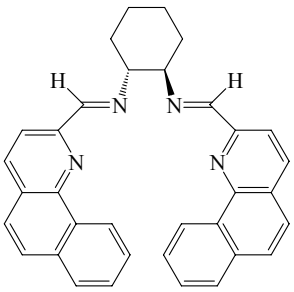

(*R*,*R*)-**5** DP-2-33-1

CD

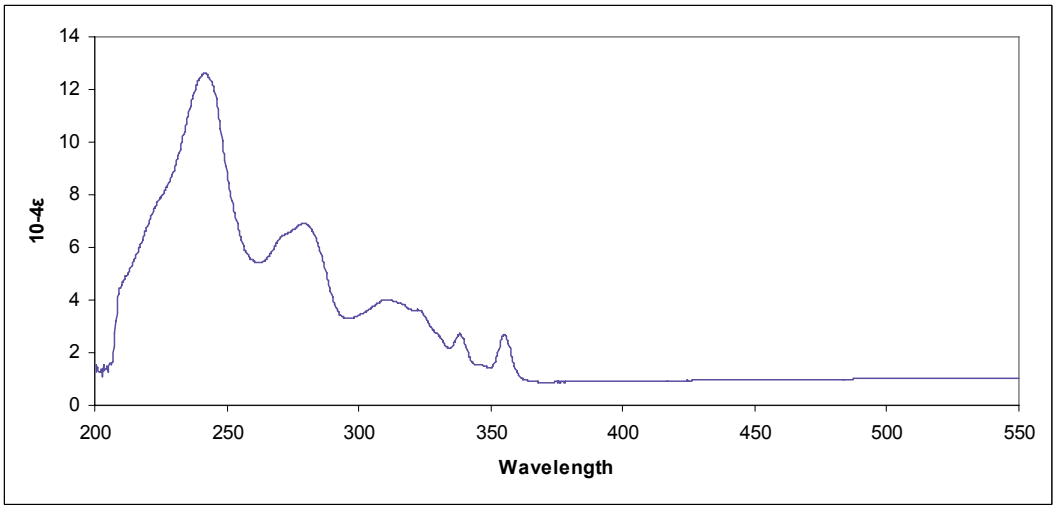

UV

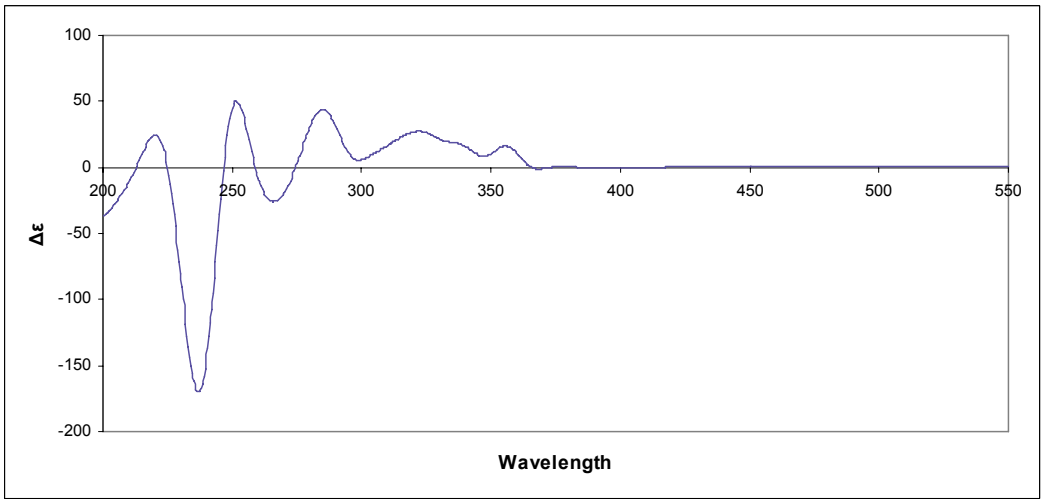

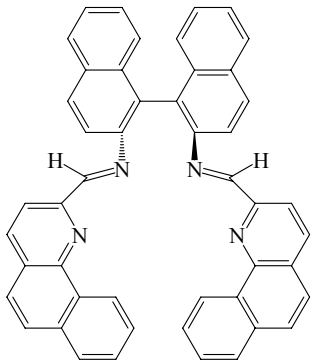

(*R*)-**6** DP-2-34-1

UV

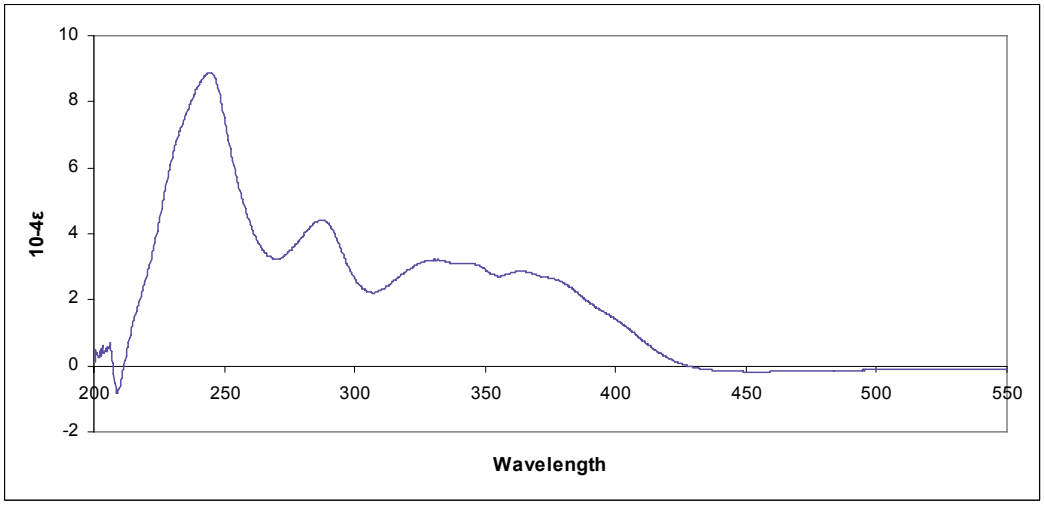

CD

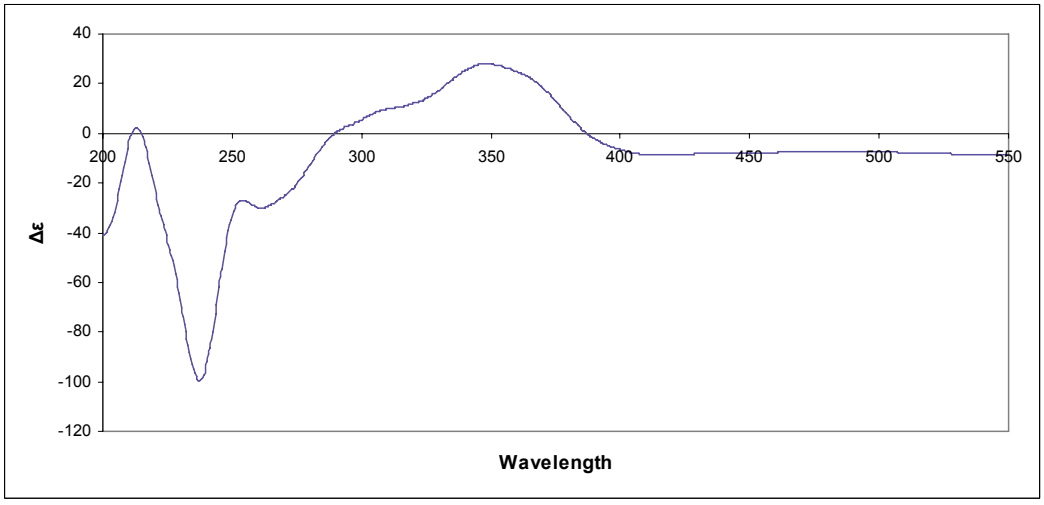

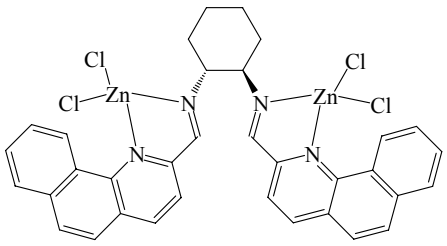

(*R*,*R*)-**8** DP-2-53-1

UV

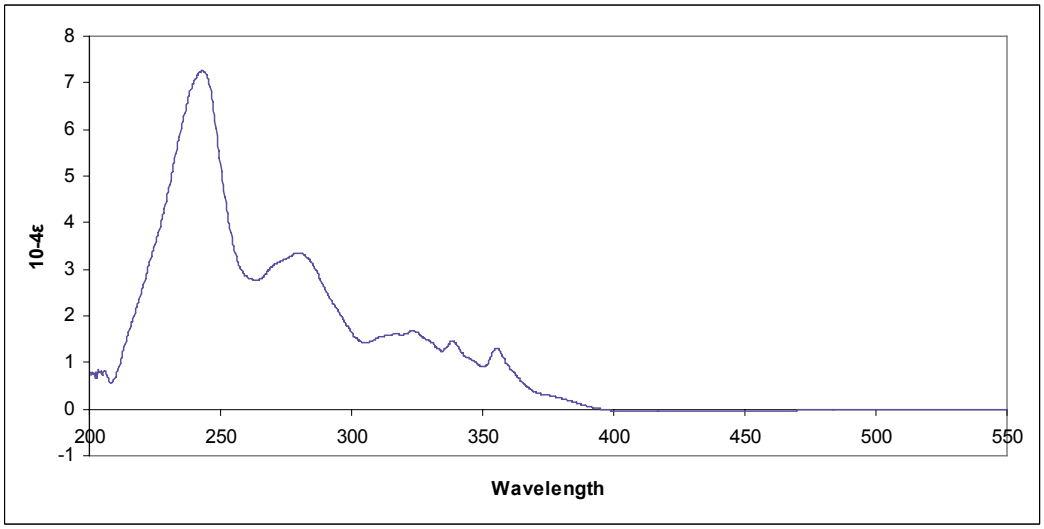

CD

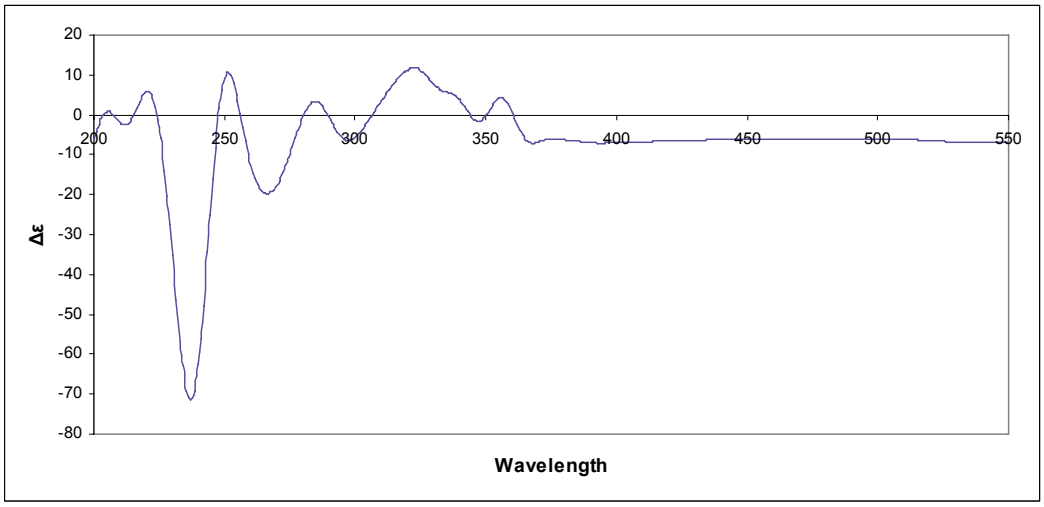

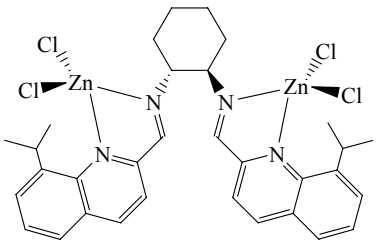

(*R*,*R*)-**9** DP-2-54-1

UV

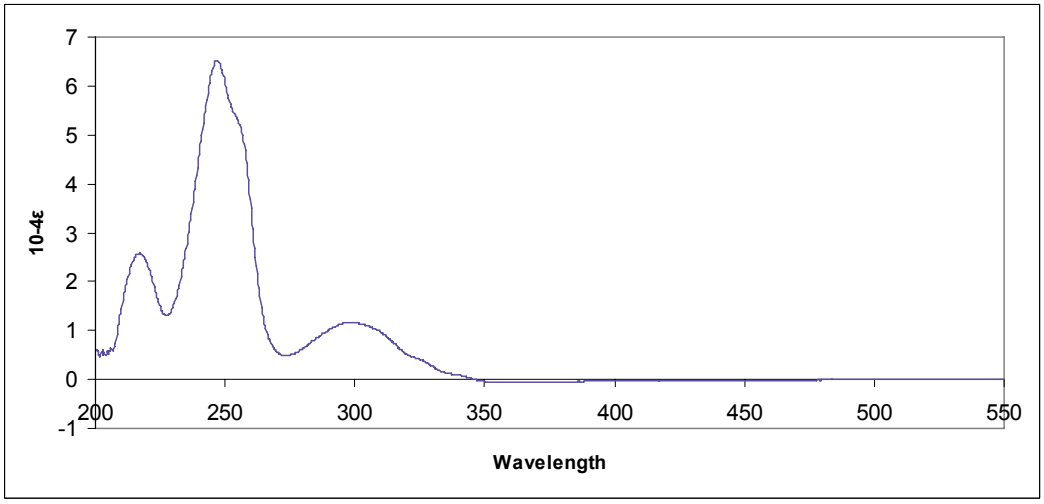

CD

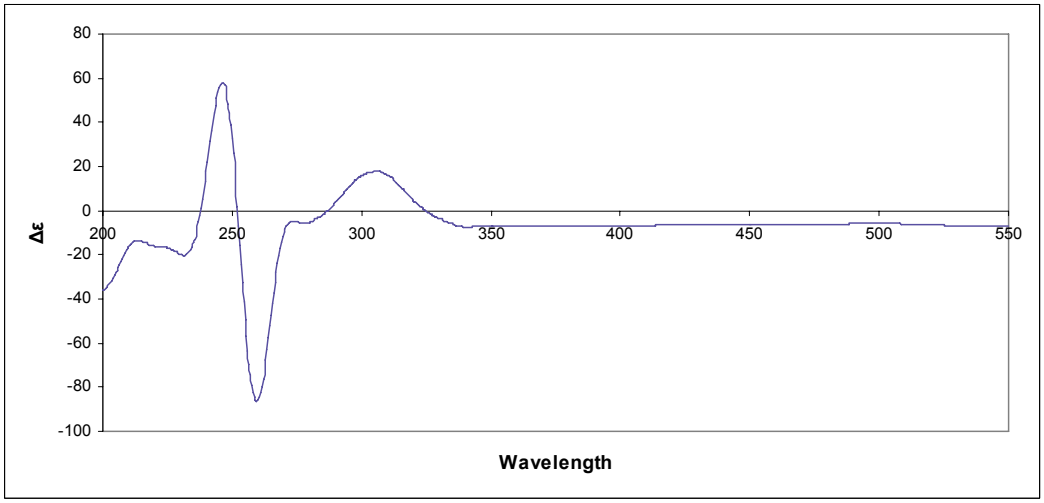

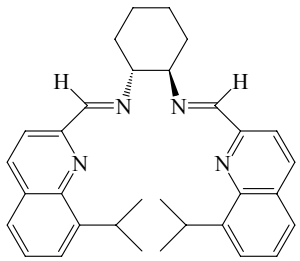

(*R*,*R*)-**10** Al-3-188

UV

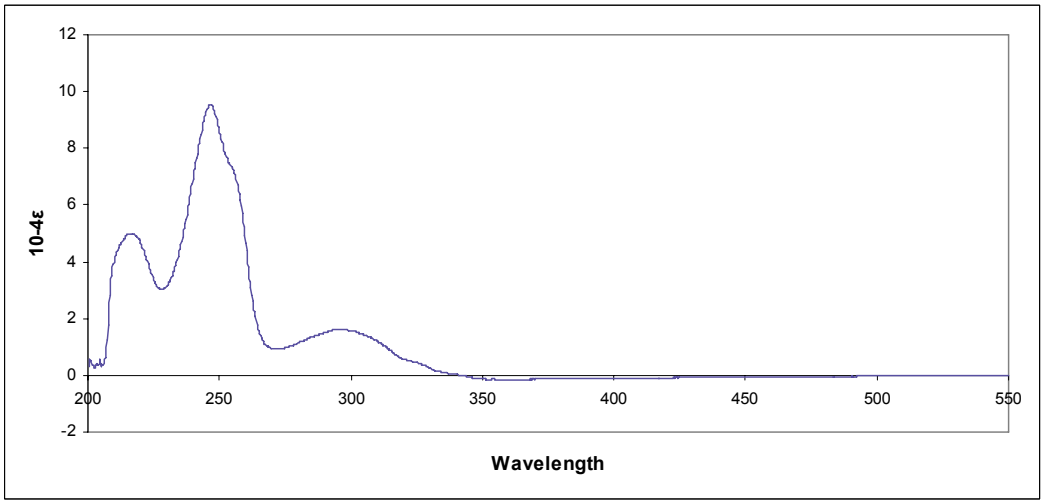

CD

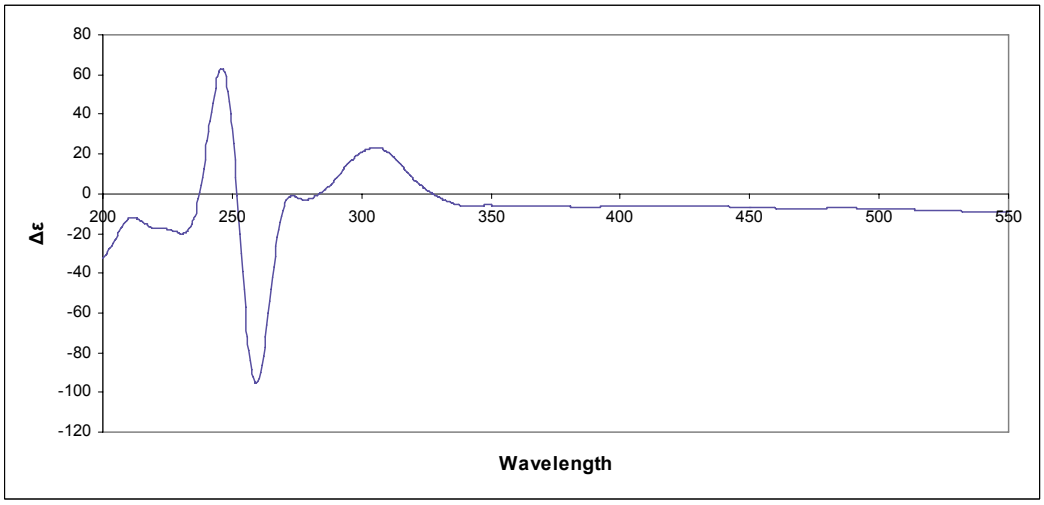

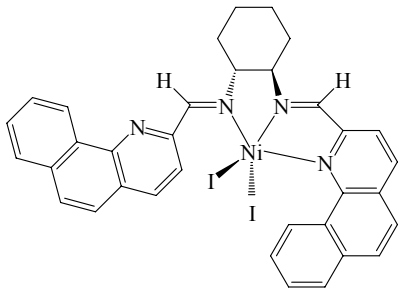

(*R*,*R*)-**11** DP-2-75-1

UV

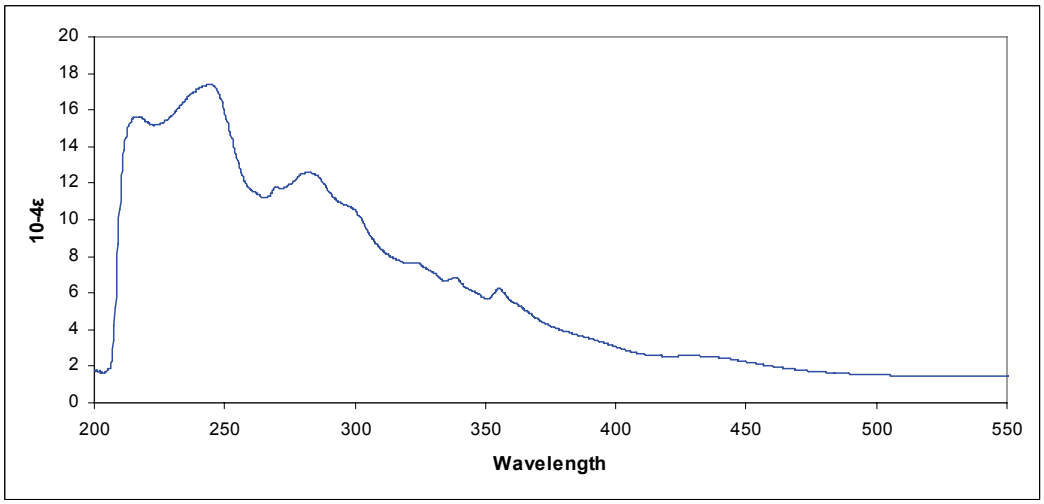

CD

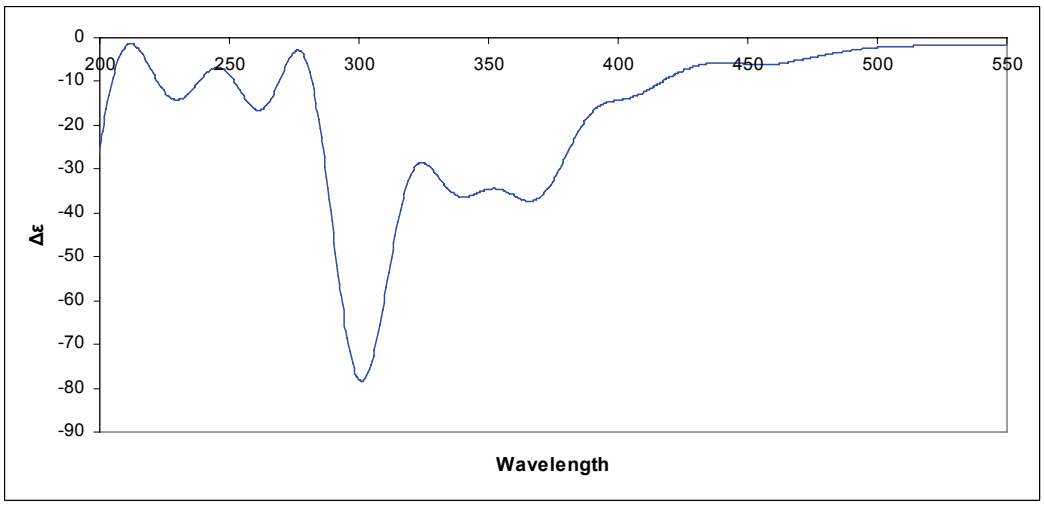

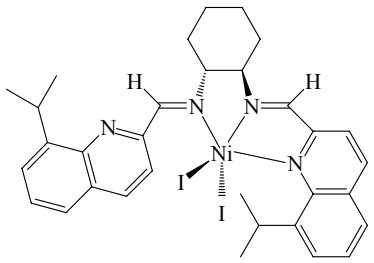

(*R*,*R*)-**12** DP-2-95-1

UV

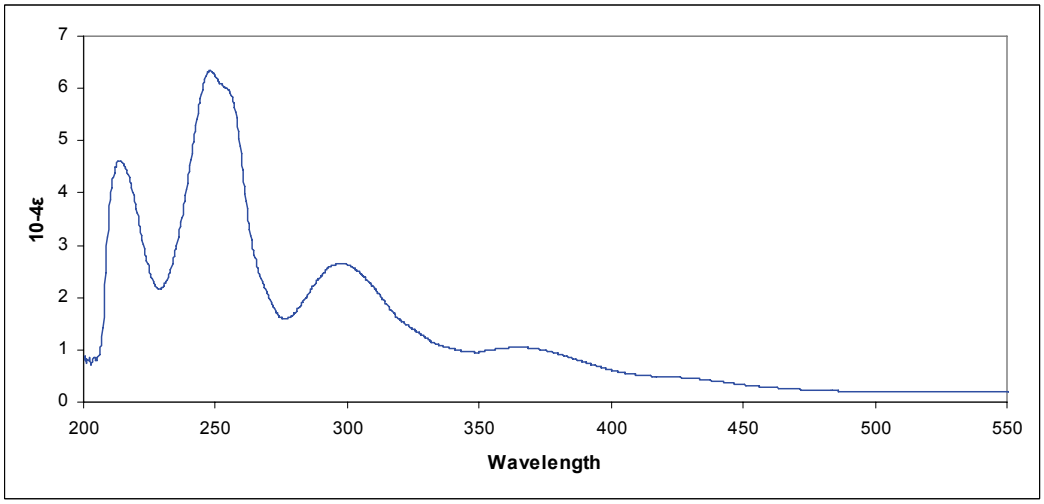

CD

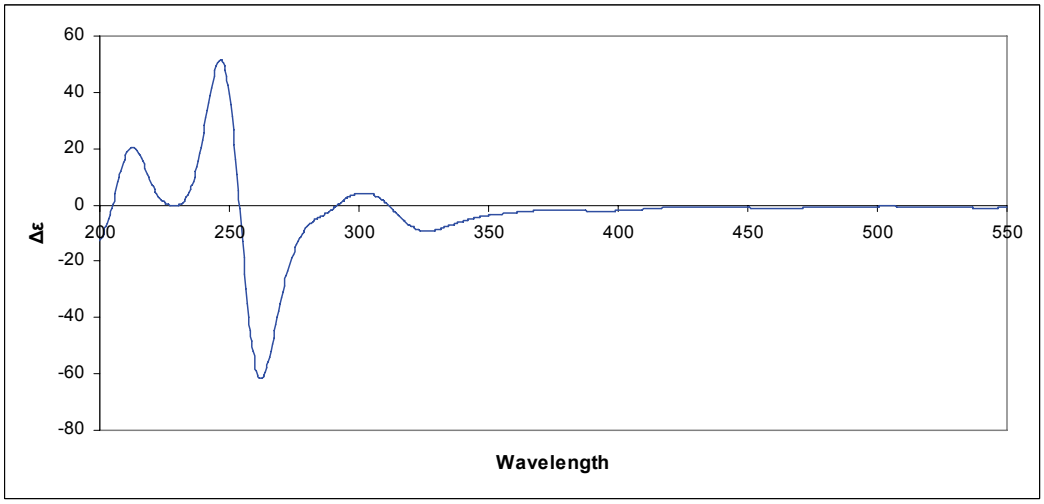

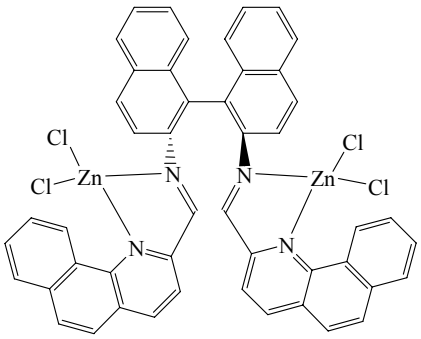

(*R*)-**19** DP-2-50-2

UV

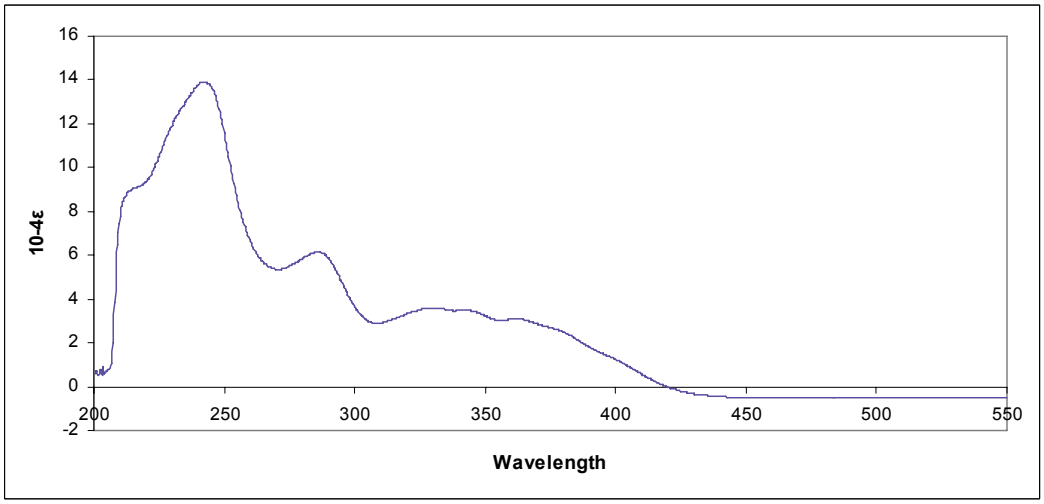

CD

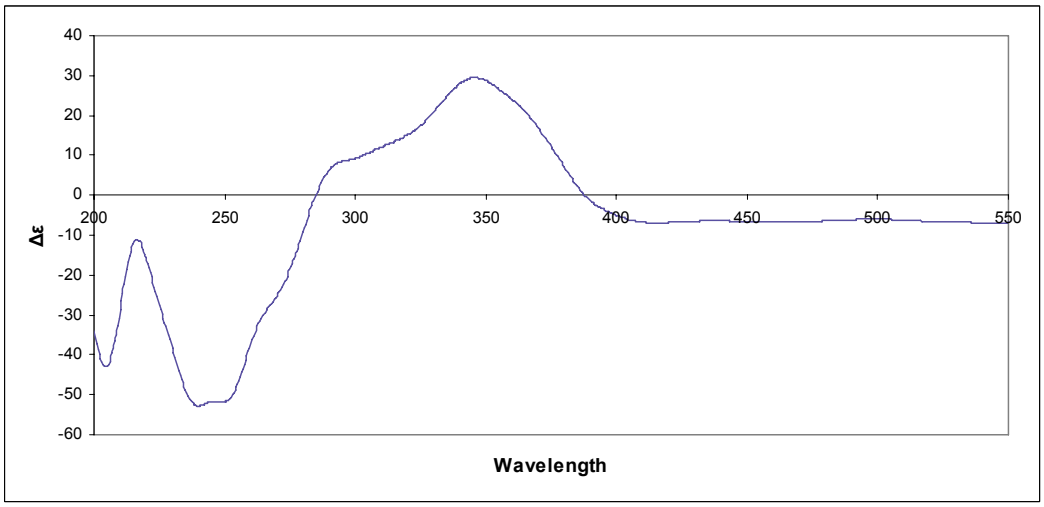

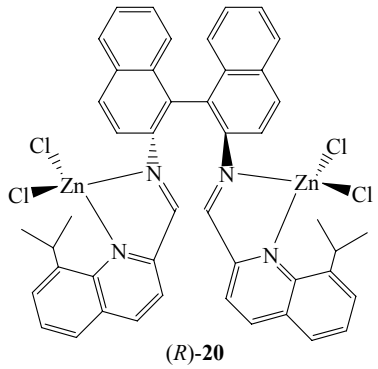

(*R*)-**20** AL-3-163

UV

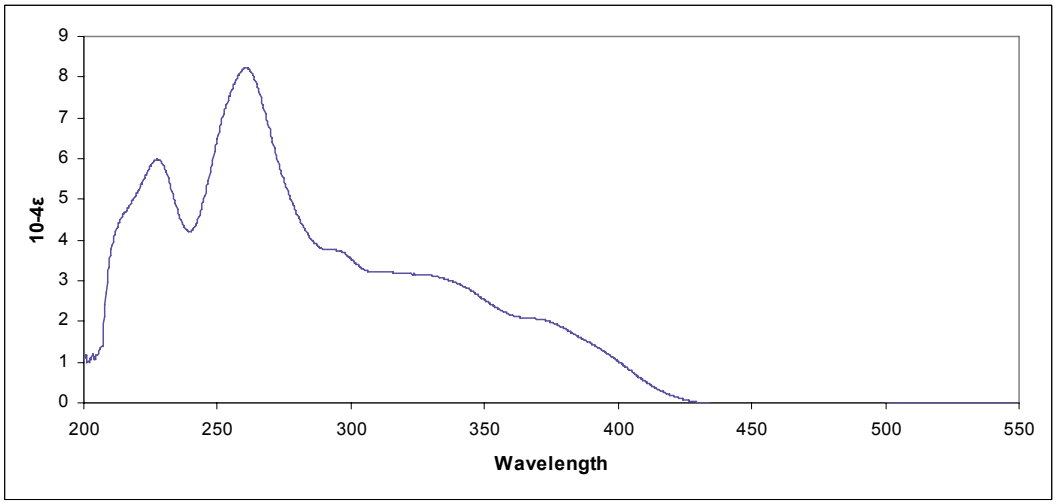

CD

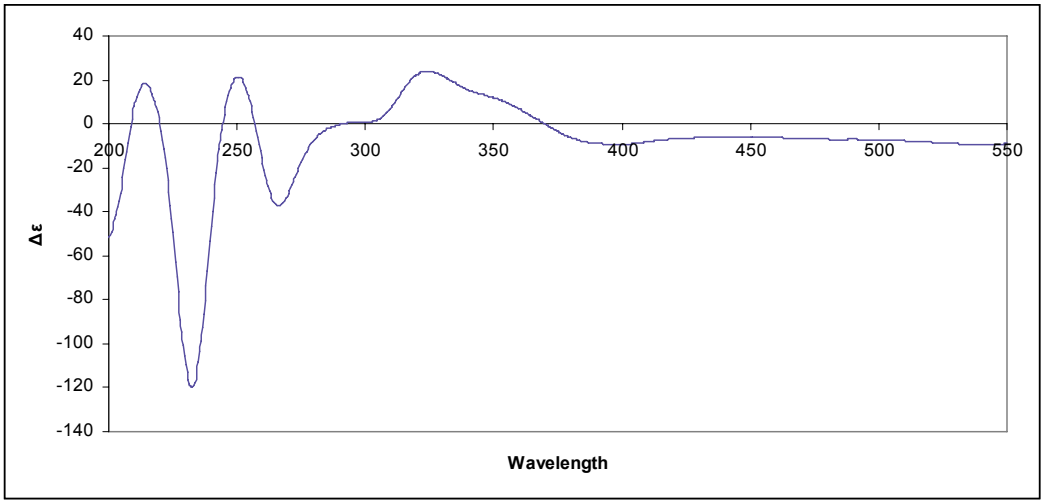

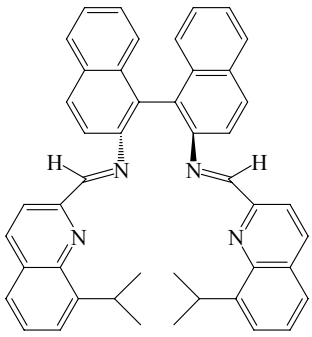

(*R*)-**22** AL-3-178

UV

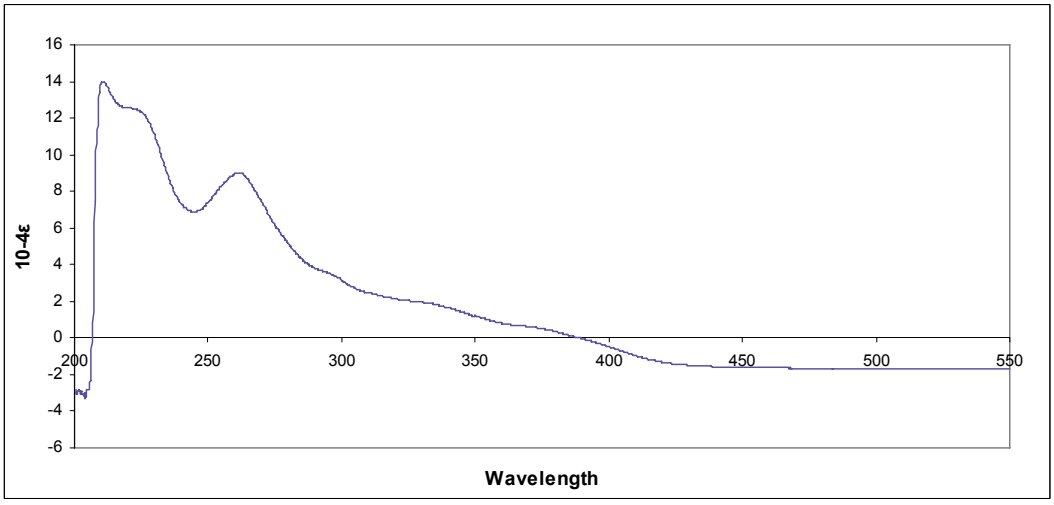

CD

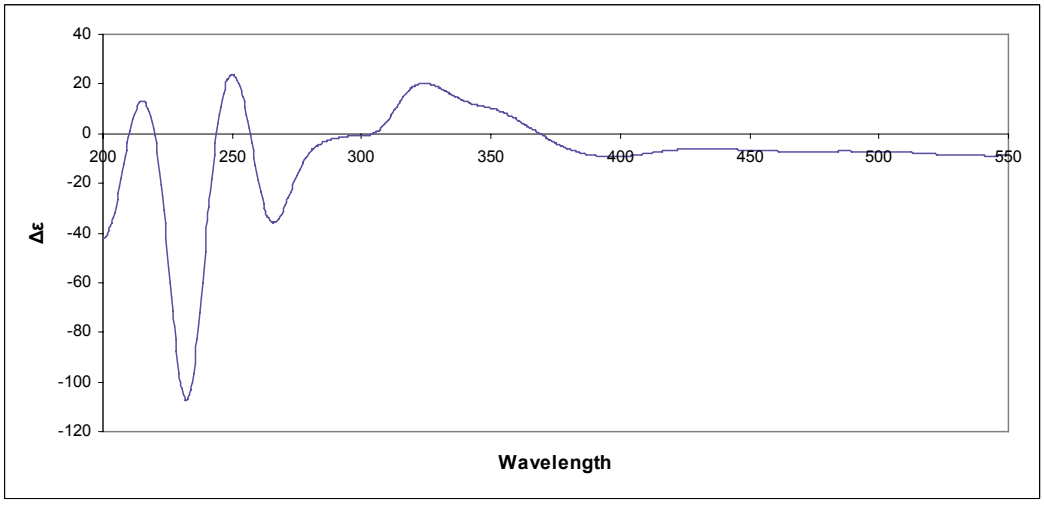

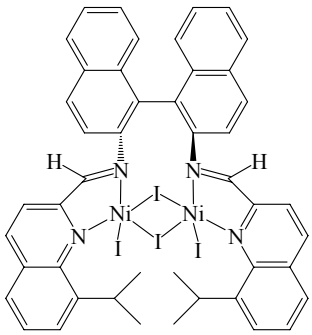

(*R*)-**23** DP-3-4-1

UV

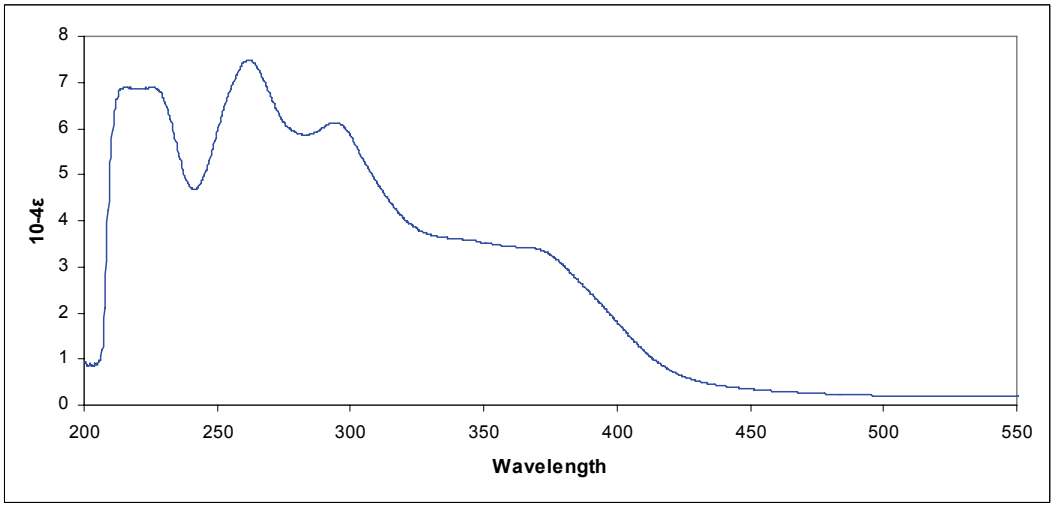

CD